The Development of a Portable Dynamometer for Upper Limb Strength and Power Assessment

By

Yassine El Alaoui

Bachelor of Applied Science, University of Windsor, 2020

A Thesis Submitted in Partial Fulfillment of the Requirements for the Degree of

MASTER OF APPLIED SCIENCE

in the Department of Mechanical Engineering

University of Victoria

We acknowledge and respect the Lək̓ʷəŋən (Songhees and Xʷsepsəm/Esquimalt) Peoples on whose territory the university stands, and the Lək̓ʷəŋən and W̱SÁNEĆ Peoples whose historical relationships with the land continue to this day.

The Development of a Portable Dynamometer for Upper Limb Strength and Power Assessment

By

Yassine El Alaoui

Bachelor of Applied Science, University of Windsor, 2020

Supervisory Committee:

Dr. Joshua Giles, Supervisor

Department of Mechanical Engineering

Dr. Mike Berger, Supervisor

University of British Columbia

Dr. Zuomin Dong, Departmental Member

Department of Mechanical Engineering

Abstract

Portable, practical assessment of upper-limb muscle function is limited by the inaccessibility of gold-standard isokinetic systems to most clinics, and the shortcomings of purely isometric devices. Clinically, isotonic (constant torque) testing enables assessment of power characteristics that isometric (static) measurements miss. Conventional isokinetic (constant velocity) systems are complex, expensive, and have a large footprint. This thesis presents the design and technical validation of a table-top dynamometer that measures upper limb muscle isometric torque and isotonic power. It uses a Brushless Direct Current (BLDC) motor and gearbox drivetrain with field-oriented control (FOC) to target a constant resisting torque. The device clamps on to a table. It has a lever arm with a padded, adjustable cuff, and records torque and velocity while the user performs voluntary movement under a target resisting torque. The goals of this work are to (i) evaluate FOC as a strategy for producing precise, constant resisting torque, (ii) develop a prototype capable of both isotonic and isometric testing, and (iii) validate constant-torque behaviour across a clinically relevant range.

During validation, the drivetrain's failure to maintain constant resisting torque was traced to gearbox inertia and velocity-dependent friction. These effects were quantified via passive deceleration tests across multiple added inertias and velocities, resulting in an empirical power-law friction fit implemented as real-time feed-forward compensation. A brake-chopper was added to stabilize the DC bus during backdriven operation. Validation with drop tests showed linear velocity-time profiles across resisting torques of 0.61-4.61 N·m and velocities of 0-22 rad/s, indicating constant resisting torque ($R^2 \geq 0.99$; RMSE = 0.11 rad/s). The prototype (≈19.2 kg; 18.9 L) maintained a constant torque. These results show that FOC with empirical friction compensation is a viable approach to portable isotonic dynamometry. Future work will increase control-loop frequency, unlock the hardware's full torque capacity (≈23 N·m), and perform clinical validation toward standardized protocols and normative datasets.

Table of Contents

List of Tables

List of Figures

Acknowledgements

I would like to thank my supervisors, Dr. Giles and Dr. Berger, for their guidance, support, and technical insight throughout this project. I am especially thankful for their patience and understanding during the iterative development of this work.

I also thank Dr. Dong for serving on my supervisory committee, and Dr. Chelvan for agreeing to be the external examiner. Their questions, comments and feedback helped strengthen this thesis.

I am grateful to the members of the Orthopaedic Technologies and Biomechanics Lab for the discussions and encouragement along the way.

This work was supported by Mitacs. Additional support from the Orthopaedic Technologies and Biomechanics lab, the University of Victoria, and the Mechanical Engineering department is gratefully acknowledged.

1. Introduction

1.1. Rationale

Upper limb dysfunction is common across neurological and musculoskeletal disorders, and in work related injuries [1], [2], and it limits basic self-care and participation in daily activities [3]. Upper limb motor function is a major predictor of health-related quality of life[4], [5]. Musculoskeletal disorders can result in major mobility limitations, loss of independence, and the need for a full-time caregiver [6], [7], [8], [9]. The pain and fatigue associated with work-related upper limb injuries are frequently linked to reduced productivity and mental health decline[10]. Individuals with neurological impairment (for example, after stroke) show weakening in shortened muscle positions and significantly reduced isometric elbow flexion and extension torque compared to controls [11].

Neurological disorders, including spinal cord injury (SCI), are also a major cause of upper limb impairment. SCI often leads to weakness and loss of voluntary control, making long-term rehabilitation necessary[12], [13]. Recent approaches such as functional electrical stimulation (FES)[14], neurorehabilitation robotics[15], [16], and regenerative treatments show potential for preserving function, slowing decline in neurodegenerative disease, and in some cases restoring movement[17], [18], [19]. Measuring their effectiveness, however, is difficult without reliable methods to evaluate static and dynamic muscle performance[20]. Accordingly, emerging interventions require proper outcome measures, or biomarkers, that quantify them both. To be meaningful, these should be easily quantifiable, repeatable, and practical for routine assessments. Elbow flexion and extension are important for everyday function. Flexion enables activities such as eating, grooming, lifting and manipulating objects. Extension, on the other hand, allows people to stand up from a chair, move from a bed to a wheelchair, or otherwise stabilize the body with the upper limbs.

Two common markers of muscle performance are strength and power. Strength in elbow flexion/extension refers to the maximum voluntary torque, where torque is the product of a moment arm and a perpendicular force ($\tau = F \times r$). Power is the rate of doing work, represented by the product of torque and angular velocity ($P = \tau \times \omega$). Power relates closely to the execution of time-constrained functional tasks in daily life [21], [22], [23]. Fine motor power predicts the ability to manipulate tools and utensils [24]. Dynamic muscle performance assessments reveal speed-dependent deficits in stroke patients, with greater impairments at increasing movement speeds, indicating that power captures additional, velocity-dependent impairments that torque measured at a fixed angle or set speed may miss[25], [26], [27], [28]. Comprehensive physiological profiling of upper limb function, including strength and power assessment, is an effective way to differentiate between healthy individuals and those with neurological

conditions [29], [21], [27]. However, strength and power measurements alone do not capture compensatory movement. Kinematic variables of movement quality such as joint ranges of motion and trunk displacement explain 51-52% of the variance in motor impairment scores, highlighting the need for standardized positioning[30].

Table 1. Summary of upper limb strength and power test types, benefits, limitations and practical aspects as relevant to dynamometry [22], [28], [31], [32], [33], [34], [35], [36], [37]

Test Type	What is Measured	Key Benefits	Key Limitations	Practical Aspects
Isometric	Strength (Torque at fixed angle)	- Simple protocols - Widely Understood - Low cost	- No velocity information - Sensitive to examiner stabilization (handheld)	- Low cost - High portability - Rapid setup - High tolerance
Isokinetic	Work/Power (torque at constant angular velocity)	- Controlled speed - Common in research - Outputs torque/velocity curves	- Constrains velocity - Bulky/expensive - Many patients fail to reach criterion speeds	- High cost - Low portability - Requires extensive training - Moderate tolerance
Isotonic	Power (torque and velocity against a constant external load)	- Mirrors daily actions - Captures velocity-dependent deficits - Better tolerated - Outputs torque/velocity curves	- Few standardized protocols/devices in clinics - Historically underused	- Mostly custom devices - High tolerance - Good safety under sub-maximal loads

There are different ways to measure muscle output, each with benefits and limitations[22]. They include isometric, isokinetic, or isotonic tests (summarized and described in detail in section 2.2). While isometric tests are often used as primary clinical assessments, and isokinetic tests are common in research settings, isotonic power is often neglected despite being a stronger predictor of functional ability [21], [23], [31], [32]. Deficits in power can appear before losses in isometric strength are detected [21], [23]. In older adults, isotonic power gains are more strongly associated with functional improvements than increases in isometric strength alone [38]. This emphasizes the importance of isotonic power and reinforces the need for practical tools to measure it.

Handheld dynamometers are a popular way to obtain isometric strength (static torque). Their effectiveness is limited by the examiner's strength and their stabilization technique[22], [33], [34]. Isokinetic testing requires devices that are often prohibitively expensive, bulky, and impractical for clinical settings[35], [36]. In addition, constraining velocity can artificially make peak torque coincide with peak power [31]. In isokinetic tests, many stroke patients cannot reach typical criterion speeds during testing (20% fail to reach 30°/s (0.52 rad/s), 68% fail to reach 75°/s (1.31 rad/s, and 90% fail to reach 120°/s (2.09 rad/s)) [28]. Most daily activities are not performed at a constant velocity, or fixed position like in isokinetic and isometric tests, respectively. Isotonic testing closely

mirrors movements in daily life involving moving objects with a fixed mass, including the body itself[31].

Despite the potential relevance of isotonic testing, and the dominance of isotonic contractions in daily activities such as lifting, standing, and pushing doors, isotonic power assessments are rare in clinics due to a lack of standardized tools and protocols [31], [39]. Clinical and research data remain limited due to technical barriers, and clinicians and researchers tend to prioritize isometric and isokinetic tests due to equipment availability and ease of implementation[31]. The ability to obtain a single explosive movement from an isotonic test can give clinicians and researchers insight into the rate of power development and an objective measure of velocity-dependent power [39], [40]. In addition, isotonic testing is better tolerated and causes less pain [37]. Dynamic muscle performance assessments were shown by Kim et al. (2005) to be more clinically relevant than torque alone since stroke patients often have speed-dependent deficits in power. This deficit can be more pronounced at higher speeds, making power measurement more relevant than torque alone [25], [26], [28]. However, many current clinical assessments of upper-limb function rely primarily on grip strength and manipulation tasks because they are simpler to administer and correlate with performance in daily activities[41], [42], [43], [44]. These assessments can be challenging for patients who cannot grip effectively (due to weakness or pain). Isotonic power testing can provide more functionally meaningful assessments for those patients, regardless of their grip ability.

Taken together, the functional relevance, feasibility and clinical timelines point to the need for isotonic power measurement in routine care. Isotonic testing typically requires heavy, expensive devices, limiting their accessibility to most clinical settings. The increasing availability and decreasing cost of high-performance, off-the-shelf motor controllers now provide the potential to build a portable device with smooth control for dynamometry.

1.2. Goals and Objectives

Building on the rationale above, the ubiquity of upper limb dysfunction due to stroke, spinal cord injury, musculoskeletal disorders and workplace injuries, combined with the emergence of new therapies has increased the need for portable and effective tools to measure upper limb function. The goal of this research is to develop a portable dynamometer capable of measuring both isometric torque and isotonic power, giving clinicians a convenient and capable tool to evaluate upper limb function. To achieve this, the following objectives are defined:

1. To evaluate the viability of field-oriented control (FOC) as a motor control strategy to produce precise and constant resisting torque.

2. To develop a table-top prototype dynamometer device capable of performing isotonic and isometric tests.
3. To validate the device's ability to maintain a constant resisting torque in the target torque range, and to measure isometric strength for healthy populations.

Data will support feasibility testing, calibration, tuning and give preliminary estimates of repeatability in a controlled setting.

1.3. Summary of Contributions

Project-Wide Roles

This thesis represents work conducted under the supervision of Dr. Joshua Giles and Dr. Mike Berger, with additional input from Colin Day. Dr. Giles and Dr. Berger, in addition to supervising, acquired funding for the project and provided financial support for component purchases and prototyping needs. All design and testing activities were carried out in the Orthopaedic Technologies and Biomechanics Lab at the University of Victoria.

Prior Work

Colin Day (BEng, Research Engineering Associate) and Evan Stefanik (BEng) were involved in the earliest work on this project which defined the initial development objectives and the choice of a motor driven solution.

Erik Bedard (BEng) developed the initial Printed Circuit Board (PCB) for isometric and isotonic testing, including circuit design and microcontroller firmware. This prototype used a different motor and controller, PCB, firmware, communication, and control strategy than those used in this thesis.

Colin Day refined the early prototype into a functional device for isometric testing, developed a daughter board and circuit for isotonic testing, and replaced the motor and controller with the models used in this thesis. The daughterboard informed the circuit in the current design but remains distinct from it.

Section 1: Introduction

Dr. Berger: Identified the need for a portable tool to measure isotonic power, outlined the requirements for the device, and identified the clinical constraints.

Dr. Giles: Helped set the overall project goals, reviewed the needs from a mechanical engineering perspective, co-defined goals, scope and technical constraints.

Yassine El Alaoui: Translated goals into actionable tasks, co-defined goals and scope, conducted literature review on clinical protocols and existing devices.

Section 2: Background

- Dr. Giles: Directed the background research, reviewed the chapter and suggested edits as needed.
- Dr. Berger: Interpreted the clinical relevance, suggested additional background, and reviewed the chapter.
- Colin Day: Provided rationale for field-oriented control (FOC).
- Yassine El Alaoui: Conducted background research and wrote the original draft (motivation, and problem framing).

Section 3: Mechanical Design

- Dr. Berger: Conceptualization (clinical need and constraints), and requirements review.
- Dr. Giles: Conceptualization (engineering constraints), requirements review, writing review and editing.
- Colin Day: Provided lessons learned from previous designs.
- Yassine El Alaoui: Drafted the physical, technical, functional, and performance requirements.

Section 4: Prototype Development and Build

- Dr. Berger, Dr. Giles: Regular design reviews and design sign-off.
- Colin Day: Drivetrain component selection (motor, controller and gearbox), troubleshooting assistance with electromagnetic noise and brake-chopper.
- Yassine El Alaoui: Mechanical design overhaul, circuit design, and firmware development for the current implementation. This includes component integration and communication, enclosure, mechanical brake, clamps, electronics, CAD/drawings, strain-gauge assembly, mechanical assembly, wiring, and writing of the original draft.
- Rodney Katz (Senior Scientific Assistant): Fabrication of the prototype, and mechanical-design advice.

Section 5: Device Characterization Methods

- Dr. Berger: Clinical performance criteria and acceptance thresholds, review and editing.
- Dr. Giles: Experimental design guidance, validation oversight, data-collection script assistance (NDI Vega motion-capture camera), review, editing.
- Yassine El Alaoui: Methodology and Design (initial system assessment, gearbox deceleration tests for inertia/friction characterization, constant-torque drop tests), design of experimental fixtures, data-collection scripts, data processing pipeline, and writing of the original draft.

Section 6: Results

- Dr. Berger: Review and editing
- Dr. Giles: Interpretation, supervision, review and editing.
- Yassine El Alaoui: Investigation (all experiments), formal analysis (parameter estimation, friction equation derivation and fit, compensation evaluation, isometric validation, data visualization), and writing of the original draft.

Sections 7-9: Discussion, Validation and Conclusion

- Dr. Berger: Clinical interpretation and applicability, review and editing.
- Dr. Giles: Validation oversight, technical feedback, supervision, review and editing
- Yassine El Alaoui: Formal analysis and synthesis, writing of the original draft.

2. Background

A clear understanding of the structures involved in upper limb mobility is essential to the development of a dynamometer capable of accurately quantifying strength and power. In this chapter, the anatomical and functional characteristics of the elbow joint are reviewed with an emphasis on muscles involved in elbow flexion and extension. In addition, this chapter presents the current power and strength measurement techniques, discusses other dynamometers on the market, and introduces the technologies used in the development of a portable dynamometer capable of measuring isometric torque and isotonic power.

2.1. Upper-limb Biomechanics

The human upper limb is a complex system dependent on the coordination between the skeletal, muscular, connective and neurovascular structures [45]. Understanding each of these is fundamental to the development of measurement devices that capture and describe their function.

2.1.1. Anatomy of the Upper Limb

The humerus is the longest bone of the upper limb. It forms the upper arm's skeletal architecture and articulates proximally with the scapula to form the shoulder joint. The shoulder is best described as a ball-and-socket joint. It gives the arm the ability to move in flexion, extension, abduction and axial rotation [46], [47]. On the distal side, the humerus meets the radius and ulna to form the elbow joint. The elbow behaves primarily as a hinge, allowing flexion and extension, and providing rotational stability during forearm pronation and supination[48]. Structurally, the distal humerus features two key components: the trochlea on the medial side, forming the humeroulnar joint, and the capitellum on the lateral side, which meets the radius at the humeroradial joint. These articulations help distribute forces through the elbow during movement and have a role in force transmission through the arm[49].

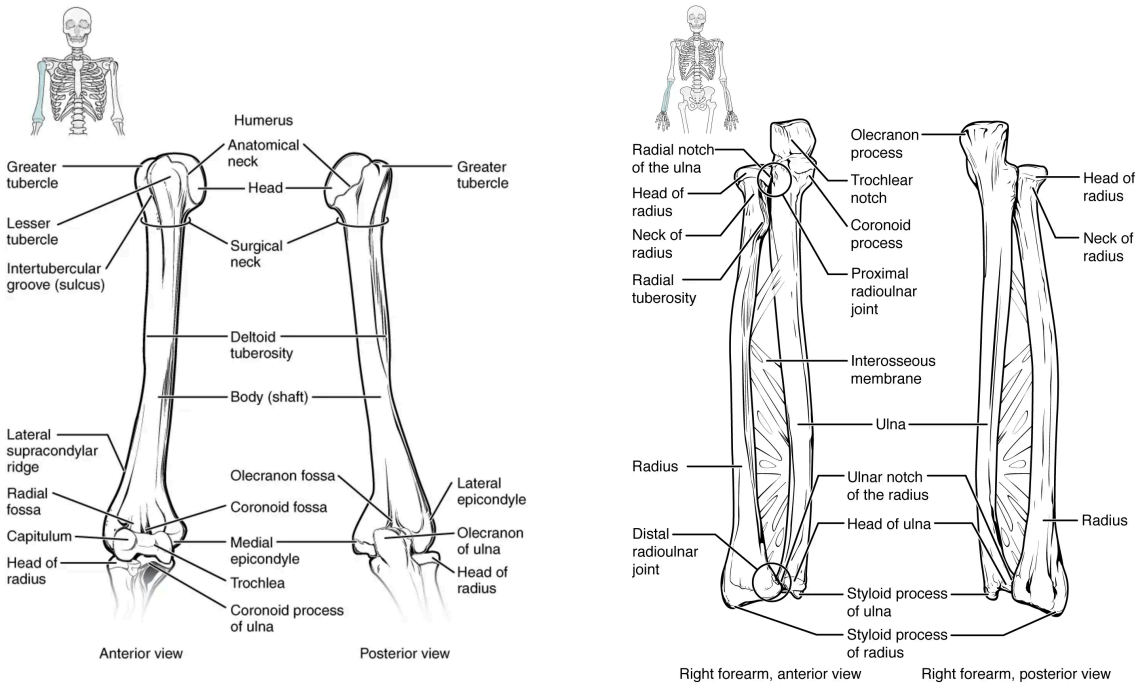

Figure 1. Upper limb bones relevant to elbow flexion/extension [50].

The elbow's stability is kept by the surrounding ligaments and joint capsules, which also help with smooth movement [48]. The articulation between the humerus and the ulna plays a key role in stabilizing the elbow at rest, but stability in dynamic movements requires coordinated muscle activation [48], [51]. Medially, the ulnar collateral ligament links the humerus to the ulna and acts as a brace against outward rotation of the elbow (i.e. valgus rotation). On the lateral side, the lateral ligament complex prevents the elbow from collapsing inward under varus stress. The entire joint is surrounded by a flexible joint capsule that adds support, especially during rapid movements and impacts [51]. Tendons, which connect muscle to bone, transmit forces generated by muscles but also contribute to joint stability. The biceps tendon is positioned to increase the range of motion, while the triceps tendon is essential to elbow extension [48]. The triceps itself is made of three heads: long, lateral, and medial, which all meet at the olecranon process of the ulna[45]. The efficient communication between these muscles and the brain is done through the brachial plexus and its network of nerves [52], [53]. Oxygenated blood and nutrients supporting muscle metabolism during high and low intensity exercise are transported to the region by the brachial artery[54].

2.1.2. Muscular Contributors to Elbow Flexion and Extension

The main drivers in elbow joint movement are the muscles. Though their primary function is to generate power, they also function as stabilizers during rapid or dynamic arm movements[48]. The brachialis is the primary and most powerful contributor to elbow flexion and is able to produce consistent force at all forearm positions. This makes it a good indicator of overall strength in flexion [55], [56]. The brachioradialis becomes more active when the forearm is pronated or neutral, and during rapid, forceful movements [45], [57]. The biceps brachii has moment arms that vary throughout the movement, but it functions primarily as a supinator [58].

The triceps brachii, the primary extensor of the elbow, can generate the large forces required for pushing tasks. It can also counterbalance the flexion forces produced by the flexors[48]. The anconeus is a small muscle that stabilizes the lateral aspect of the elbow during rapid extension. It stabilizes the elbow joint and helps in fine-tuning movement patterns [48], [59]. The coordinated activation of all these muscles is required for smooth, controlled, and efficient elbow motion. Neural recruitment, feedback, and activation is necessary to generate force, regulate joint angles, control speed, and protect the joint [48], [51], [59], [60].

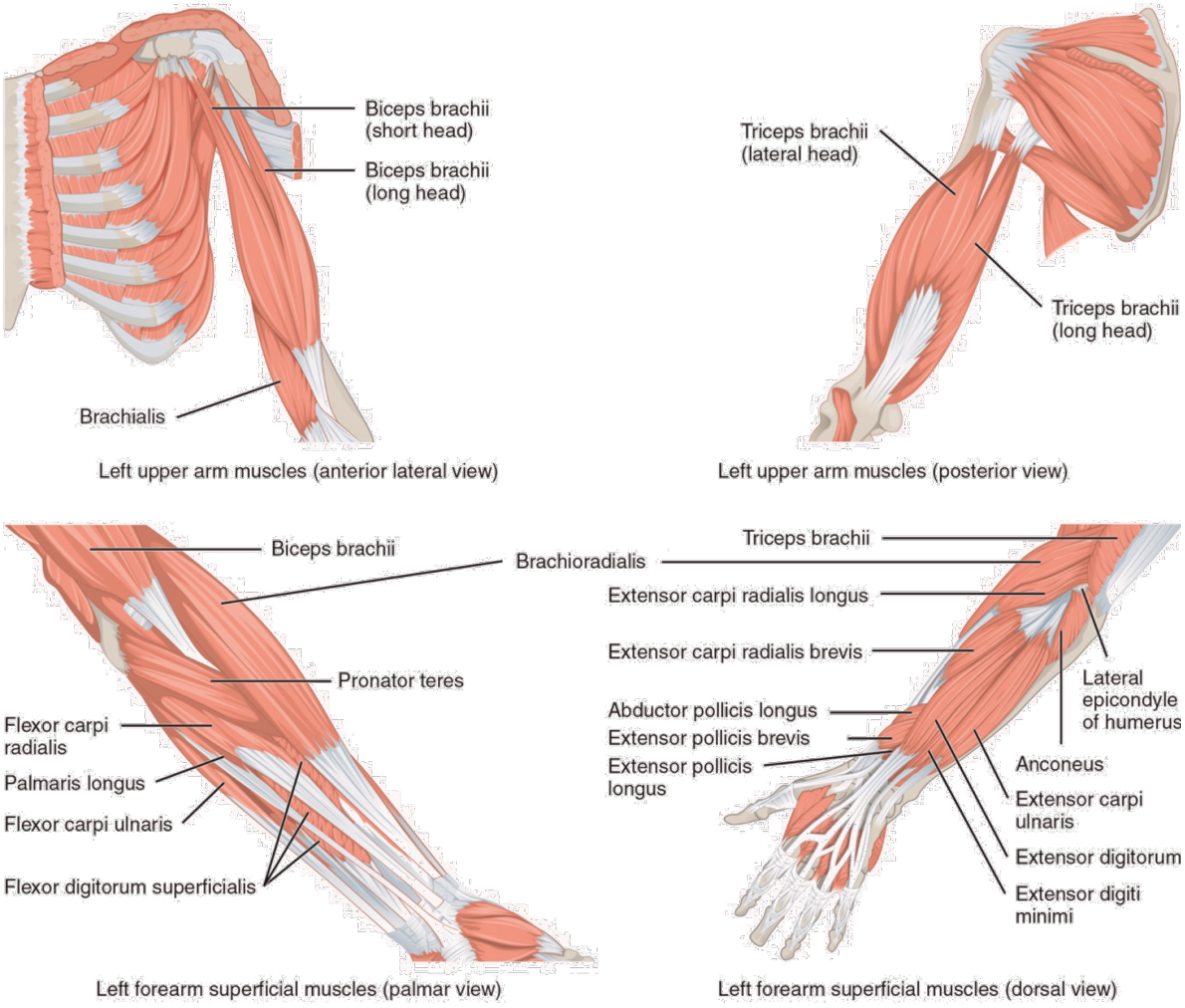

Figure 2. Primary muscles involved in elbow flexion and extension [45].

2.1.3. Mechanisms of Muscle Contraction

Muscles produce static and dynamic outputs by generating movement with three main types of contraction: isometric, isokinetic, and isotonic[61], [37]. Isometric contractions occur when a muscle produces force without changing in length. These types of contraction are essential to posture and joint stabilization. Isometric testing's simplicity, ease of administration, and reproducibility make it a popular method to assess strength [61], [33]. Isotonic contractions occur when the muscle changes length against a constant load. Isotonic contractions can be concentric when the muscle shortens as it produces force, or eccentric when the muscle lengthens or stretches. For example, lifting then lowering a weight in a controlled manner represents a cycle with a concentric and eccentric contraction, respectively [61], [62].

Isotonic contractions are more representative of everyday activities because velocity is unconstrained while the load is constant. The underlying mechanism can be explained by the sliding filament theory of muscle, where actin and myosin filaments interact by sliding past each other as they form cross-bridges. With increased velocity, the time available for cross-bridging is reduced, and less force can be produced. This is consistent with experimental results that show that the maximum power is typically observed at intermediate velocities, and explained by the force-velocity curve, which illustrates the inverse relationship between the two variables during muscle contraction[63], [64], [65].

Isokinetic contractions occur when angular velocity is constrained and constant. This form of contraction typically occurs when specialized equipment is used and produces continuous torque plots. Isokinetic testing gives insight into peak torque and muscular endurance but fails to represent the variable speeds that occur in everyday activities[31], [66].

The rate of force development (RFD) is the slope of the force curve at the start of muscle contraction. It is an important parameter in characterizing the dynamic performance of a muscle. It depends on motor unit recruitment and the contractile properties of the individual muscles. Improvement in RFD correlates with better performance in athletic movements and in daily activities that require rapid force generation such as fall prevention[67], [68], [69].

2.1.4. Biomechanical Implications for Functional Performance

Each aspect of functional performance depends on the relationship between multiple biomechanical factors. Maximum isometric torque, for example, is achieved at a joint angle of approximately 90° because the moment arms of the biceps brachii and brachialis are optimal near that position [70], [71]. Moment arms, muscle lengths, joint angles, and muscle fiber types are all factors affecting performance [64]. For isotonic contractions, high forces can be generated at lower angular velocities, but power is limited by the low speed. At higher speeds, the capacity to generate force is reduced. As such, the force-velocity relationship is hyperbolic. The highest power output is obtained where the force and speed are balanced.[63], [72]

Efficient force transmission is facilitated by adequate joint stability [48]. Muscle co-contractions provide this stability, with passive support from ligaments and joint capsules. This prevents misalignment, excessive loading, and other possible mechanisms of injury[73], [74].

2.2. Strength and Power Measurement in Biomechanics

As reviewed in[22], [75], clinicians and trainers use various forms of muscle strength and power assessment. The accuracy of these assessments is essential to clinical diagnostics and athletic performance evaluation. Quantifying, standardizing, and understanding these parameters helps diagnose neuromuscular impairments, track rehabilitation progress and customize training protocols. Each measurement technique has its advantages and limitations.

2.2.1. Assessment Techniques

Assessment methods range from qualitative tests to advanced laboratory instrumentation. Manual Muscle Testing (MMT) is one of the most widely used initial assessment methods. The technique involves the clinician resisting a patient's contraction and grading it on a standardized scale, typically from 0 (no strength) to 5 (full strength) [22], [76], [77]. MMT is limited by its subjectivity and reliance on the clinician's strength [22], [76], [77]. Inter-rater reliability is limited, and the applied resistance is not standardized. As a result, scores are not directly comparable across clinicians [78], [79]. MMT's coarse scale, despite its +/- modifiers, introduces step sizes that may not capture small and clinically meaningful improvements[22], [78], [80]. For example, a stronger patient who scores 5, will still score 5 if they improve.

Figure 3. Elbow flexion strength assessment using MMT(left) [81] and HHD (right) [82].

Hand-held dynamometers (HHDs) provide a relatively inexpensive, objective measure of isometric force or torque [22], [83]. Despite the device itself being able to accurately sense forces, HHD results can be influenced by the tester's ability to stabilize the device and match the patient's force. Like MMT, HHDs depend on the rater's strength and their ability to stabilize their arm and the patient's limb [34], [84]. Consequently, greater error

can occur with HHD when the patient can output high force or overpower the clinician[34].

Isometric dynamometry is often used to obtain the maximum voluntary contraction, which is used as a measure of baseline strength [85]. This form of measurement is highly accurate and repeatable, but it fails to capture the dynamic properties of muscle contraction[86].

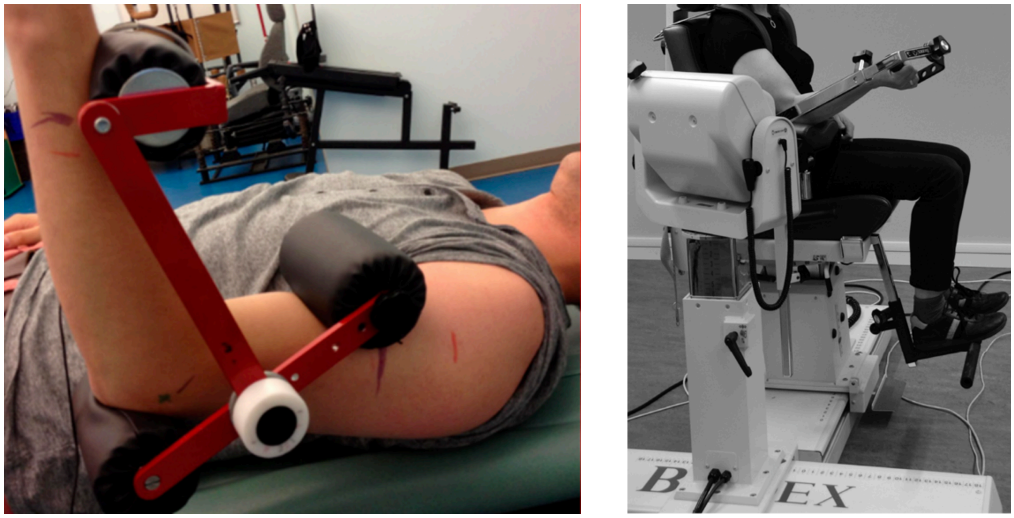

Figure 4. Fixed isometric (left) [87] and isokinetic dynamometry (right)[88].

With Isokinetic dynamometry, continuous torque measurement across a motion for multiple trials at varying speeds allows researchers and clinicians to obtain torque-velocity curves[89] and evaluate muscular endurance[90]. Isokinetic dynamometers artificially constrain movements to a constant velocity, which does not accurately represent the variable speeds that occur during daily movements [85], [91].

2.2.2. The Case for Isotonic Dynamometry

Isotonic testing simulates real-world conditions[31] by imposing a constant load while the joint moves[92]. Assessing only isometric and isokinetic qualities may overlook clinically relevant information available from isotonic power measures [31]. The development of a convenient and easy to use isotonic dynamometer would allow a more comprehensive understanding of muscle performance, and more research data on this under-used power measurement.

Velocity data collected under constant load allows calculation of rate of force development (RFD) [39], an established predictor of balance, fall risk and athletic performance[69]. Deficits in isotonic power can be detected before changes in isometric strength, supporting its use for early diagnosis[21], [23], [25], [68]. A portable

dynamometer capable of static and dynamic assessments could provide torque-velocity profiles, rate of force development, isometric torque and isotonic power in a single session[39], [93], and bridge the gap between bulky laboratory equipment and the portability required in clinical practice[36], [94].

In summary, while isometric tests are common and well-documented, they only give an estimate of the maximum force produced by a muscle group. They do not give a full picture of a patient's muscle performance. Isokinetic tests can provide important information regarding muscle fatigue and endurance, and isotonic tests can give torque-velocity data in a setup that better simulates daily activities. A combination of all three approaches to quantifying muscle function can give more insight to the clinician into the condition of their patient.

2.3. Existing Dynamometers and Their Limitations

Existing dynamometers, although repeatable and reliable, have several limitations that need to be addressed. This section reviews some of the dynamometers available on the market and identifies key areas where improvements are needed.

2.3.1. Overview of Current Devices

In this thesis, measurement accuracy refers to how close a measurement is to the true (reference) value, while precision describes how close repeated measurements are to each other. In practice, repeatability means precision when the same operator repeats the same procedure with the same equipment and environment. Reproducibility is precision when the operator, instrument, location or other environmental factors have changed [95]. Reliability, in the context of rehabilitation measurement, describes how consistently a test gives the same result when the same person uses the same protocol. Intra-rater reliability is when the same rater measure the same person multiple times, while inter-rater reliability is when multiple raters measure the same person with the same protocol/device. Test-retest reliability refers to obtaining roughly the same result when the same person is tested with the same protocol at different times (either later in the day, or on a different day). [96].

Dynamometers fit into distinct categories depending on the metric they measure and how they operate. Handheld Dynamometers (HHDs) such as the MicroFET 2 (Hoggan Scientific, Salt Lake City, UT, USA) are used to measure isometric strength[97]. They require the tester to hold the device against the patient's limb while they generate force. A valid test can greatly depend on the examiner since they need to stabilize the patient and resist their motion. If the subject is stronger, the tester will be overpowered or fail to stabilize the device, causing variability in the results[33], [34], [98].

To eliminate some of that variability, fixed-frame isometric systems were developed. They secure the patient's limb onto the device, while it measures isometric strength [87](typically with a load cell). Though these devices are accessible to clinics, they only serve a single function. Multi-purpose systems tend to be large, expensive, and impractical. The lack of portability is an important limitation when it comes to clinical adoption of new devices [36], [97].

Isokinetic dynamometers, such as the Biodex (Biodex Medical Systems, Shirley, NY, USA), are often used for detailed muscle performance evaluations. They can provide continuous reporting of torque throughout a full range of motion at a constant velocity. The Biodex System 4's documentation lists concentric speeds of up to 500deg/s and torques of up to 680 N·m, with a torque accuracy of ±1% of full scale and a 16-bit analog resolution[92]. The System 3's torque standard error is measured at 0.33 N·m [99]. This form of power measurement is well documented in literature, but these devices require extensive training, take a large footprint, and need expensive setup and calibration. The Biodex System 4 Pro, for example, measures 132 x 165 x 152 cm. It requires an additional data station and accessory cart. The total floor space occupied by the system is 6 m^2 and has a total weight of 612 kg [100]. These devices are therefore not accessible outside of specialized facilities or research laboratories[75], [101].

Less technologically complex dynamometers are also used in research to simulate real-world dynamic loading and provide measures of isotonic power. These dynamometers use mechanisms like weight stacks or pneumatics as the source of a near-constant external load. These devices are often poorly standardized, have limited repeatability, or suffer from an inconsistent load control due to their inability to maintain a constant resistance across varying movement velocities[31], [39], [102]. Purely mechanical systems such as weight stacks and pneumatic devices lack standardized, load-invariant resistance profiles and do not provide continuous torque across the range of motion [39], [103]. The variety of isotonic dynamometer designs in use by laboratories and clinics, lead to significant variability in measurement approaches between studies[37]. The lack of standard protocols makes it difficult to compare results. This is in contrast to isokinetic dynamometers, which have established and validated protocols [37]. Finally, depending on the technology used in isotonic dynamometers, velocity related effects can cause changes in the load experienced by the user during movement[102].

2.3.2. Experimental and Functional Approaches to Isotonic Dynamometry

There have been many attempts at achieving constant or quasi-constant torque for dynamometry. Each approach has its strength and limitations. These include but are not limited to passive mechanical resistance, passive electromagnetic absorbers, field-controlled frictional or viscoplastic brakes, and active programmable resistance.

Passive mechanical constant resistance systems use passive elements, usually constant-force springs, constant-torque springs or cams/spools to approximate a constant output force or torque over a specific range[104], [105], [106], [107], [108]. Their main strength for isotonic dynamometry is that they can be compact, low-cost and stable. They are, however, limited by the range where the resistance is constant. The limitation can be either a specific angle/deflection range, or a direction of motion. Practical performance depends on friction/hysteresis and geometry. Changing the load experienced by a subject would require hardware changes or manual reconfiguration[105], [107], [108].

Passive electromagnetic absorbers include eddy-current and particle brakes. Eddy-current braking torque is produced by induced currents moving through a magnetic field. As the rotor moves, it experiences a changing magnetic flux which induces an EMF (electromotive force), driving an eddy current in the conductor and producing an opposing force that scales with speed [109], [110]. Constant torque can be achieved by tracking the torque and adjusting the excitation current so the measured torque and desired torque stay the same. While this approach is effective, the system generates very little torque at rest since it depends on rotation, and some implementations become difficult to control at lower speeds[111]. Particle brake torque is produced by magnetizing ferromagnetic particles in a gap, so they produce shear in the particle medium. Constant torque can be achieved by tracking the torque and adjusting the applied field/current to increase or decrease shear and obtain the desired output torque [112]. This approach is viable but is subject to hysteresis effects and requires calibration and characterization to maintain consistent resisting torque under dynamic use. Both of these methods are passive, meaning they cannot actively drive, assist, or overcome the limb [112], [113].

Active programmable resistance via pneumatics or motor-driven torque control can produce a specific force or torque profile. In Henderson's implementation, a pneumatic cylinder with pressure sensors and proportional valves is used to estimate actuator force with a pressure-feedback controller. The authors note that their system is accurate for slow movement and encounters control limitations at higher excitation frequencies due to fluid dynamics and compressibility[114]. Motor driven solutions use closed-loop control to emulate a commanded load torque and reject disturbances [115], [116], [117], [118], [119]. For isotonic dynamometry, the main strength of motor-driven torque control is that constant torque can be a direct software setpoint over a wide velocity range (including near zero)[115], while preserving the functional capability to assist or overpower if needed in the future. Complexity is the main disadvantage of these methods. They require sensors, calibration/verification, and advanced motor controllers to achieve stable, accurate torque[115], [116], [117], [118].

2.3.3. Reliability Considerations

Reported reliability varies depending on the tool and operating modes. For MMT, since the method uses an ordinal scale, agreement is summarized with a kappa statistic that accounts for chance agreement. A kappa value of 0 indicates the agreement is no better than chance, and 1 means there's perfect agreement [76], [78]. Kappa values around 0.8 are considered substantial agreement [80]. One major weakness of MMT is when the subject has near-normal strength, where distinguishing 4+ from 5 becomes difficult, and kappa values can be in the 0.02-0.13 range [78]. For elbow flexion in people post-stroke, Gregson et al. reported a quadratically weighted kappa, of 0.85-0.87 (inter-rater) and 0.81-0.96 (intra-rater). For elbow extension, they reported 0.92-0.94 (inter-rater) and 0.86-0.93 (intra-rater)[120]. For HHD, intraclass correlation coefficients (ICC) are commonly used. ICC is a reliability metric for continuous measurements, and represents how similar repeated measurements are relative to between-subject variability [96]. Brookshaw et al. reported intra-rater ICC = 0.969 in elbow flexion, and 0.975 in elbow extension. Inter-session ICC in flexion was 0.854, and 0.909 in extension. Inter-rater reproducibility for elbow extension was much lower with ICC = 0.575 [87]. Regarding the full-scale dynamometers like the Biodex System 3 Pro, test-retest reliability ICC at 60 °/s (1.05 rad/s) was 0.95 for elbow flexion, and 0.92 for elbow extension, with a standard error of measurement of 2.6-2.9 N·m, and a smallest real difference (SRD) of 7.1-8.0 N·m [88].

Other factors affecting reliability include patient positioning, sensor sensitivity, calibration differences, operator training, and inter-operator variability that can complicate rehabilitation assessment and reduce reliability[22], [34]. Rigorous calibration and standardization are essential for reliable measurements[121].

2.3.4. The Rationale, Feasibility and Benefits of a Portable Isotonic Dynamometer

The limitations of existing devices point to the need for a tool that can assess isotonic power with higher precision while remaining portable. A device that can achieve both isometric torque and isotonic power would allow clinicians to obtain a more comprehensive functional assessment without the drawbacks of expensive and impractical laboratory-grade equipment. Advances in brushless DC motor technology, and motor control strategies, allow devices to have high torque-to-inertia ratios, low friction, low torque ripple and can provide consistent torque control during rapid velocity changes[122], [123]. Off-the-shelf FOC-capable controllers for BLDC motors have made it possible to make such high-performance devices with smaller sizes[122].

A device capable of measuring both static (isometric torque) and dynamic (isotonic power) muscle performance metrics gives a more complete understanding of upper

limb function. It allows the clinician to measure velocity-torque profiles, rate of force development, and static force generated at various joint angles. These parameters can be used to quantify baseline status, the response to interventions over time, and give insight into neuromuscular physiology/pathophysiology. The identification of early neuromuscular deficits, the selection of appropriate therapies and the design of targeted rehabilitation protocols can also be affected by such outcome measures [42]. A device that enforces a standard position, has real-time control, and includes digital signal processing can make the results nearly independent of the operator, improving reliability and repeatability for clinical research, diagnostics, and rehabilitation. In addition, a device that addresses this need could make the detection of subtle changes in patient progress much easier to interpret and enable continuity of care.

2.4. Field-Oriented Control

Motor control strategies all have their advantages and limitations. Field-oriented control (FOC) is an important motor control technology that is quickly becoming more popular in applications that need precise torque control. Unlike traditional methods, FOC independently adjusts the torque and the flux, making it ideal for applications that require constant torque during rapid velocity changes[124], [125], as is the case for isotonic dynamometry. This section details the principles of FOC and how the technology can benefit the proposed system.

2.4.1. Fundamentals of Field-Oriented Control

Field-oriented control, sometimes called Vector Control, is used in BLDC motors to mathematically transform the three-phase motor currents into two orthogonal components (vectors)[126]. The three-phase currents are transformed into a rotating d-q reference frame aligned with the rotor's magnetic field[124], [126]. This allows the motor to have a smooth torque output, high efficiency, precise control and negligible torque ripple[125]. In this frame (the rotating FOC rotor-flux d-q coordinates), the d-axis current i_d sets the flux, and the q-axis current i_q generates torque [124], [126]. The independent control of each of these two currents is what gives FOC precise torque control regardless of the motor's behaviour.

For surface-mounted BLDC motors, the electromagnetic torque is given by:

$$T = \frac{3}{2} p \psi_{PM} i_q \text{ [127]} \tag{2.1}$$

Where T is the torque in N·m, p is the number of pole pairs (dimensionless), $\psi_{PM}$is the permanent-magnet flux linkage in Wb, and i_q is the q-axis current in A (all in the rotating d-q frame)[124], [126].The torque equation shows that the q-axis current is the

only contributor to torque. The controller therefore minimizes i_d by setting it to 0 to avoid unnecessary flux changes and regulates i_q to control the torque[126].

For the backdriven dynamometer application, maintaining a constant resisting torque means keeping the torque-producing current (i_q) at its setpoint while the inverter supplies enough voltage on the torque axis to overcome the motor's own generated voltage (back-EMF), which increases with speed [124]. Because the inverter can only generate a limited phase voltage, set by the DC-bus, once the required voltage exceeds that limit, the PWM saturates, and the current controller cannot maintain i_q. The resisting torque drops as a result[124]. Separately, when backdriven, power flows into the DC link and raises the bus voltage. The controller's internal protections cause it to reduce its outputs (PWM and current), so it once again stops maintaining i_q (and therefore torque)[128], [129].

A brake-chopper is a safeguard that momentarily switches a resistor onto the bus to provide a sink that dissipates the excess energy, maintaining the DC-bus voltage below thresholds, allowing the PWM operation to function normally so the FOC current loop can keep tracking i_q, and constant resisting torque can be maintained up to the true limits of the drive [128], [129]. The brake-chopper is activated when the voltage exceeds a setpoint, and is deactivated when voltages return to normal [122].

Modern FOC controllers are small, relatively inexpensive, and can adjust to disturbances within microseconds [126]. This makes them perfect candidates for the isotonic dynamometry application, since the motor and controller will have to react to an external driving torque (from the subject) that will be rapidly varying.

2.4.2. Advantages Over Alternative Motor Control Methods

Sinusoidal and trapezoidal control, the traditional BLDC motor control strategies, have limitations that make them unsuitable for isotonic dynamometry. Sinusoidal controllers apply a smoothly varying sinusoidal voltage to the motor windings. Their inability to control torque and flux independently results in speed-dependent torque characteristics[124]. For a dynamometer, this means the resisting torque would not stay constant if the patient's movement speed varied, which would compromise the validity of isotonic power measurements. Trapezoidal control is the easiest to implement and requires the least computational resources, but it produces the greatest amount of torque ripple during commutation[130]. This ripple manifests as noise in the measurements. It can also cause discomfort and a choppy feel for the patient using the device [131]. Both control strategies have back-EMF profiles that introduce significant measurement and control errors in backdriven applications such as dynamometry. This back-EMF causes speed-dependent regenerative torque, causing the net torque to deviate from the setpoint as movement speed changes [124], [125]. FOC controllers, in

contrast, treat back-EMF as a disturbance and cancel it in real-time [132] as long as the inverter isn't saturated and the DC bus stays within safe limits[124], [128].

FOC control of BLDC motors (when compared to six-step commutation) significantly reduces torque ripple even during rapid velocity changes [125]. The accuracy and precision of these controllers is what allows them to provide constant resisting torque and accurate measurements with a traditional BLDC motor. The current control loop of some off-the shelf drivers, such as the TMCM-1636, is in the kHz range [122]. This enables sub-millisecond torque control during rapid speed changes, as is experienced during isotonic tests.

2.4.3. Implementation Considerations for Dynamometry

Advances in modern microcontrollers, signal processing, and hardware miniaturization have made the implementation of FOC much more cost effective and viable for prototyping and device development. ARM-based microcontrollers can now complete the complex transforms required for FOC in real-time while keeping costs low [125]. They can be purchased at any major electronics distributor. Specialized FOC chips can be purchased with all sensor interfaces, power electronics, and necessary algorithms in a plug and play package [122], significantly reducing development time and project complexity.

Many inner-rotor BLDC motors already have a lower mechanical inertia compared to brushed motors or outer rotor designs, which is important in systems that need to respond quickly to changes external forces without measurement error [133]. Low inertia is particularly important in dynamometry because it minimizes effort required for weaker patients to initiate movement. At the same time, a high inertia could mask subtle but clinically meaningful changes in velocity or power output for stronger patients [134], [135]. The integration of FOC further increases the responsiveness of the system [122]. The combination of low inertia and precise torque control allows the dynamometer to provide a constant resistance across the full range of human movement speeds, from very slow and weak patients to the rapid and explosive movements generated by athletes.

In addition, FOC systems can operate in many modes. For isometric testing, the system can maintain zero velocity while measuring applied torque. It can be supplemented with an external brake and load cell. For isotonic testing, the controller can be switched to constant torque mode while measuring the velocity. The flexibility of modern FOC controllers and the ability to switch their operation mode with software reduces the need for complex switching mechanisms and allows the end user to operate the system in isometric, isokinetic and isotonic modes [123].

2.4.4. Clinical Relevance and Performance Benefits

The benefits of FOC translate directly to dynamometry. The precise torque control, the speed at which it can respond to changes, and the separate control of torque and flux eliminate the velocity-dependent torque variations that affect other isotonic dynamometer designs. This ensures that regardless of the speed at which the patient is moving, the resistance remains constant. This should translate to accurate measurements, and increased reliability.

The rapid dynamic response of FOC systems enables the dynamometer to adapt quasi-instantaneously to changes in user effort, providing a natural feel and preventing the jerky or unstable resistance that can occur with slower control systems[131]. The smooth operation can be important for the adoption of the technology since it can reassure patients who are nervous around medical devices, or those who have limited strength[136].

3. Mechanical Design

3.1. Design Requirements

This chapter describes the design requirements for an upper-limb dynamometer capable of measuring isometric strength and isotonic power. These requirements are informed by the previous prototype, feedback from clinical partners, and evidence from academic literature to ensure the device is portable, usable, repeatable, and cost-effective.

To meet these needs, the proposed dynamometer combines isometric strength and isotonic power measurement in a portable and cost-effective design. Portability significantly increases assessment frequency in clinics, leading to more data, better monitoring, and improved outcomes[137], [138]. Therefore, ease of use, setup, and teardown are essential design requirements.

3.1.1. Functional Requirements

For a comprehensive assessment of the upper limb, both static and dynamic muscle performance metrics need to be captured. The combined assessment gives researchers and clinicians more insight into neuromuscular function compared to individual and isolated measurements[23], [67], [86], [139]. This supports decisions on the type of therapeutic approach, the treatment intensity, and the progression criteria [42].

3.1.1.1. Measurement Capabilities

Several design challenges need to be addressed to achieve the measurement capabilities required for the full range of potential users. The device needs to be sufficiently rigid to prevent deformation during isometric testing because that could introduce measurement errors [85]. Conversely, the weight of the torque arm needs to be as low as possible, so the inertia is easy to overcome by the weakest patients in isotonic power testing[134]. The arm must be able to withstand a maximum voluntary contraction (MVC) of 78 N·m, which represents the peak elbow flexion in healthy men [89]. The dynamometer must provide resisting torque up to 20 N·m so that it can assess up to 25% of maximum voluntary contraction across the full range of potential users[39], [140], from those with neuromuscular impairments to high performance athletes. 20% MVC was identified as a load adequate to obtain maximal shortening velocity and velocity-dependent power [140], making 25% a reasonable target for initial isotonic dynamometry prototyping. The minimum recommended velocity sampling rate for rate of force development studies is 500Hz, with most studies suggesting a minimum of 1000Hz [68], [141], [142].

3.1.1.2. Testing Configurations

The dynamometer needs to be designed in a way that allows the participant to move in a full range of motion for the elbow joint. A variety of upper arm positions need to be tested, so the ability to adjust the initial position is essential. The device needs to test elbow flexion and extension without any hardware changes between tests, to give clinicians the ability to easily adapt the device to their testing protocols. To ensure standard positioning between sessions and operators, the dynamometer must stabilize the patient's limb, isolate the tested muscle groups, only operate within safe bounds, and ensure that the user can only move in the intended plane.

3.1.2. Physical Design Requirements

3.1.2.1. Portability

One of the primary reasons why state-of-the-art measurement tools are not used as frequently in clinical settings is the lack of portability [137], [143]. Though accuracy and repeatability are essential, a device that is too impractical will rarely be used if other options (even if less accurate) are available [98]. Recent studies on medical devices had clinicians report a more positive experience with portable devices when compared to stationary ones [144], [145]. A device can be considered portable if a single person can carry it, deploy it, and pack it up on their own.

As such, the total weight should stay near 15-20kg to allow easy transportation. Occupational health guidelines indicate that professionals can safely carry 23kg [146, pp.

762–763] without risk of musculoskeletal injury during routine tasks [147], justifying the maximum weight target. The device should need minimal disassembly for transportation or storage, to ensure that its deployment is trivial. In addition to weight constraints, portability requires manageable dimensions. As such, the device should stay under 60 x 40 x 30 cm when packaged[148], allowing it to be manipulated by a single person[146], [149].

3.1.2.2. Mounting System

To remove barriers to adoption, the mounting system for the device needs to be secure enough to allow reliable measurements. It also needs to be compatible with the furniture or surfaces available in most clinics, so that purchasing additional furniture or fixtures is not required. The ease of setup and teardown would allow a clinician to use the device in multiple clinics or store it away between uses. An adjustable, secure, and non-marring clamping mechanism would prevent damage to existing furniture and allow the clinician to mount the device to any available surface. The clamp, if easy to engage or release, would improve the device's portability and make it more practical in busy clinical environments. A quick-mounting device that can be adjusted to fit any potential mounting surface will ensure that the dynamometer can be deployed rapidly, without special tools or training.

3.1.2.3. Mechanical Design

To capture an accurate profile of muscle performance, measurement tools need to capture data over a wide angular range. The mechanical linkage between the rotating elements needs to ensure that angular motion is smooth and repeatable. The design tolerances need to consider the need for repeatability in measurement.

To offer enough adjustment and meet the requirements for isotonic dynamometry in elbow flexion and extension, the dynamometer needs two rotational elements, each allowing 360 degrees of rotation. This will give the operator the ability to adjust the upper arm and forearm mounts separately. The device needs to allow the examiner to lock the position of the upper arm while allowing the forearm to move freely during dynamic tests. This will provide the versatility needed for isometric strength tests at any joint angle, and isotonic power tests with any initial position. The system must stay fixed during isometric tests, without slip, while still giving unrestricted motion during dynamic tests. This can be achieved with a mechanical brake on the freely rotating arm, that can function as a safety stop as well. The transition between the two testing modes needs to be seamless, requiring little to no adjustment, so the clinician and user can follow a test protocol without interruption. Finally, a modular design can allow adaptability for future applications, where the arm can be changed to measure different joints in or beyond the upper limb.

3.1.2.4. Materials and Construction

Durability, weight, and mechanical performance are the main considerations when selecting components and raw materials. Patient comfort and clinical practicality are important to ensure clinical adoption[136], [150]. The structure needs to be strong and rigid enough to allow good measurement accuracy. Load-bearing components need to handle at least 120% of the maximum expected user strength to account for a factor of safety and prevent failure when stronger patients are using the device. A balance between strength, rigidity, weight and portability needs to be found, and the device needs to accommodate anyone from low strength patients to high-performing athletes without sacrificing measurement accuracy.

The surfaces in contact with patients require materials suitable for clinical environments. The likelihood of causing skin irritation, and the ability to clean and sanitize between users, are both important factors in material selection. As the FDA (U.S Food and Drug Administration) highlight in their human factors, usability engineering and medical device reports, material selection and surface treatments should prioritize comfort and cleanability for all patient-contacting components[151], [152], [153].

3.1.3. Technical Requirements

3.1.3.1. Sensor Integration

For both diagnostic and research purposes, data acquisition needs special consideration. To capture the rapid force fluctuations in muscle contraction, a high sampling rate is necessary. A target of 1000Hz should be the goal for velocity measurements during isotonic torque tests. The selected sensors must be accurate and precise enough to allow reliable measurement of isometric torque and isotonic power. Load cells are often used for isometric strength measurements[154], typically made with strain gauges [155]. When coupled with high-resolution analog-to-digital converters (ADCs) and fast microcontrollers, they can be extremely accurate. The ADS1256, for example, can provide a maximum sampling frequency of 30 kSPS (samples per second) [156]. In practice, this allows oversampling followed by filtering to reduce noise while still achieving the targeted 1kHz for torque-velocity measurements. For dynamic tests, the motor itself requires an encoder to obtain accurate velocity measurements, and support field-oriented control.

Sensor calibration should follow a simple, repeatable, and well-documented process to allow the user to verify sensor readings with known values and build confidence in the results.

3.1.3.2. Data Acquisition

To maximize versatility, two operating modes should be considered for the device. In standalone mode, the device should be completely independent, with its own internal signal conditioning, amplification, filtering, and with enough internal memory for a day of data-collection. This reduces barriers to field use and increases portability.

Most laboratories already have workflows for sensor data acquisition. The second operating mode should aim to integrate the device within those workflows. Analog outputs on the dynamometer will enable interfacing with commercial data-acquisition systems (DAQs.) They should transmit conditioned voltages proportional to torque and angular velocity to ensure compatibility with standard lab hardware.

The greatest advantage of the dual-mode approach is its ability to reduce the training requirements by integrating directly into existing workflows, without sacrificing portability when used in situations where DAQs are unavailable.

3.1.3.3. User Interface Requirements

The user interface (UI) must be easy to use with little technical training. It should clearly display torque and velocity values in real-time, because real-time visual feedback was shown to increase maximum voluntary contraction[157] and average peak torque during isokinetic exercise[158]. It must also require minimal steps between test positions, automatic storage of test results, and clear status indicators. Recent studies demonstrated that the user experience is a significant factor affecting the adoption of new devices or technologies in clinical settings [136], [159], and that poor interface design can cause errors unrelated to device malfunction[160]. The UI should allow the device to function in stand-alone mode, so that it can be used in situations where a full computer-based setup is unavailable.

3.1.3.4. Measurement Parameters

As stated in section 3.1.3.2, the device must record and report raw-time-synched torque and angular-velocity data from the motor controller's digital outputs, and from the onboard digital to analog converter (DAC)'s analog outputs. This allows each laboratory to calculate the metrics they need, with their own protocols and processing pipelines. At minimum, the device will report:

1. Maximum voluntary contraction (MVC) as Peak Isometric Torque (N·m)
2. Rate of force development (RFD) (N·m/s)
3. Time to peak torque (s)
4. Torque-Velocity profile from isotonic trials (deg/s)

These parameters were selected for their cross-study comparability, and their widespread use. MVC is a standard strength metric, and is used as a reference for setting resistance torque in isotonic tests (as %MVC) [22], [39], [66]. RFD can be computed multiple ways, though the time to peak torque, the average slope from contraction onset to 200ms, and the peak slope from that same window can all be computed directly from torque time series[31], [68], [142]. Finally, torque-velocity profiles can be obtained directly from the same raw digital logs or analog outputs [31], [66], [72], [85], and power can be calculated from torque and angular velocity.

3.2. Implementation Considerations

3.2.1. Component Selection and Cost

The balance between cost and performance is the primary consideration during component selection. The device is intended to be used in a variety of healthcare settings. Some will be remote clinics, or clinics with limited resources. Keeping the final cost of the device as low as possible is therefore essential.

Modern, low-cost, ARM-based microcontrollers have enough power to control the motor and complete the calculations needed for FOC[122], [123], [126]. Measurement quality remains one of the most important aspects of the device, so the stability and reliability of each component should be evaluated.

The use of off-the-shelf components in a modular design approach reduces development costs by enabling the use of existing libraries, simplifying the implementation, and reducing the troubleshooting. These components are all independently tested, standardized, and validated. Long term, this ensures that the device is easy to repair, and that components are widely available. This strategy also future-proofs the device by allowing new modules to be easily added for more functionality.

To keep the costs low, some strategic compromises will be necessary. The majority of the budget should focus on the motor, gearbox and controller components. The motor and controller's capabilities will directly determine the ability to generate and control the resisting torque, and the gearbox will have an important effect on measurement errors. These are the critical areas that will ensure the device has its best possible performance. The enclosure can then be designed around these components to sustain the maximum loads that will be experienced, allow a variety of mounting positions, and appear as non-threatening as possible to patients.

3.2.2. Cost Targets

Beyond the initial component costs, the value proposition should consider maintenance and operational costs. According to Mitchell et al., if the device retains long-term value, a higher initial purchase price can be justified [161].

Handheld dynamometers have a price range between $200 for the most basic devices [162], and $2500 for the more advanced ones [163]. They can measure force or torque but are unable to measure power. Isokinetic systems, while feature-rich, sacrifice portability to offer full features. They cost $45,000 [100] to $100,000 [164, p. 17], [165]. To bridge the gap between the portable but limited devices, and the full-featured but fixed devices, a $5,000 to $10,000 price point will position the portable dynamometer as an affordable way to obtain advanced features in smaller clinics. This price represents approximately 10-30% of the cost of gold-standard devices [164]. If the measurement precision and repeatability is achieved, this would make the device a great option for power measurements.

For long term viability, the modular design limits repair costs since a damaged component can easily be replaced, and whole-system replacement will be unlikely. Regarding the mechanical design, using design for manufacturing principles ensures that production expenses are as low as possible.

3.2.3. Maintenance Requirements

A final product that works out of the box and requires little to no maintenance is the goal. It must maintain accuracy over long periods without needing recalibration. An annual calibration protocol, with little disruption to the clinic's operation, would ensure the device's long-term reliability without limiting adoption.

Serviceability is also an important consideration in the device's design. Its modular nature permits individual component replacement and repairs without requiring a full factory return. Easily swappable modules will minimize equipment downtime. A minimum of 5 years of service life will ensure the annual cost of ownership is low, with a longer life, and increased functionality justifying a high initial investment when compared to the basic handheld dynamometers.

Maintenance procedures aimed at reducing disturbances to clinical workflows, and a design that focuses on keeping the device in service as long as possible with minimal and easy maintenance will keep the device competitive over time. Maintenance documentation, with detailed procedures, diagnostic protocols, and step-by-step repair guides can add to the value proposition.

3.2.4. Clinical Usability

The portable dynamometer must be effective at measuring torque and velocity for the largest possible patient population. To measure the weakest patients, the inertia of the motor and the gearbox will be the main limiting factors. The motor's power will affect the upper resisting torque limit that the device will achieve. More powerful motors tend to have a higher inertia, so a good balance will need to be achieved. To standardize the position, the device must provide enough support to stabilize the patient's limb, and restrict the movement to stay within the intended plane. The contact areas between the patient and the device need to have enough adjustment to fit all patients, including those with impairments, without sacrificing the stability or the standard position.

The dynamometer should be easy to operate and require very little training. To achieve this, visual guides, clear instructions, and intuitive controls are necessary. Modular designs can be confusing when they require assembly. Clear instructions help reduce errors, and a design that makes it difficult to assemble components incorrectly is ideal.

The device should also fit seamlessly into existing workflows with the option to use it stand-alone, or to include it as a part of greater ecosystem. The clamping mechanism should be adjustable for most tables, while giving the user an option to mount it securely and permanently.

Finally, the operation should require minimal changes during tests. For example, rather than changing the attachments between isometric and isotonic tests, the device should be able to run both tests sequentially. This would keep the patient in the same standard position, reduce the time needed between full protocols, and reduce the set-up time between different patients.

3.3. Performance Requirements

3.3.1.1. Precision, Accuracy, and Reliability

Due to its nature as a measurement device, precision (how closely repeated measurements agree with each other) and accuracy (how close a reported value is to the true value, or a known reference) are the most important metrics affecting the dynamometer's success in research and clinical settings. The device must be reliable over its full range of torque and velocity, with comparable accuracy to standards expected by the clinical and research communities.

Isokinetic dynamometers such as the Biodex are the current gold standard. Elbow flexion studies designed for such devices have protocols with fixed velocities ranging from 12°/s (0.21 rad/s) to 300°/s (5.24 rad/s)[166], [167], [168]. Healthy adults, when

tested for their maximum movement velocity at the elbow joint, can achieve 1140°/s (19.90 rad/s) in flexion, and 1600°/s (27.93 rad/s) in extension[169]. These should therefore be the velocity targets. Peak torques in isometric tests at a 90° joint angle can reach up to 78 N·m for elbow flexion in healthy males, and approximately 10 N·m less for elbow extension [89], [90], [170]. In isokinetic tests, peak torque at 60°/s (1.05 rad/s) can reach 67-77 N·m for healthy males [90], with lower torques at higher velocities and for healthy females. Healthy males without resistance training had an average of 49.9 ($\pm$ 8.5) N·m peak torque[90].

The device should target a torque measurement accuracy of ±1% of full scale across the entire measurement range to match the Biodex [92, p. 160]. The system's linearity when calibrated against reference weights must target an $r^2 \geq 0.99$ to ensure accuracy, calibration validity, reliability, and comparability across sessions[171]. The coefficient of variation when compared to load-cell-based isometric tests should be minimized below 5% [172], [173], [174]. Test-retest, inter-rater, and intra-rater reliability are typically quantified using the Intraclass correlation coefficient (ICC)[88], where 0.75-0.90 is considered good reliability and values above 0.90 are considered excellent[96].

The Biodex System 3 had a measured torque standard error of 0.33 N·m, which can serve as a practical benchmark for the development of the portable dynamometer[99]. In stroke survivors, the smallest real difference (SRD) in elbow flexion/extension is 7-8 N·m at 60°/s, indicating that a minimum change of 7 N·m between repeated measurements needs to be detected for it to be clinically meaningful[88]. A target resolution of less than 1 N·m would ensure quantization does not limit the ability to detect clinically meaningful changes. A recent long-term reliability study of the Biodex had a moderate to good result for test-retest reliability with intraclass correlation coefficients ranging from 0.48-0.81 at 60°/s (1.05 rad/s) (moderate to good) and 0.77-0.87 at 240°/s (4.19 rad/s) (good to excellent)[175]. For this portable dynamometer, a target of 1% torque measurement error at full scale using the best fit straight-line method should be the target.

These performance metrics will determine the device's usefulness in clinics and research labs, but its long-term viability will depend on its ability to maintain the initial calibration over time. A minimum of 6 months under normal use, with periodic field calibration using calibrated weights is the minimum acceptable goal. This will ensure that the device does not need to be sent to the manufacturer routinely and will limit the interruptions to normal clinical operations.

Long term reliability will require prolonged use of the device, under a variety of conditions. Periodic testing of the first functional prototypes will validate that the device can perform well over its lifetime. The use of high-quality strain gauges for isometric tests, and a reliable motor controller for the isotonic tests, will improve the reliability of

the dynamometer. Temperature compensation, and a sealed housing can address environmental factors like humidity and day to day fluctuations.

4. Prototype Development and Build

4.1. Drivetrain

The components that form the mechanical core of the prototype are the motor and gearbox. The output shaft of the gearbox is rigidly attached with a custom machined coupling that allows a mechanical disc brake to be attached, along with the torque arm that will be rotated by the patient. These components are all shown in Figure 5.

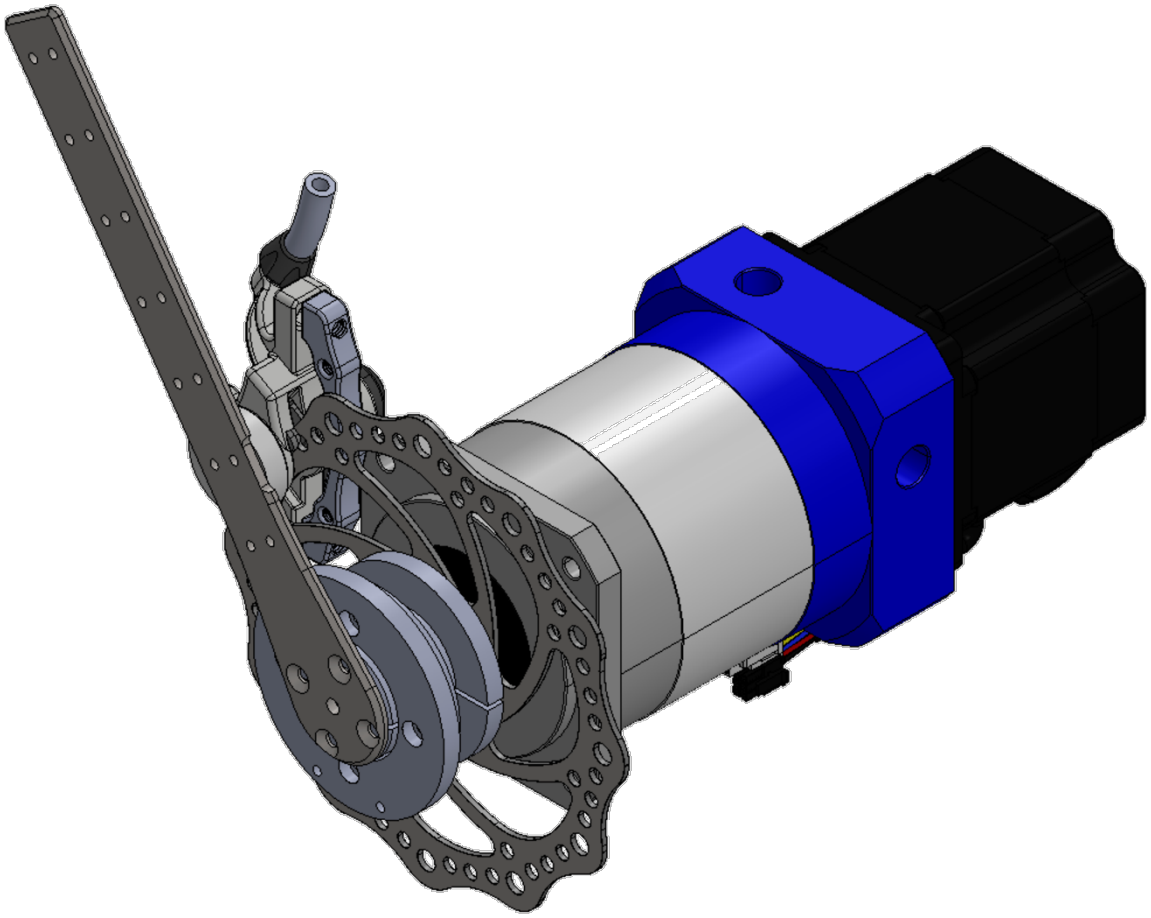

Figure 5. Drivetrain assembly rendering (SolidWorks).

4.1.1. BLDC Motor[176]

The Lin Engineering BL34E34-01D-05RO Brushless DC (BLDC) motor was chosen for its electrical and mechanical specifications, and its availability through online distributors.

Its specifications align well with the design requirements. The motor's key specifications are:

- Max Speed 4500 RPM
- Rated Torque: 0.72 $N \cdot m$
- Peak Torque: 1.44 $N \cdot m$
- Rated Current 7.49A
- Back-EMF Constant: 7.03Vrms/krpm
- Moment of Inertia: 0.000108 $kg \cdot m^2$
- Weight: 2.56 kg

Given the peak torque of 1.44 $N \cdot m$, with a 16:1 gearbox (discussed in Section 4.1.2), the system can provide a total of 23.04 $N \cdot m$. The maximum expected elbow torque is 78 $N \cdot m$[92]. meaning this motor and gearbox combination can provide up to 30% MVC for the strongest subjects when operating at its peak. The short bursts required for individual tests and the time that the motor spends below its peak should allow it to function without generating excess heat. Healthy subjects can reach 27.93 rad/s (1600 °/s) in extension (less in flexion). The motor's max speed of 4500 RPM (471 rad/s) becomes 29.5 rad/s at the output shaft of the gearbox. The motor's peak angular velocity is therefore just beyond the needs of the application. In addition, this motor's three-phase BLDC design, with integrated hall sensors and optical encoder make it compatible with a variety of controllers, including those that use FOC.

4.1.2. Planetary Gearbox[177]

The Anaheim Automation GBPH-0902-NS-016-AA341-625 is a two-stage planetary gearbox with lifetime lubrication. This gearbox achieves the desired gear ratio while keeping maintenance as low as possible. Its low backlash, though not a design constraint, is important if future applications require the dynamometer to alternate directions during a test.

- The gearbox's key specifications are:
- Ratio: 16:1
- Rated Output Torque: 1487 in-lb (168 $N \cdot m$)
- Rated Input Speed: 4000 RPM
- Backlash: $\leq$ 16 arc-min

- Efficiency: ≥ 94%
- Weight: 4.5 kg

The maximum torque on this system is expected to occur during maximum (isometric) voluntary contractions (78 $N \cdot m$)[89]. This is well below the gearbox's rated 168 $N \cdot m$, and the disc brake will be engaged during those tests. The maximum torque the gearbox will be subjected to is the 23 $N \cdot m$ the motor can resist with during dynamic tests.

4.1.3. Mechanical Disc Brake

For isometric tests, the motor's holding torque is insufficient to fully resist most healthy subjects, which is why a mechanical disc brake was incorporated in the design. The rotor is rigidly attached to the output shaft of the gearbox and the torque arm. This configuration allows the assembly to rotate indefinitely, which gives the clinician the ability to choose the angle for isometric tests. In addition, mechanical disc brakes are standard components used in bicycles. As such, they are inexpensive, widely available, and easy to repair or replace. An off-the-shelf braking mechanism, with the rotor, caliper brake lever, and brake cable also kept development costs to a minimum. The RUJOI Bike Disc Brake Kit, with aluminum calipers, 160mm rotor, and tool-free adjustment was selected for its low weight, availability, and easy tuning.

5.1.4. Torque Arm

The custom torque arm was designed to be as light as possible, so the inertia that the weaker patients needed to overcome could be minimized. The arm needed to withstand the maximum torque for isometric tests without observable bending, or plastic deformation. It was manufactured out of stainless steel. This material gave it a more polished appearance and is easy to clean. Two small notches on the torque arm gave the ability to add strain gauges to measure the torque on the arm directly, through its bending.

4.2. Enclosure and Body

4.2.1. Enclosure

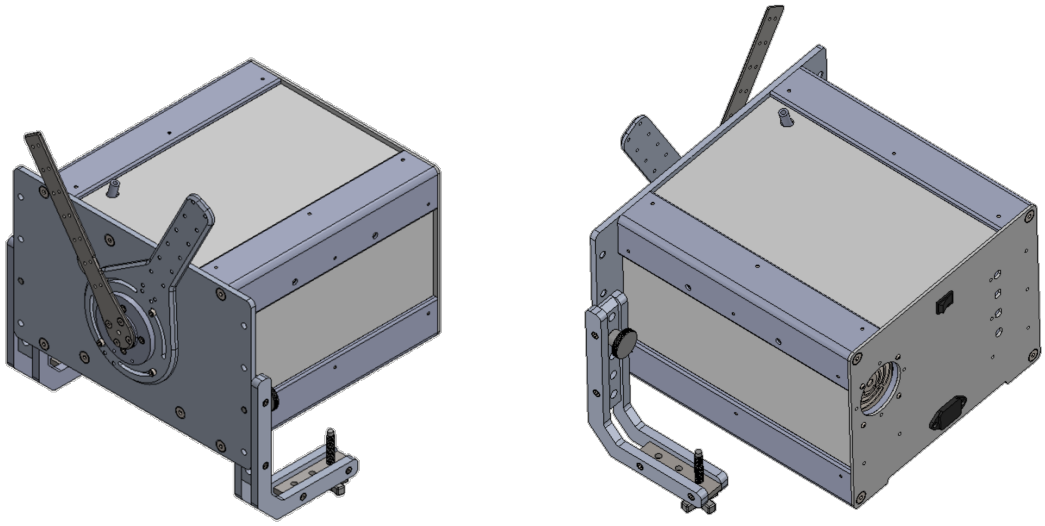

Figure 6. Portable dynamometer enclosure and mounting structure.

The outer enclosure of the dynamometer, shown in Figure 6, consists of a post and plate design for strength and rigidity without adding excessive weight. The 4 posts are made of aluminum extrusion. The white panels on the top, both sides, and back, are made of a composite material that protects the electronics while having a negligible effect on the total mass. The back panel has cut-outs for the power-supply fan, the power cord, an on-off switch, and BNC connectors.

The enclosure's outer dimensions are 31.5 x 29.5 x 20.3 cm. This is significantly more compact than the Biodex System 4 Pro (132 x 165 x 152 cm), which requires an additional clinical data station (64 x 48 x 104 cm) and an accessory cart (85 x 51 x 102 cm)[100]. The total mass of the portable dynamometer is 19.23kg, only $\approx 3\%$ of the Biodex System 4 Pro (612kg).

4.2.2. Front and Bottom Panels

The front (shown in Figure 6), and the bottom panels are both made of aluminum. While the composite material was sufficiently strong to protect the internal components, it cannot withstand the demands of the clamping mechanism (discussed in section 4.2.3). In addition, the front panel serves as the mounting point for the entire drivetrain and needs to carry the weight of the heaviest components (the motor and the gearbox). The bottom panel has rubber feet mounted to it, to keep the dynamometer from

slipping during transportation or while it is rested on a table. The bottom panel also has thru holes and threaded holes so that direct mounting is possible, if a permanent mounting solution is desired.

4.2.3. Clamps

To give the dynamometer the maximum portability and compatibility with clinics, a versatile mounting solution was needed. The clamping mechanism (Figure 6) developed for this prototype mounts to the back of the front panel, on the sides of the dynamometer. It is secured by thumb screws, allowing the operator to attach and detach the clamps without tools. Multiple positions are available for the clamps, giving the clinician options to match most table thicknesses they might encounter. The c-shape of the clamp is formed by the clamp arms, the front panel, and the bottom panel of the enclosure. The clamp arm has threaded holes and thumb screws to fine tune the clamping force and ensure the dynamometer is rigidly attached to the intended surface.

4.3. Electronics

4.3.1. Motor Controller[122], [123], [126]

The motor is driven by the Trinamic TMCM-1636 controller. The module was selected for its built-in support for FOC, its ability to handle the demands of the motor, and its high performance. The controller has a rated output of 1000W at 48V and can provide up to 60A peak current. These specs are more than enough to handle the motor's requirements of 48V at a peak of ≈ 15A and give a generous margin of error to ensure stability and performance even under rapid load changes.

The TMCM-1636 integrates all the hardware and firmware required for closed-loop FOC, including a fast current control loop at 100 kHz. This allows the motor to maintain a constant resisting torque even if the subject's speed varies in the middle of an isotonic test. The controller has built-in support for hall sensors, absolute, and incremental encoders, which gives it the flexibility required for prototype development and the ability to extend features in future iterations of the dynamometer. The current iteration uses an optical absolute encoder with 1000 counts per revolution (CPR) for rotor position feedback.

In addition to its control capability, the TMCM-1636 was chosen for its software support and programmability. The TMCL-IDE, a software provided by the manufacturer, accelerates prototype development by allowing the user to test the motor/controller in a plug and play method. It allows features to be turned on and off and gives visual feedback of all sensors. Once the desired combination of features is found, a microcontroller can then be used to set those parameters when the motor is turned on.

The TMCM-1636 also supports CAN & UART for communication with other microcontrollers, has various GPIO (General Purpose Input and Output), built-in overvoltage protection, and the ability to use a braking resistor. Its multiple input and output options also allow interfacing with data acquisition systems.

4.3.2. Microcontroller [178], [179], [180]

The STM32F407G-Disc1, a discovery board that features an STM32F407VGT6 microcontroller with a 32-bit ARM Cortex-M4 core and a floating-point unit was chosen as the main controller for the dynamometer. The device can operate at clock speeds up to 168 MHz, with 1MB of flash memory and 192 KB of SRAM. These specifications ensured that the microcontroller could keep up with the rapid calculations that may be needed as part of a custom control loop on top of the Trinamic built-in controller, while addressing the constant stream of inputs.

The discovery board was ideal for this prototype due to its extensive peripheral options. It includes a 12-bit ADC, and an integrated DAC, which can be used to process strain gauge data, and output analog signals to external data acquisition systems. In addition, the discovery board features USART, SPI, I^2C, and CAN interfaces for communication, so current and future applications could seamlessly be integrated. The board also features multiple timers and PWM generation.

Ultimately, this microcontroller was chosen for its strong balance of processing performance, peripheral flexibility, and accessibility, making it well suited to controlling the dynamometer's main operations.

4.3.3. Power Supply [181]

The Meanwell SE-600-48 regulated switching power supply was selected for its ability to provide up to 48V and 600W, which exceeds the motor's rated 300W and leaves enough room to operate at peak load. The power supply also allows voltage adjustment, has a quiet integrated cooling fan, overload, over-voltage, short-circuit and over-temperature protection. This ensures that the prototype, operator and patient are safe.
The SE-600-48 has a hardware switch to select the input voltage (90-132 VAC/180-264 VAC, 47-63Hz), making it usable in a variety of clinical and laboratory environments. The power supply weighs 2.1kg, making it a reasonable choice for the portable dynamometer.

4.3.4. Strain Gauge Assembly [182]

The torque on the arm was determined using a pair of Micro-Measurements S5145 foil strain gauges whose outputs were interpreted into torque based on an experimental calibration. Specifically, two 350 Ω active gauges were used in a half-bridge

configuration, with the other half of the Wheatstone bridge completed using two fixed 350 Ω resistors. This specific configuration ensured that the two strain gauges, placed on opposite sides of the torque arm, would have an additive effect thus improving the signal to noise ratio, while also eliminating temperature effects. The S5145 strain gauges have a 0.76 mm grid length, and compact overall dimensions of 2.41 x 1.60 mm, which allowed the gauges to be mounted securely anywhere on the torque arm. They were placed on the thin edges, as far as possible from the neutral axis, so that the maximum signal can be obtained from the minimal bending of the stainless-steel torque arm.

The half-bridge was connected to a Texas Instruments ADS1256 analog-to-digital converter (ADC). The ADS1256 is a 24-bit delta-sigma ADC with a maximum data rate of 30kSPS. The chip includes a low-noise programmable gain amplifier (PGA) with gains from 1:64, allowing the direct amplification of the millivolt-level half-bridge outputs. Communication with the microcontroller is handled through 5V-tolerant SPI interface, and the board itself provides self-calibration for offset and gain errors. The ADS1256 has existing Arduino libraries that enabled rapid prototyping with the intent to integrate its functionality directly with the main STM32F407 microcontroller, reducing complexity and communication needs.

4.4. Final Prototype

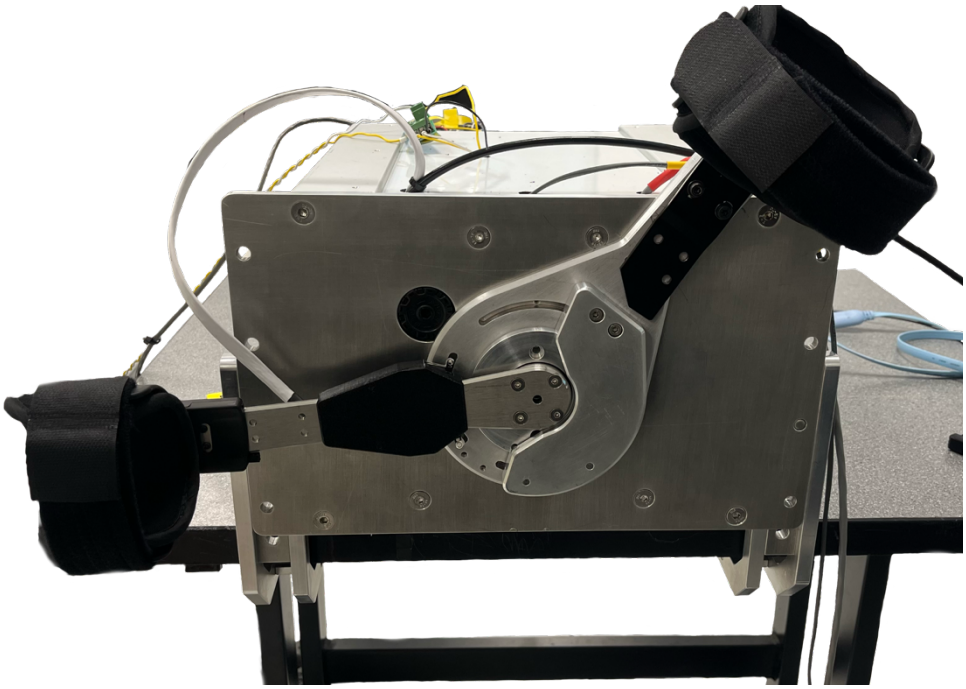

Figure 7. Final prototype of the portable dynamometer mounted to a Table.

The final touches include soft cuffs with hook-and-loop straps, a strain gauge cover and an optional aluminum hard stop for additional safety during testing. The hook-and-loop

straps allow the clinician to adjust the cuff width to match the patient. They are removable for easy cleaning or replacement and ensure that the patient's arm stays in the correct position throughout the test. The plastic strain gauge cover ensures that the gauges are protected from damage and secures the cable to prevent accidental pulls from disconnecting the delicate strain gauge wires.

The final cost of the device prototype is in the $4000-$5000 range depending on regional variations in component pricing and manufacturing costs. At the time of writing, the motor can be purchased for $551[183].The gearbox costs $750[184], while the motor controller costs $474[185]. The power supply is $148[186], and other miscellaneous electronics (ADS1256, brake-chopper parts, microcontroller, connectors and wiring) individually cost $20-$50. For sensing, most components are included with the motor and controller, though the strain gauges cost $45 each. The total expected bill of materials is in near $3000 once we include aluminum extrusions, panels/cutouts, hardware and fasteners and cuffs. Depending on the machining, finishing, and assembly costs, this finished unit price can reach $4500-$5000.

5. Device Characterization Methods

To begin the development process of the isotonic motor system, an initial assessment was needed to benchmark the setup as recommended by the motor controller manufacturer. The findings from that benchmark led to a systematic characterization of the gearbox's friction and inertial properties, the development of a friction compensation procedure, a technical validation against known weights and an analysis to process the acquired measurements. Each step was completed with its own fixtures as required by the experiment, and informed design of the dynamometer. The analysis of the results evaluates the dynamometer's performance and establishes its suitability for the dynamometer application.

To obtain meaningful muscle performance results, a thorough understanding and characterization of the measurement system itself is necessary. Physical properties of each component in the dynamometer's drivetrain, such as frictional losses and inertial characteristics, can introduce systematic errors into measurements. Therefore, these sources of error need to be properly quantified and accounted for. Friction, for example, always opposes the direction of motion. If the patient is producing torque and the dynamometer is resisting, an uncompensated friction will act against the patient and in the same direction as the dynamometer's resistance, leading to a higher than intended total resisting torque. Similarly, inertial properties influence the relationship between applied torque and the resulting acceleration as indicated by Newton's second law:

$$\tau = I\alpha \tag{5.1}$$

A multi-stage calibration process was therefore required to ensure accurate measurements of isometric strength and isotonic power. This process was designed to first identify the magnitude of the system's internal resistance, then to determine empirical compensation parameters for the gearbox inertia and its velocity-dependent friction for dynamic compensation.

5.1. Initial System Assessment

Preliminary investigations were the first step in understanding the dynamometer's baseline behavior. The primary goal was to determine if the combined motor-gearbox assembly could maintain a constant resisting torque when backdriven. Drop tests were chosen for this initial assessment because gravity provides a consistent external load (via calibrated weights) to the system's output shaft. This ensures that the observed dynamic response is entirely attributed to the system, with no variation in applied load. The entire test setup involved the motor, gearbox, a pulley system with a wheel on the gearbox output shaft, and known masses. A motion tracking camera was used to track the wheel's rotation, and measure the angular velocity of the gearbox output shaft.

A custom laser-cut plywood wheel with a 15cm radius was attached to the gearbox output shaft with a 3D-printed coupling. The plywood wheel had a passive reflective marker array (3 markers) rigidly attached on its surface for kinematic tracking. The markers are part of the NDI Polaris Vega optical motion capture system, which includes a camera that tracks at 250Hz (Northern Digital, Waterloo, ON, Canada). The entire test setup is shown in Figure 8.

Figure 8. Initial system characterization setup for drop tests.

In these tests, the BLDC motor was operated in a specific velocity control mode: the target velocity was set to zero, while the maximum permissible motor torque was systematically varied across trials. This control strategy caused the motor to resist the motion but only up to a pre-determined maximum torque limit. Observing the system's actual motion using external measurement from the validated motion tracking system gave insight into the net torque balance, which includes the internal resistive forces like friction. Specifically, the applied external torque caused by gravity on the falling mass is constant. The resulting wheel velocity-time profile should increase linearly (due to the constant angular acceleration) if the motor torque is constant. A constant resisting torque would reduce the net torque on the wheel, resulting in a constant acceleration with a lower magnitude. Any deviation from the ideal behaviour, such as a non-linear velocity-time profile, would indicate additional resistive effects in the system. Testing with various resisting torques could reveal a trend or pattern that can be characterized.

Results of this assessment are presented in detail in the next chapter; however, the primary takeaways from these initial phases were as follows:

- the motor-gearbox system was unable to achieve a constant acceleration (i.e. linear velocity curve) when backdriven by a constant external load.

- the motor-only tests revealed that the motor itself was effective and consistent at achieving a linear velocity profile when resisting an external load; no gearbox was present in this configuration.
- gearbox-only tests did in fact show non-linear velocity increases and variable characteristics for different levels of applied torque.
- high velocities (such as those obtained with a low resistance and high external torque) resulted in bus voltage transients that exceeded nominal supply voltage.

These initial benchmark findings confirmed the need for a thorough characterization and calibration approach aimed at isolating, quantifying and compensating the gearbox's inertia and friction, as well as the implementation of a brake-chopper to avoid the bus voltage increases. The following section details the methods used to achieve this characterization.

5.2. Gearbox Inertia and Friction Characterization

Although the initial tests provided an indication that the friction in the gearbox had a significant effect on the system's ability to function as intended, it did not systematically characterize that effect. Thus, the next logical step was to conduct this characterization. However, this required knowledge of the gearbox's rotational inertia, which was not provided by the manufacturer. Thus, to develop an effective error compensation method, it was necessary to undertake characterization of the inertial and frictional properties of the gearbox.

5.2.1. Experimental Protocol (Deceleration Tests):

For rotational motion, Newton's second law states that:

$$\sum \tau = I\alpha$$

Where $\sum \tau$ is the net torque, I is the inertia of the system, and α is the angular acceleration of the rotating system. Taking the directions into consideration, the equation becomes:

$$\tau_{user} - \tau_{motor} - \tau_{friction}(\omega) = I_{total}\alpha \tag{5.2}$$

With the user driving the system, τ_{user} is the torque applied by the patient, as required by the test. The motor's torque, τ_{motor}, acts in the opposite direction to resist the motion. Since friction always acts opposite to the motion, and that the output shaft of the motor is moving in the same direction as τ_{user}, then $\tau_{friction}$ is in the same direction as τ_{motor} (both motor torque and total friction resist the user).

The compensation mechanism, once all parameters are determined, can subtract the friction (converted to the equivalent motor current) from the target torque. This would remove the effect of friction during the assessments and result in more precise and meaningful results.

A simple drop test that measures the acceleration via changes in velocity, will not discriminate between the inertial effects and the frictional effects. Both are unknown and need to be determined separately. Therefore, a custom experimental setup and a deceleration-based protocol were implemented (shown in Figure 9).

The protocol involved measuring the passive deceleration of the gearbox output shaft with different rotational inertias and across different initial velocities. The motor was used to accelerate the gearbox, with the added weight discs, to a pre-determined velocity. Once that velocity was reached, and held for a few seconds to confirm that the system was stable, the motor was decoupled from the gearbox. This instantly reduced the motor torque (τ_{motor}) to zero, leaving friction as the only torque ($\tau_{friction}$) acting against the rotation of the gearbox and mass system. The deceleration (α) of those masses can then be entirely attributed to friction. The total inertia ($I_{total} = I_{gearbox} + I_{known\_weights}$) is unknown, but $I_{gearbox}$ is constant in all tests.

The fundamental equation for these tests is:

$$\tau_{friction}(\omega) = I_{total} \times \alpha(\omega)$$

Systematic measurements of deceleration (α) from a range of initial angular velocities (ω), for different total inertias (I_{total}) will result in a friction torque value for each velocity.

Since the only variable altering friction between these tests is velocity, for each initial velocity condition we have:

$$\omega_1 = \omega_2$$

$$\tau_{friction_1} = \tau_{friction_2}$$

$$(I_{gearbox} + I_1) \times \alpha_1 = (I_{gearbox} + I_2) \times \alpha_2$$

$$I_{gearbox} = \frac{I_1\alpha_1 + I_2\alpha_2}{\alpha_2 - \alpha_1} \tag{5.3}$$

In this equation, I_1 and I_2 are two different known weights, α_1 and α_2 are the measured passive decelerations of those weights. The two tests (1 & 2) both begin with the same initial velocity. This procedure was systematically repeated in a range of 0-3250RPM (0-340 rad/s)motor velocity range for each of the available weight configurations (8N to

56N, at 8N increments). Friction in geared transmissions is often speed-dependent, so testing at multiple initial velocities was important. This procedure should result in slightly different $I_{gearbox}$ values for each inertia and deceleration pair, due to experimental variability. Since the gearbox is the same in all tests, an average value can be used as the likely true value.

A comprehensive empirical relationship between the friction and velocity could be calculated from known velocities, decelerations, inertias and the fundamental equation $\tau_{friction}(\omega) = I_{total} \times \alpha(\omega)$. The resulting best fit equation related the friction torque magnitude to the angular velocity magnitude using a power law relationship:

$$\tau_{friction\_magnitude} = a_\tau \cdot |\omega|^{b_\tau} + c_\tau \quad (5.4)$$

where a_τ, b_τ, c_τ are coefficients found empirically through this procedure, and $|\omega|$ is the absolute angular velocity (rad/s). $a_\tau$is a scaling factor in $\frac{N \cdot m}{rad/s^{b_\tau}}$, and c_τ is an offset in N·m.

5.2.2. Experimental Setup

The experiment was designed to allow the gearbox's properties to be measured, without the motor's influence. A 3D-printed motor-gearbox coupling, which enabled the rapid and manual removal of the motor while it was spinning, was critical to the success of this experiment. It allowed the gearbox's passive deceleration to be observed without any active or external torque. When the motor was removed, the only torque acting on the gearbox was its own internal friction. To determine the inertia, a machined aluminum fixture with a rotating shaft supported by bearings, was mounted to the gearbox output shaft. This fixture was secured to the table and allowed a set of 8N calibrated weights to be added as needed (up to a total of 56N). These disc-shaped weights changed the total rotating inertia (I_{total}) of the system in a known manner. The systematic change of initial velocity and total inertia made it possible to compare system dynamics and mathematically separate the effects of inertia and friction. A 3D-printed wheel on the rotating shaft held passive markers for kinematic tracking via the NDI Polaris Vega system.

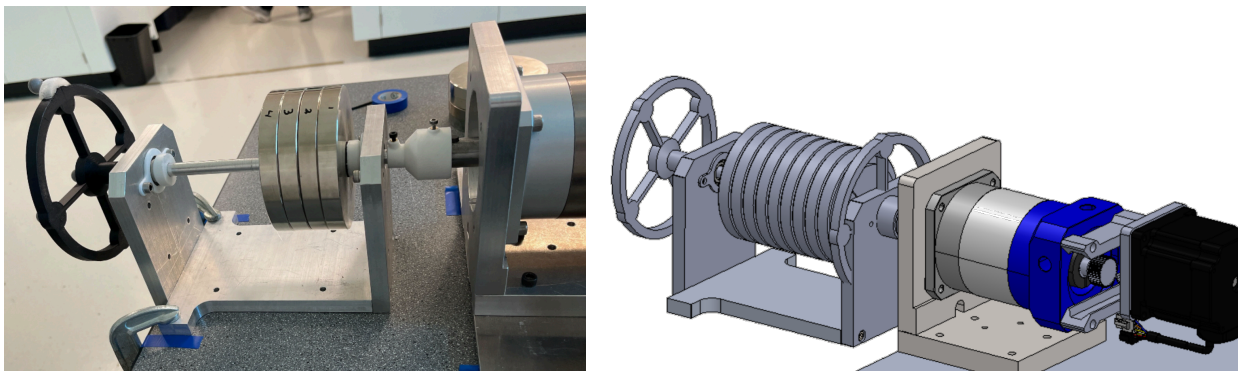

Figure 9. Fixture for gearbox inertia and friction characterization.

5.3. Friction Compensation Selection & Validation Experiments

The fixture and experiment described in section 5.2, and its associated analysis, established the gearbox's inertia. With the experimentally determined inertia, the friction profiles could be calculated from the deceleration values (also obtained through the same experiment). A friction equation was developed, and a compensation algorithm was implemented within the dynamometer's microcontroller. This led to a validation phase with two primary goals: 1) to confirm that the friction compensation accurately nullifies the frictional losses of the gearbox, and 2) to assess the ability of the dynamometer to maintain a constant resisting torque against a known external load. Drop tests, like those used in the initial benchmarking, were used in the fully assembled and calibrated system.

5.3.1. Test Setup

For the validation experiments, the dynamometer was fully reassembled. The quick-release motor fixture used in the deceleration tests was removed, and the motor was coupled and bolted to the gearbox as intended by the manufacturers. The same 30cm diameter plywood wheel used in the initial benchmarks was mounted directly to the gearbox output shaft for the validation drop tests, with the same steel wire and pulley. The weight used for this setup, with its mounting hardware, was measured as 6130g. Similar to the initial tests, this weight was suspended and released manually. It applied a known external torque of 9.02 N·m on the gearbox output shaft (Figure 8). Kinematic data was obtained from the motor's own encoder, as intended in the final configuration of the dynamometer.

5.3.2. Test Protocol: Dynamic Torque Control (Drop Tests)

The validation experiments tested the calibration, the compensation algorithm, and the brake-chopper. The friction compensation equation derived from the calibration procedure in section 5.2.1, with the friction coefficients obtained experimentally, were implemented into the motor control loop running on the dynamometer's microcontroller unit (MCU).

The principle behind this validation is straightforward: in an ideal system, applying a constant external torque via a suspended weight that drops (T_{weight}) will result in a constant angular acceleration of the wheel. Applying a constant resisting torque (T_{motor}) will reduce the net torque. This will still result in a constant angular acceleration, but it will have a lower magnitude. In the real system, however, gearbox friction ($T_{friction}(\omega)$) also acts on the shaft. In this scenario, friction opposes the direction of rotation of the wheel and goes in the same direction as the motor's resisting torque. The total torque resisting the falling weight is therefore $T_{motor} + T_{friction}$, with $T_{friction}$ increasing with velocity. This results in a non-linear change in velocity and thus the acceleration is not constant. Velocity increases at a decreasing rate.

During a test, the MCU receives encoder outputs at a high frequency for the motor's angular velocity (ω). It used the friction equation (derived from the fit described in section 5.2), to calculate the expected friction torque magnitude at that instant. This calculated friction torque was then subtracted from the motor's maximum allowable torque in a feed-forward manner. The adjusted motor command $\tau_{command}$ was therefore calculated as

$$\tau_{command} = \tau_{target} - \tau_{friction}(\omega) \tag{5.5}$$

where $\tau_{friction}(\omega)$ represents the calculated compensation torque, and τ_{target} is the intended constant resisting torque. This instructs the motor to produce a maximum torque that decreases as velocity (and therefore friction) increases, allowing the total resisting torque to remain constant.

The torque felt by the patient during an isotonic power test should be constant despite velocity fluctuations in natural muscle movements, and regardless of the patient's strength. With an accurate friction compensation equation, the resisting torque stays constant even as the velocity changes. A successful calibration and a good compensation will result in a linear velocity profile during a drop test. If the velocity increases linearly with respect to time, then the acceleration is constant. A non-linear velocity profile would indicate that further characterization is needed and that the compensation strategy is inadequate.

5.3.3. Validation of Isometric Mode

To assess the dynamometer's static measurement accuracy, the arm's load cell measurements were compared to known calibrated weights. The calibrated weights were suspended from the dynamometer's lever arm at the forearm restraint's mounting point. This mass (m) creates a known torque (τ) on the centre of rotation ($\tau = m \times g \times r$). In this equation, g is gravitational acceleration, and r is the lever arm. The dynamometer was held in a static position (isometric mode), and the torque reading from the strain gauges, digitized by the ADS1256 module, was recorded and compared with the known values.

5.4. Data Analysis

The raw kinematic data acquired by the NDI Polaris Vega during the initial benchmarks, and during deceleration tests required post-processing to extract meaningful parameters and calculate the system's properties. The analysis was completed using custom scripts developed in MATLAB 2023a (The MathWorks, Natick, MA, USA). The Curve Fitting Toolbox and the Statistics and Machine Learning Toolbox contained essential functions to this analysis. The workflow involved data import, signal conditioning, kinematic calculations, model fitting and error analysis. A systematic workflow, described in this section, was used to extract the information needed to develop the friction compensation.

5.4.1. Raw Data Processing and Kinematic Calculation

The raw motion capture output from the NDI Toolbox software was obtained in CSV format and contained quaternions. This data was used to calculate the dynamometer's output shaft angular velocity with MATLAB's angvel function (angvel(q, timestep, 'frame')). The function computes the angular velocity in the fixed coordinate frame from the time series of quaternions (q), using the known 250Hz sampling rate to determine the time-step. Initial and terminal artifacts were removed, and a Savitsky-Golay filter (MATLAB's sgolayfilt function, implemented in the filterData function) was used to reduce noise. Segments of zero/near-zero velocity were removed to isolate the periods of actual motion relevant to the analysis.

For the deceleration test data used to determine the friction and inertia of the gearbox, further processing was required. To identify the relevant passive deceleration phase, the algorithm starts at the end of the dataset and works backwards. A sliding window of 10 frames is used to analyze slope. A linear fit is used in each window while the slope is negative (deceleration). This stops when the slope becomes positive or zero, indicating the end of the constant velocity portion of the test, and the beginning of the deceleration phase. This data is extracted. The outer 25% of data points on both ends

are removed to ensure that only the central portion is kept. The goal is to obtain the instantaneous deceleration for that specific initial velocity. A linear regression (fitlm) was then applied to the deceleration segment to determine the deceleration during that phase. Key metrics, including the weight, initial velocity, trial number, and calculated mean deceleration were added to a data structure for further analysis. Finally, representative deceleration values for each unique experimental condition (Weight/Initial Velocity combination) were calculated by taking the median of all 6 trials. These results were saved so they could be used in the inertia and friction calculations.

5.4.2. Inertia and Friction Parameter Estimation

The calibration involved using the processed deceleration data to estimate the gearbox's rotational inertia and develop a friction equation.

First, the rotational inertia of the gearbox output and fixture ($I_{gearbox}$) was calculated. This was done using the data from deceleration tests performed with different known added weights (8N, 16N, 32N, 48N, 56N). For each weight category, a mathematical equation (specifically, a two-term power law):

$$\alpha(\omega) = a_\alpha \cdot \omega^{b_\alpha} + c_\alpha \tag{5.6}$$

where ω is angular velocity (rad/s), α is angular acceleration (rad/s^2), and a_α, b_α, and c_α are fitted coefficients. a_α is a scaling factor with units $\frac{rad/s^2}{rad/s^{b_\alpha}}$, $b_\alpha$is dimensionless, and c_α is an offset in rad/s^2. The equation was fitted to the measured deceleration ($\alpha(\omega)$) data using non-linear least squares regression (fit function from MATLAB's Curve Fitting Toolbox). In this equation, the resulting fitted deceleration curves ($\alpha_1(\omega)$ and $\alpha_2(\omega)$ for two different weight tests 1 and 2) were then used in a two-point formula derived from $\tau = I \times \alpha$. Based on the principle that friction torque is independent of the added inertia at a given velocity, the following formula, as implemented in inertia.m, allows for the isolation of $I_{gearbox}$:

$$I_{gearbox} = \frac{I_1\alpha_1 - I_2\alpha_2}{\alpha_2 - \alpha_1}$$

where I_1 and I_2 are the known inertias added by the weights for tests 1 and 2 respectively, and α_1 and α_2 are the corresponding measured decelerations at a specific velocity ω. The calculated $I_{gearbox}$ values obtained from comparisons between different pairs of weight tests and across different velocity points were averaged to obtain a final estimate (I_{avg}) and its standard deviation (I_{std}).

With the gearbox inertia found, the velocity-dependent friction torque ($\tau_{friction}(\omega)$) was calculated and modeled. For each test weight condition, the friction torque at various

velocities was computed using the relationship $\tau_{friction}(\omega) = I_{total}\alpha(\omega)$, where I_{total} was the sum of the calculated gearbox inertia (I_{avg}) and the known added weight inertia (I_{weight}), and $\alpha(\omega)$ was the deceleration obtained from the previously fitted passive deceleration curve for that weight. The friction torque values calculated across all different weight tests were then averaged at each corresponding velocity point to obtain a mean friction-velocity profile, and the standard deviation. Finally, the friction equation (5.4), selected for its agreement with experimental data when compared to other options, was applied to the averaged friction-velocity data. The parameters were estimated by fitting the standard MATLAB Curve Fitting Toolbox library model 'power2' (which corresponds to $y = a \cdot x^b + c$) to the averaged friction magnitude versus velocity magnitude data, using non-linear least squares regression. The absolute velocity $|\omega|$ accounts for the friction magnitude regardless of direction, with the correct application opposing motion handled in the control implementation. The resulting model coefficients and associated confidence intervals (confint, Statistics and Machine Learning Toolbox) represent the calibrated friction estimation for the gearbox, which was saved for use in the validation phase and real-time control.

6. Results

6.1. Introduction

This chapter presents the outcomes of the experiments detailed in the preceding methodology section. A systematic characterization of the motor, the gearbox, and the fully assembled system give the information needed to ensure the dynamometer can reliably provide a constant resisting torque.

In section 6.2.1, an initial benchmark of the assembled system is completed to assess the ability to maintain a constant resisting torque under load. This step was completed using the software provided by the manufacturer of the motor controller, with no brake-chopper. This benchmark identified a significant deviation from the expected constant torque. Subsequent benchmarks of the motor (section 6.2.2) and gearbox (section 6.2.3) established a significant gearbox velocity-dependent friction profile, which forms the basis of the compensation implemented in the final control system. A full characterization of the gearbox in section 6.3 results in a friction compensation curve that can be used to account for friction when controlling the dynamometer. Section 6.4 presents the results of the final validation, with the same procedure as the initial benchmarks, to ensure that the changes to the system achieved the desired goal: provide a constant resisting torque while the motor is backdriven by an external load.

Throughout this chapter, emphasis is on presenting quantitative results and their immediate technical implications. These results are given with appropriate statistical

analysis and visualizations to facilitate the understanding of the system's performance. Discussion of the results is provided in Chapter 7.

6.2. Initial System Characterization

6.2.1. Full System Drop Tests

The initial system characterization, a benchmark of the unmodified assembly, with stock manufacturer software, provides insight into the original system's behaviour. Ideally, the built-in control options would provide a constant resisting torque when given the appropriate command. The available control modes are Position mode, Torque mode, and Velocity mode. Position mode allows the user to specify a relative position to the controller, with max torque, velocity and ramp-up/ramp-down limits. The controller will then move the motor to that position. Torque mode allows the user to specify a current, and the controller will provide that current to the motor, which will rotate as fast as it can given the setpoint (and therefore allowable torque). Finally, velocity mode gives the user the ability to specify a velocity, and the controller would attempt to rotate the motor at that constant velocity regardless of the load.

A series of drop tests (not shown) were completed to establish the combination of settings that would give a constant resisting torque. Position mode, with a pre-set maximum torque and initial position, attempted to return to the initial position at the end of the test. This mode was eliminated as a candidate because this was not the desired behaviour. Torque mode provided a constant torque against a falling weight but would continue to energize the motor at the end of the test until the controller was told to stop. This caused the device to continue attempting to lift the weight, a behaviour that could potentially injure a patient if their arm stops providing torque that is greater than the motor's. This mode was also eliminated as a candidate. Velocity mode, with a constant velocity of 0, and a current limit corresponding to the maximum desired resisting torque, was the only method that fulfilled the required clinical test procedure of providing a resisting torque under load while ensuring that the motor would not move when a patient was not actively driving the motor. The benchmarking results shown below, and all subsequent tests, use the controller's velocity mode with a specified maximum allowable torque.

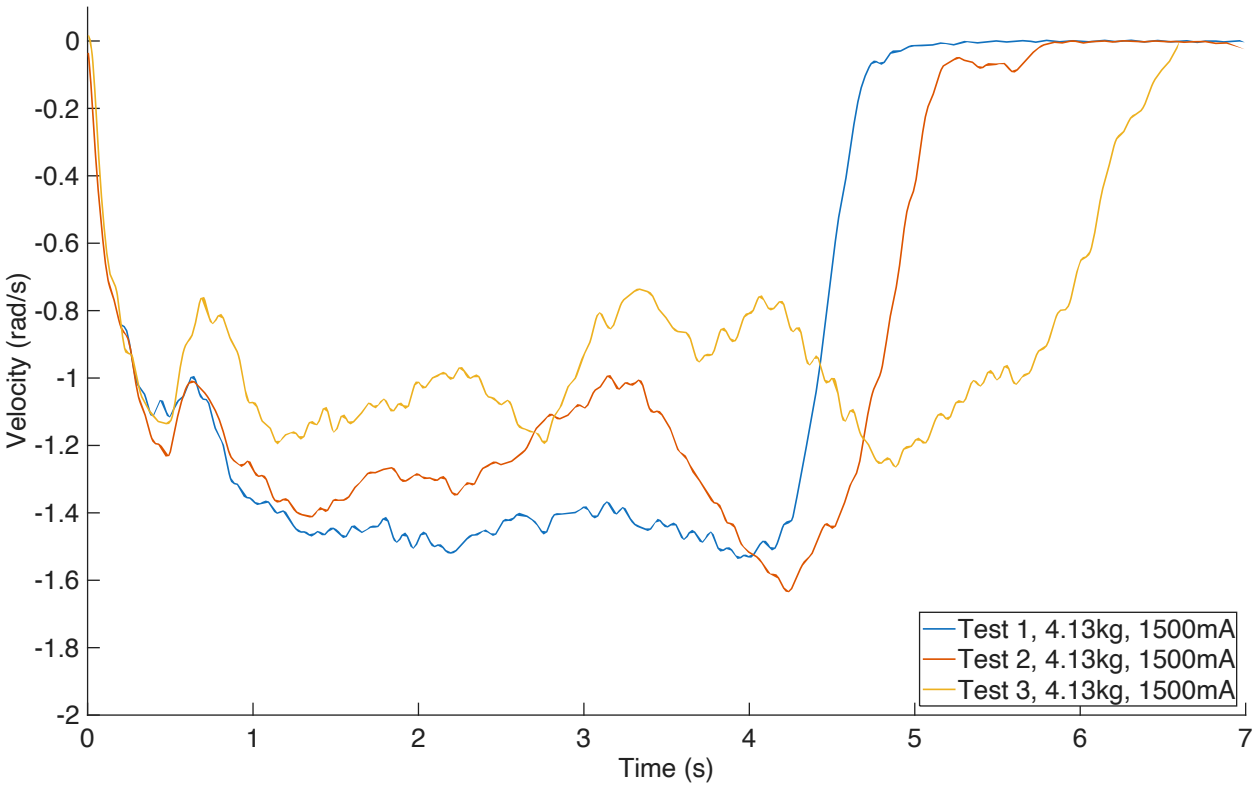

Figure 10. Full-system drop test with 4.13kg weight and 1500mA (2.31 N·m) resistance.

As seen in Figure 10, the velocity exhibits a rapid initial acceleration, followed by a decreasing rate of increase, ultimately plateauing near constant value until the end of the drop. Minor trial-to-trial variations in initial conditions and mechanical losses account for the differences in magnitude but do not affect the general trend.

Under a constant external torque such as these drop tests, a system with a constant resisting torque would have a constant angular acceleration and a linearly increasing velocity-time profile. The observed non-linear behaviour and apparent plateau indicate that the internal resistance of the system changes, confirming that the drivetrain does not provide constant resisting torque in its default state. This motivates the subsequent characterization.

One more test was done with 5.5kg and 500mA (6.7% of max torque) of resisting torque, to test higher velocity drops. This is equivalent to a theoretical resisting torque of 0.77 N·m at the test wheel.

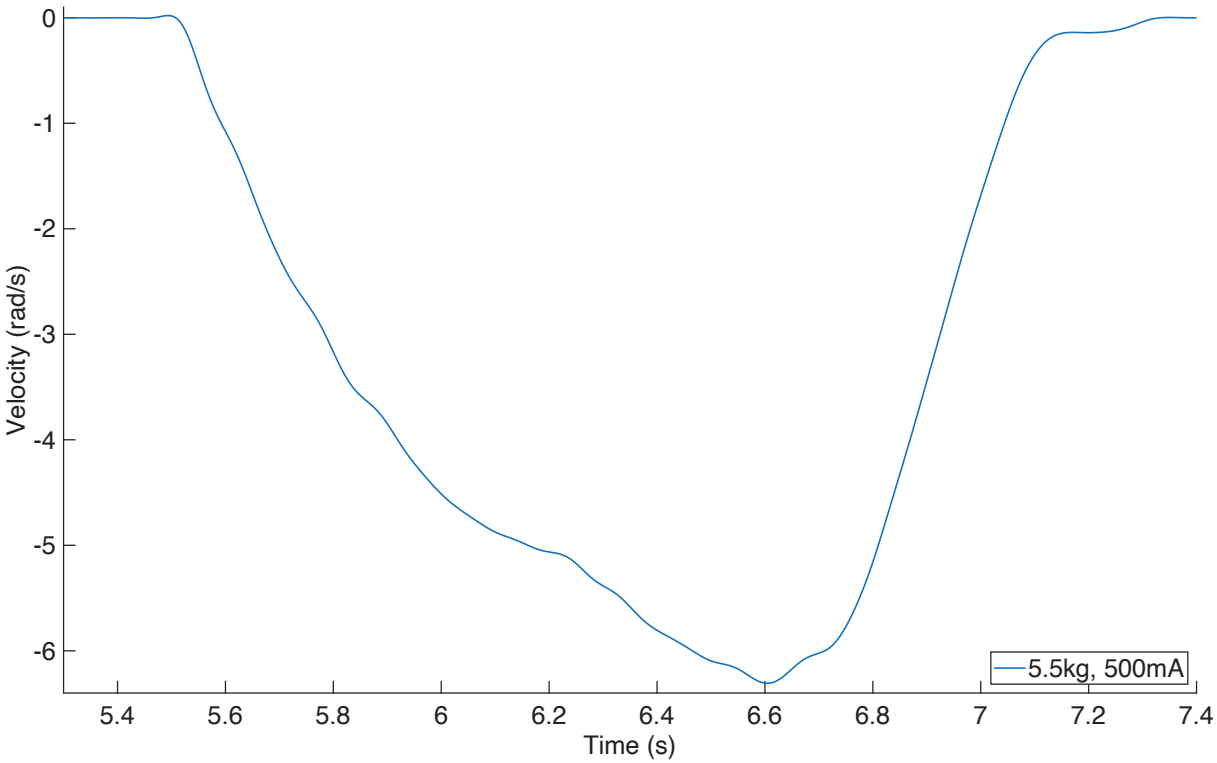

Figure 11. Full system drop test with 5.5kg weight and 500mA (0.77 N·m) resistance.

A rapid initial acceleration is observed once again in Figure 11, followed by a decreasing rate of increase in velocity until the end of the drop. The drop stopped due to impact with the ground before a plateau could be reached. In addition, a large voltage spike was observed at higher velocities, so further testing was stopped to prevent damage to the electronics.

6.2.2. Motor-Only Drop Tests

To further characterize the system and isolate the source of the observed decreasing rate of increase in velocity, drop tests were completed using the motor alone. The adapted fixture allowed for an identical test without the gearbox. The following tests were all done with a weight of 250g, and various resisting torques. 250g is 0.37 N·m at the wheel, or 51% of the motor's rated torque when the wheel is attached directly to the motor shaft, without a gearbox. Representative data from tests that clearly illustrate the overall trend is shown in Figure 12 and a summary of the results is given in Table 2.

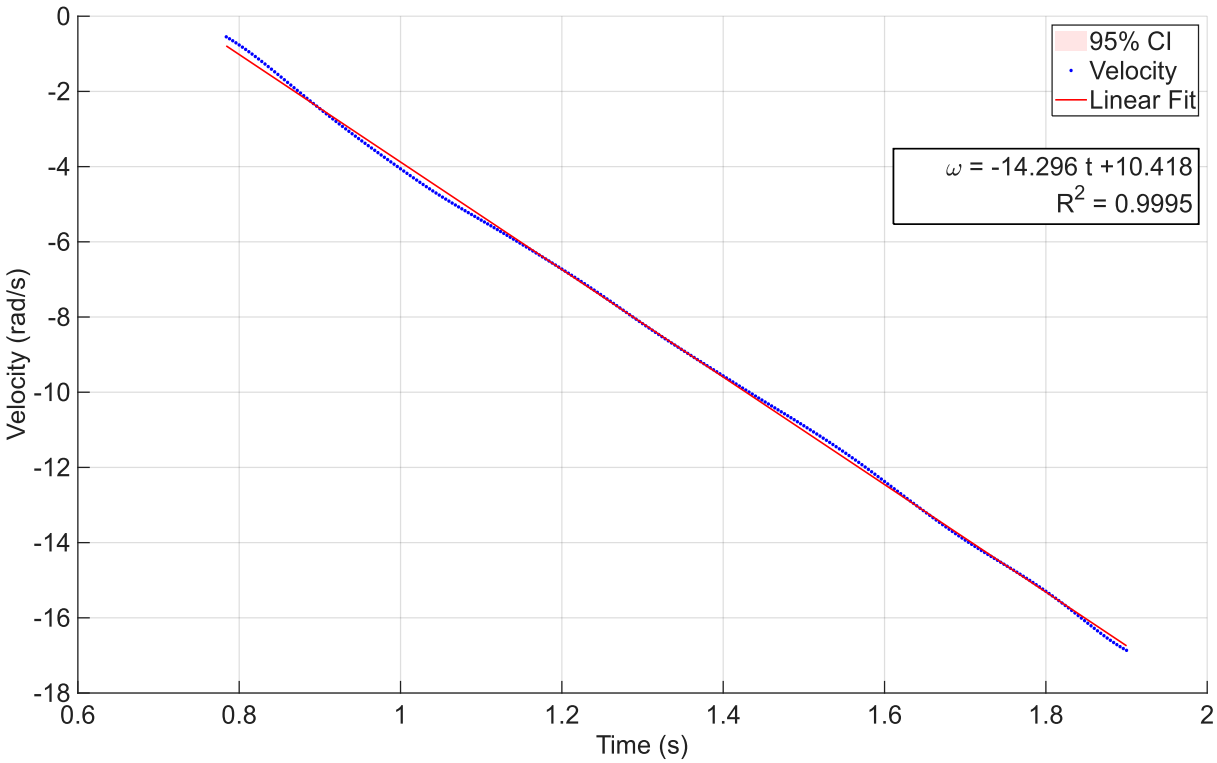

Figure 12. Motor-only drop test configuration with 250g weight and 1500mA (0.14 N·m) resistance.

Velocity data when the motor is set to provide a constant resisting torque with a maximum allowable current shows a nearly perfect linear velocity vs time curve, indicating that the acceleration of the falling mass is constant as intended. The same test was repeated at constant torque increments of 500mA to verify that this relationship is obtained over a full range of velocities and resisting torques. The statistical summary in Table 2. indicates that the linear relationship is obtained consistently in all tests within the tested range, and that the higher the torque, the lower the acceleration. This is visualized in Figure 12, where the linear relationship between resisting torque and acceleration of the falling mass is clear.

Results presented in Table 2 refer to the velocity vs time curves from which Figure 12 was generated. The mass was suspended with a pulley, and steel wire, tied to a 30cm plywood test wheel directly coupled to the motor shaft. Slopes are obtained by motion capture at 250Hz, followed by circle fitting, filtering, polynomial differentiation and linear regression. Values represent the average and standard deviations of 3 tests per resisting torque. Torque values (in N·m) are theoretical torques based on the motor's torque constant.

Table 2. Statistical Summary of Constant Torque Drop Tests with a 250g Mass.

Resisting Torque (mA)	Resisting Torque (N·m)	Slope (rad/s^2)	R^2	RMSE (rad/s)	Linear Fit Equation
500	0.0481	-22.837 ± 0.052	0.9998 ± 0.000002	0.0830 ± 0.0008	v = -22.837 t + 14.506
1000	0.0961	-18.533 ± 0.118	0.9998 ± 0.000019	0.0720 ± 0.0035	v = -18.533 t + 14.771
1500	0.1442	-14.222 ± 0.093	0.9995 ± 0.000050	0.0901 ± 0.0134	v = -14.222 t + 10.815
2000	0.1923	-10.161 ± 0.094	0.9996 ± 0.000124	0.0738 ± 0.0112	v = -10.161 t + 8.792
2500	0.2403	-5.886 ± 0.039	0.9995 ± 0.000213	0.0592 ± 0.0145	v = -5.886 t + 4.787
3000	0.2884	-2.112 ± 0.138	0.9968 ± 0.000925	0.0917 ± 0.0106	v = -2.112 t + 1.289

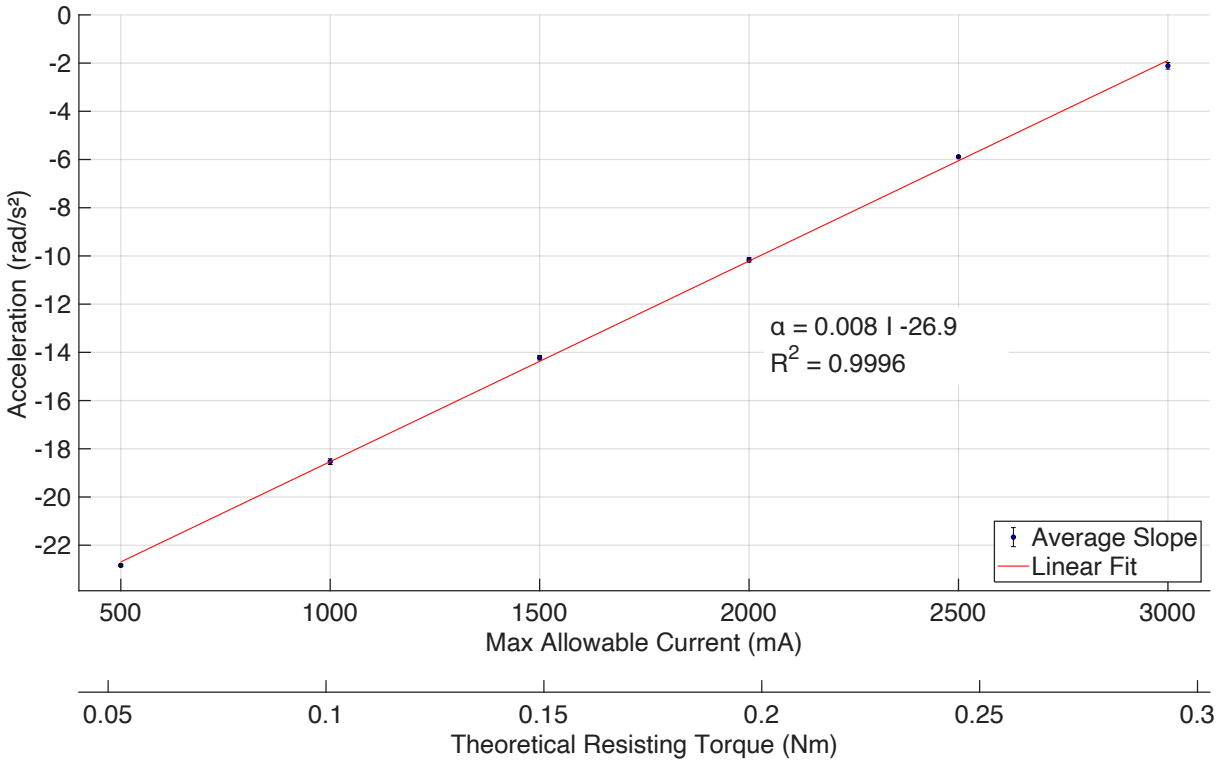

Figure 13. Relationship between maximum resisting current and angular acceleration.

6.2.3. Gearbox-Only Drop Tests

To identify the contribution of the gearbox, a series of drop tests was completed with the same test setup as the motor-only tests. The gearbox was rigidly attached to the same test wheel with passive tracking markers. A wire from the wheel to a pulley held a mass at the other end. Since no motor was used in these tests, no measure of resisting

torque was taken. Figure 14 shows the typical gearbox behaviour when subjected to drop tests with different masses. The velocity profile appears similar to the initial full system benchmarks, suggesting that the gearbox is the source of the non-linearity. For each of the weights, a decreasing rate of increase in velocity is observed. Increasing the mass resulted in a more rapid increase in velocity, and a greater velocity on impact with the ground.

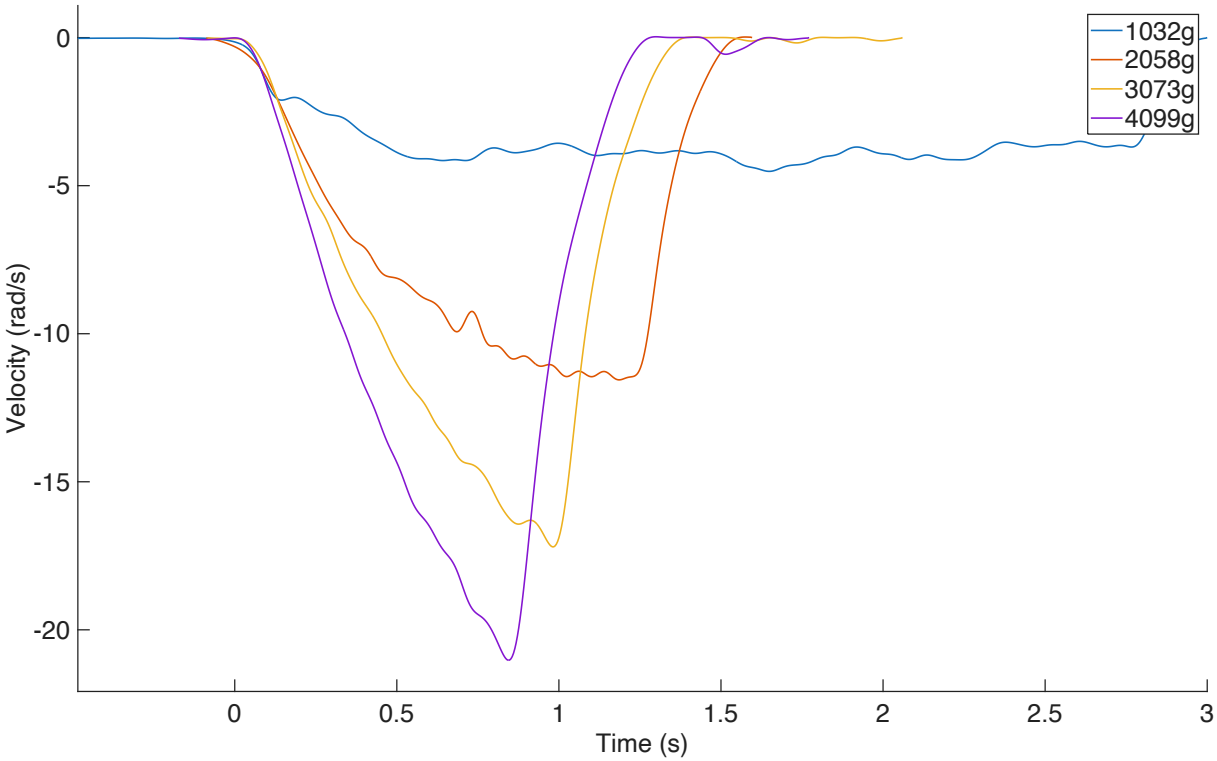

Figure 14. Velocity profiles from gearbox-only drop tests.

6.3. Gearbox Characterization

6.3.1. Inertia and Friction Testing (Passive Deceleration)

To characterize the frictional effects causing the decreasing rate of increase in velocity, the custom passive deceleration testing fixture described in 5.2.1 and 5.2.2 was used. Weights were mounted on a rack attached to the output shaft of the gearbox. The motor was used to accelerate those weights to a fixed velocity, then decoupled from the gearbox to allow it to decelerate passively. Figure 15 shows the typical velocity profile for these tests, with the raw and filtered data overlaid to show the filter's effects, and the region isolated for further analysis overlaid in green.

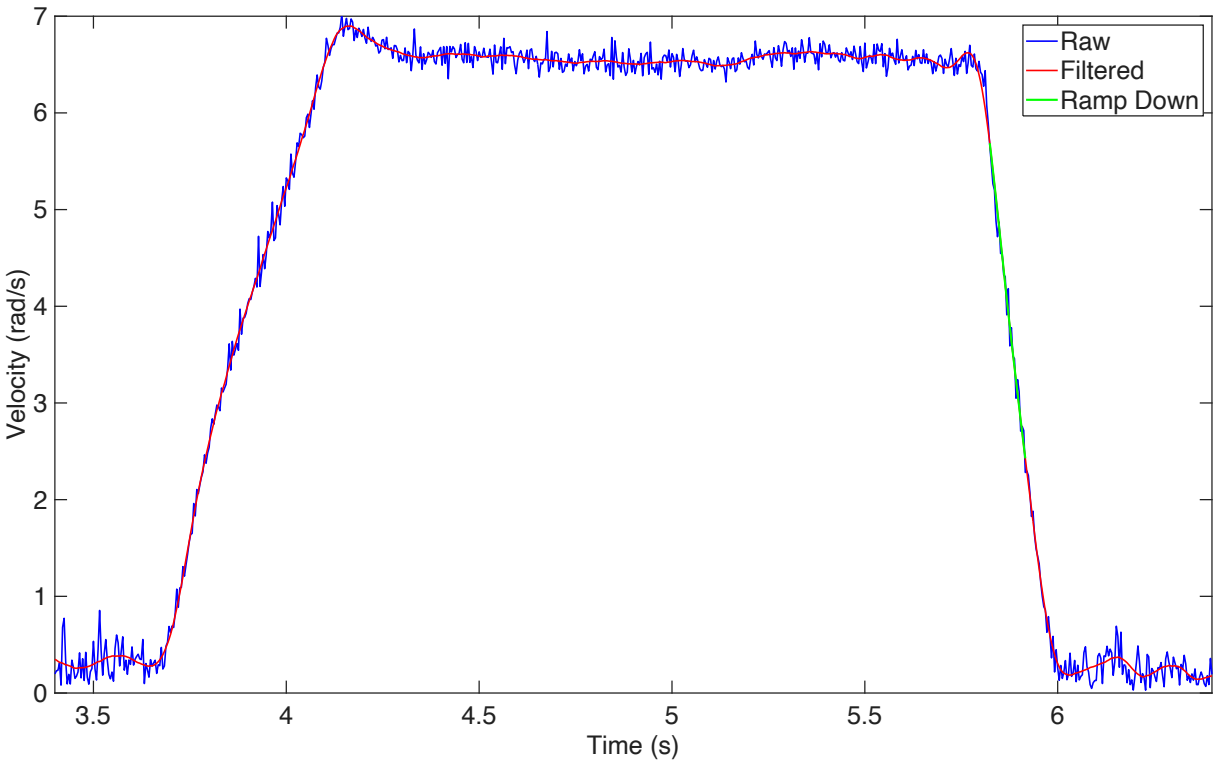

Figure 15. Representative velocity trace from passive deceleration testing.

The feature of interest for all tests is the slope of the passive deceleration phase, where the velocity drops to zero. Approximately 2/3 of the deceleration phase is used for the remainder of the analysis because the control system is designed to sample velocity and compensate in real-time. As such, a value for the instantaneous passive deceleration for each initial velocity is the data needed for the compensation algorithm.

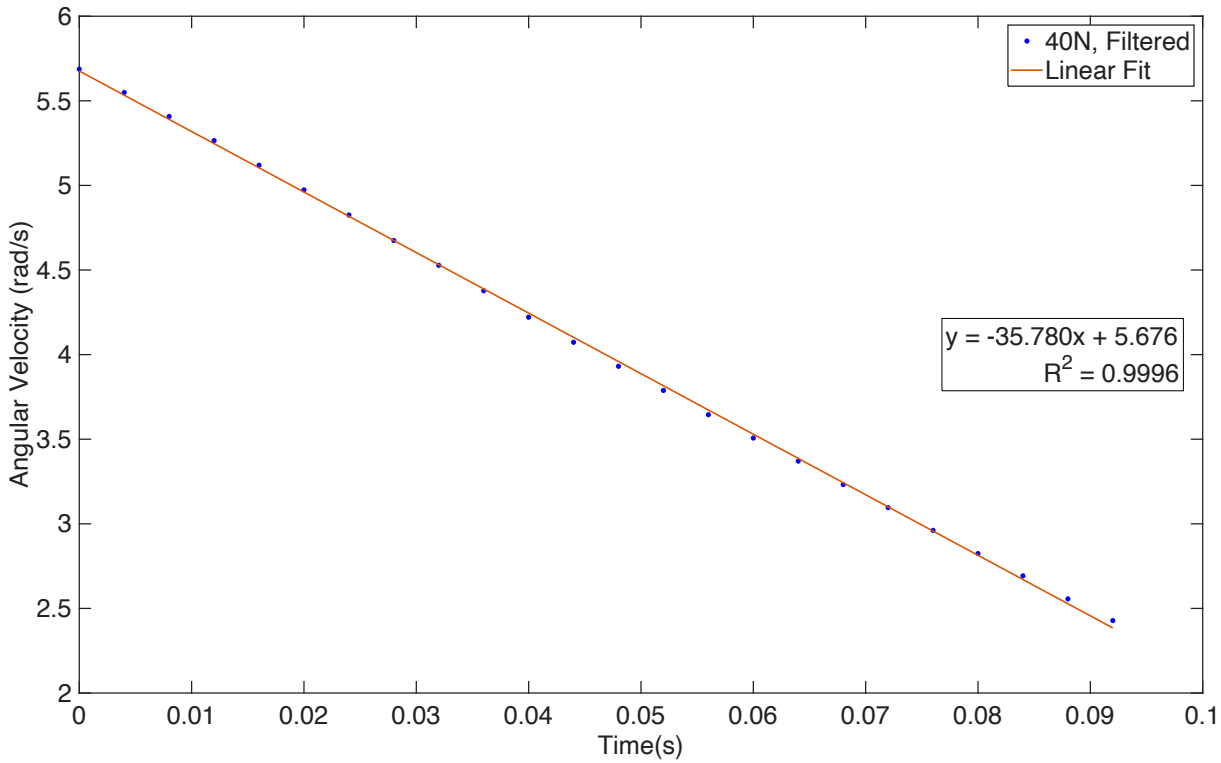

Figure 16. Deceleration phase extracted from passive deceleration test.

Table 3. Summary statistics of gearbox inertia and friction deceleration tests, 40N $[0.00525kg \cdot m^2]$ load.

Gearbox Input Velocity (rpm)	Gearbox Output Velocity (rad/s)	Median Deceleration	Deceleration Std	Average R^2
150	0.982	-8.357	2.519	0.990
200	1.309	-12.058	1.107	0.993
250	1.636	-16.048	1.229	0.993
300	1.964	-18.978	1.779	0.992
350	2.291	-21.359	0.533	0.993
400	2.618	-21.818	2.985	0.990
450	2.945	-25.275	2.210	0.995
500	3.272	-27.346	1.664	0.994
550	3.600	-27.040	1.153	0.991
600	3.927	-29.786	0.903	0.997
650	4.254	-30.259	1.657	0.996
700	4.581	-30.352	0.754	0.998
750	4.909	-32.110	1.415	0.999
800	5.236	-32.581	2.204	0.999
850	5.563	-33.478	1.133	0.999

Gearbox Input Velocity (rpm)	Gearbox Output Velocity (rad/s)	Median Deceleration	Deceleration Std	Average R^2
900	5.890	-35.518	3.337	0.999
950	6.218	-37.193	1.646	0.999
1000	6.545	-36.182	0.804	0.999
1250	8.181	-40.115	1.318	0.998
1500	9.817	-50.816	3.737	0.999
1750	11.454	-48.495	8.578	0.998
2000	13.090	-52.890	3.409	0.998
2250	14.726	-58.091	4.328	0.999
2500	16.363	-65.189	1.855	0.999
2750	17.999	-58.191	4.998	0.999
3000	19.635	-58.114	6.431	0.999
3250	21.271	-57.350	4.297	0.999

Initial velocities are expressed in rpm as this is the unit used by the motor controller, and actual setting used. Equivalent velocities at the output shaft are presented for consistent units with the rest of the report. The summary data in Table 3. shows a general trend of higher decelerations for higher initial velocities, suggesting a velocity dependence to the deceleration, and a velocity dependent source of friction. Tests for the 40N ($0.00525kg \cdot m^2$) are shown, but the entire procedure is followed at 8N increments from 8N to 56N.

The median values are then used to plot a deceleration curve (40N curve shown as a representation of the typical results). A 2-Term Power Law fit is used to represent the data. The R^2 value is given as a measure of fit quality.

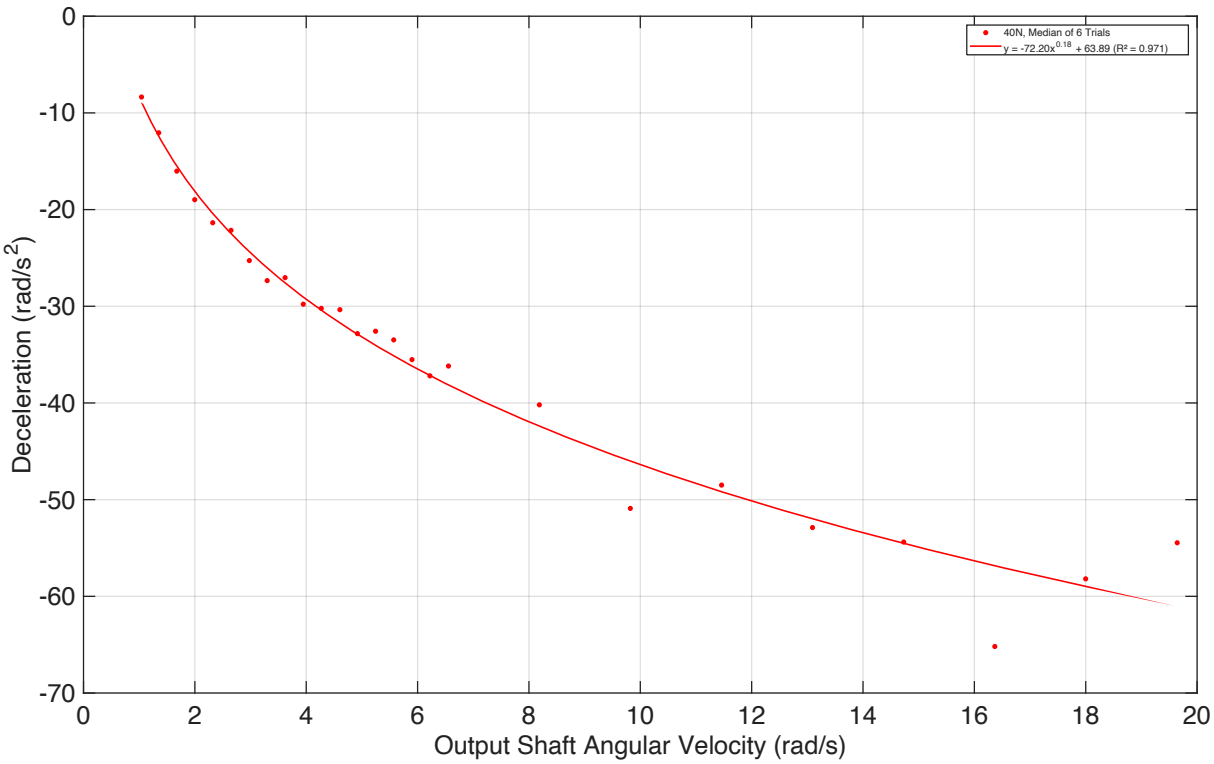

Figure 17. Measured deceleration as a function of angular velocity.

As seen in Figure 17, the power law with the equation $\omega = -72.20x^{0.18} + 63.89$ has a coefficient of determination R^2 of 0.971, indicating an excellent fit with the data. The data and resulting equation indicate that the higher the initial velocity, the higher the deceleration for any given added inertia. The rate of increase in deceleration is much greater for the lower initial angular velocities than it is for the higher ones. Data is acquired at smaller initial velocity intervals below 6.5 rad/s to better capture that rapidly changing rate of decrease.

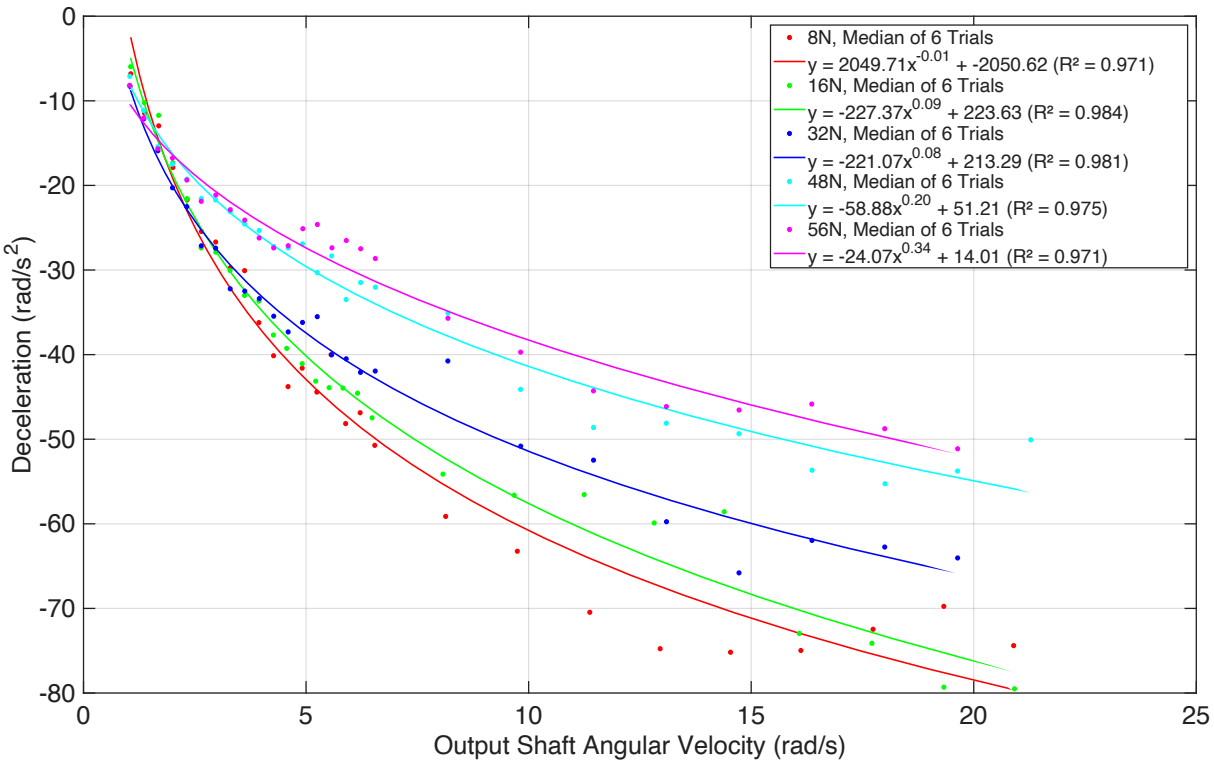

Figure 18. Summary of deceleration curves across all tested and velocity combinations.

The summary deceleration curves in Figure 18 show that the trend seen for the 40N tests is consistent for the entire range of added inertias. In addition, these curves suggest that the higher the inertia, the slower the deceleration, and that the variation appears predictable.

The difference in deceleration between two tests, with different weights, is then used to solve for the system's inertia using the rotational equation of motion. Since this results in multiple inertia values (one for each deceleration curve pair), the rest of the analysis follows a leave-one-out cross-validation approach to select the inertia and friction coefficient combination that best describes the entire system.

6.4. Leave One Out Analysis

To determine the optimal inertia and friction coefficient, a leave-one-out cross-validation approach was used. For each iteration, all test data was used except for the data from one of the additional weights. The resulting inertia and coefficient combination was used to predict the results from the excluded weight data, then tested against that actual data to evaluate the error. This was repeated for each of the weights. The iteration that led to final coefficients in the current version of the dynamometer is detailed below.

6.4.1. Experimental Determination of Inertia

Once the deceleration curves for all included weights are generated (tests from the 40N weight are excluded in the example shown in Figure 19), the difference in decelerations between each pair of weights can be used to determine the system's inertia. The two highest and lowest values for each pair of weights are removed to account for measurement uncertainties. The mean (average) of all pairs is then used as the estimate of the rotational inertia of the system. The mean inertia resulting from this analysis is $0.011kg \cdot m^2 \pm 0.005kg \cdot m^2$. The effectiveness of the approach is demonstrated in the cross-validation results (Table 5.3), where the inertia and friction combination with the lowest prediction error (RMSE = 0.798) when tested against excluded experimental data is used as calibration constants to achieve a constant resisting torque. The final validation demonstrated that this method worked in practice.

6.4.2. Empirical Friction Equation

With the inertia of the gearbox known, the deceleration curves can be used to obtain the friction in the gearbox for each weight. Since friction should only depend on the velocity, the friction curves should be the same in theory. Experimentally, there is some slight variation with an average standard deviation of 0.03 N·m across the tested velocity range (max 0.07 N·m at the lowest speed). This corresponds to an average coefficient of variation of 6.5%. These are therefore calculated and averaged into a singular friction curve that can be used to calibrate the gearbox.

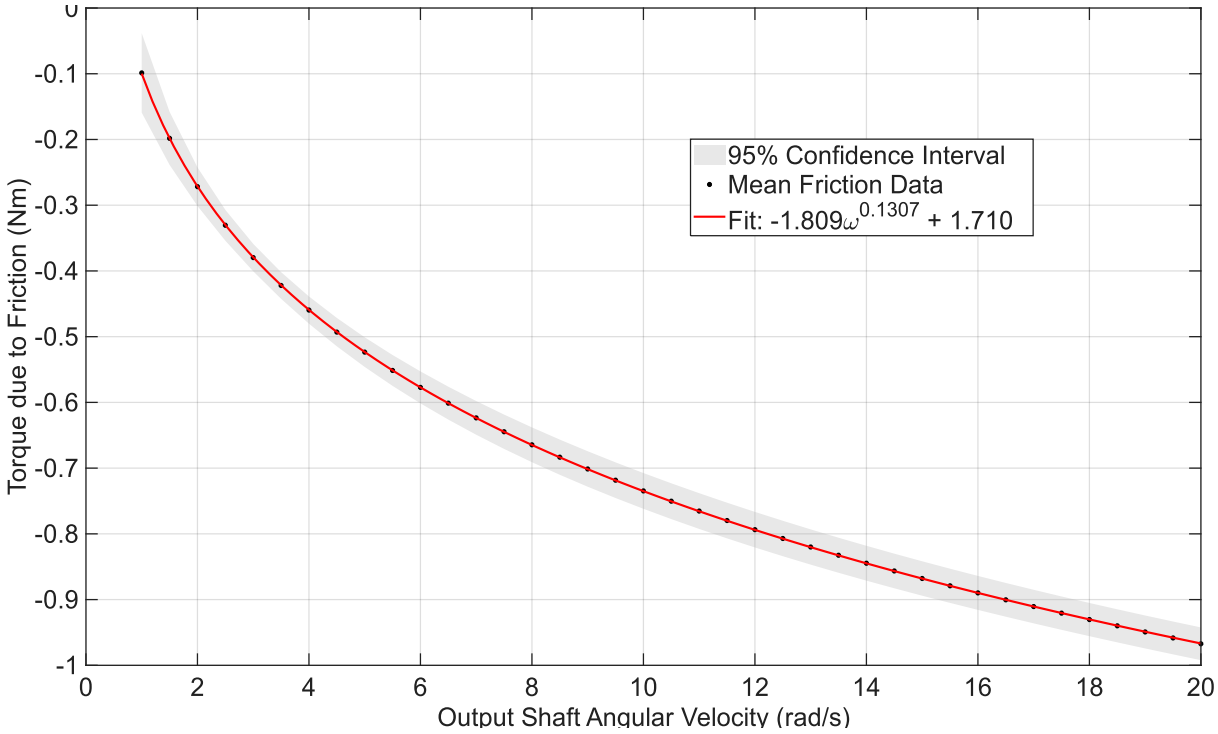

Figure 19. Empirical gearbox friction with confidence interval.

The curve shown in Figure 19 results in the following equation:

$$T_{\text{friction}} = -1.809 \cdot \omega^{0.1307} + 1.71$$

This entire process is done with the full dataset, systematically removing one of the weights and testing with the remainder of the data. The curve formed by the parameters from the 40N leave-one-out analysis are shown because it was ultimately the combination that had the lowest error when compared to the actual test data (Table 4) and worked in practice.

6.4.3. Friction Equation Validation

The equation developed above is used as a theoretical friction curve to plot the expected deceleration of the 40N dataset. This predicted curve is then compared to the actual deceleration values in that dataset to calculate the error.

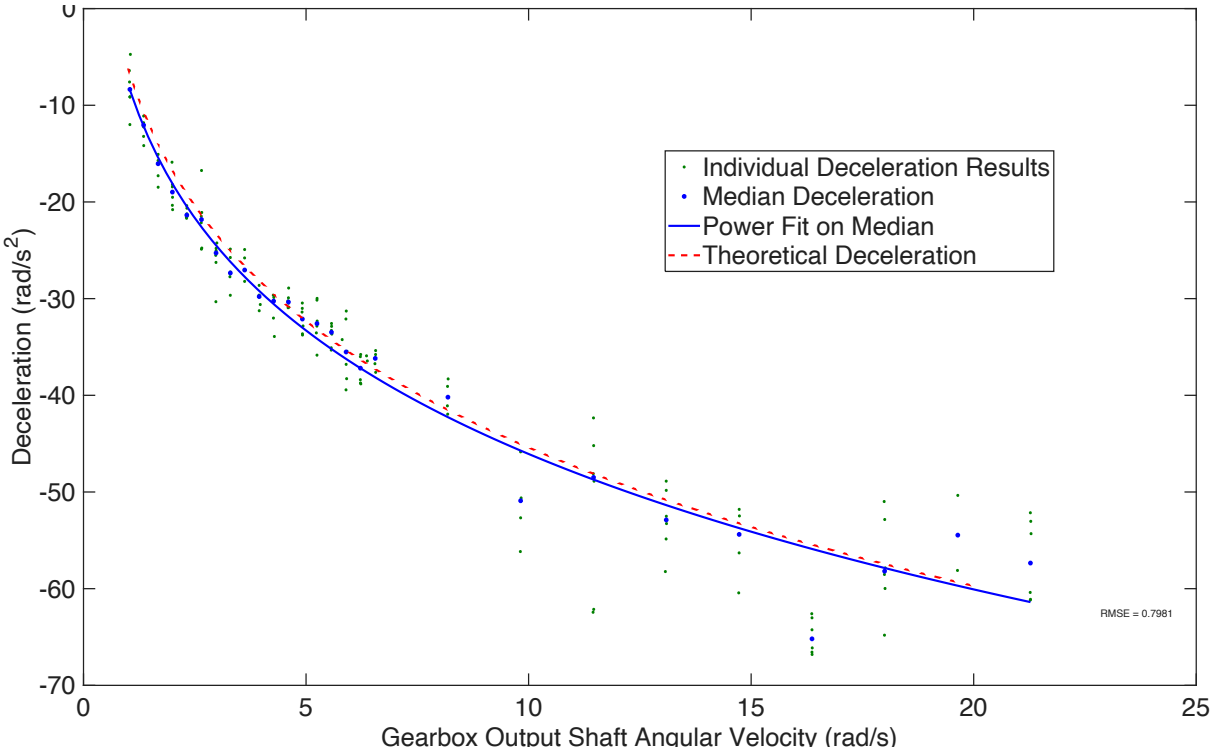

Figure 20. Predicted versus measured deceleration for leave-one-out validation.

The results of each iteration of the leave-one-out analysis, with the goal of selecting the parameters that best predict the behaviour of the system is in Table 4.

Table 4. Error analysis for each of the leave-one-out friction results

	Inertia		Coeffi cient	95% Confidence		Coeffi cient	95% Confidence		Coeffi cient	95% Confidence		
Test Weight /Left Out	Avg	Std	a	-	+	b	-	+	c	-	+	Root Mean Square Error
8	0.00768	0.00325	-1.06	-1.07	-1.06	0.164	0.163	0.164	0.965	0.959	0.972	7.16
16	0.00836	0.00381	-1.32	-1.34	-1.31	0.142	0.141	0.144	1.23	1.21	1.24	1.64
32	0.00860	0.00289	-1.17	-1.18	-1.15	0.159	0.157	0.160	1.07	1.05	1.08	3.13
40	0.0109	0.00532	-1.81	-1.83	-1.79	0.131	0.129	0.132	1.71	1.69	1.73	0.798
48	0.0111	0.00540	-2.08	-2.11	-2.06	0.118	0.117	0.119	1.98	1.96	2.01	1.46
56	0.0114	0.00532	-2.28	-2.30	-2.26	0.113	0.112	0.114	2.19	2.17	2.21	2.35

The model that best predicts the behaviour of the missing dataset is the one developed while leaving the 40N data out. The friction curve described by the empirically determined coefficients from that data predicts the actual deceleration observed in inertia/friction tests with 40N of added weight, with an RMSE of 0.798.

6.5. Compensation Validation Results

Prior to validating the system over the entire range, a brake-chopper was implemented to address the large voltage spikes encountered during the initial benchmarking. Figure 21 shows the effects of the brake-chopper in high energy tests, replicating the high voltage spike condition seen during initial system testing to assess the efficacy of the brake-chopper in protecting the electronics.

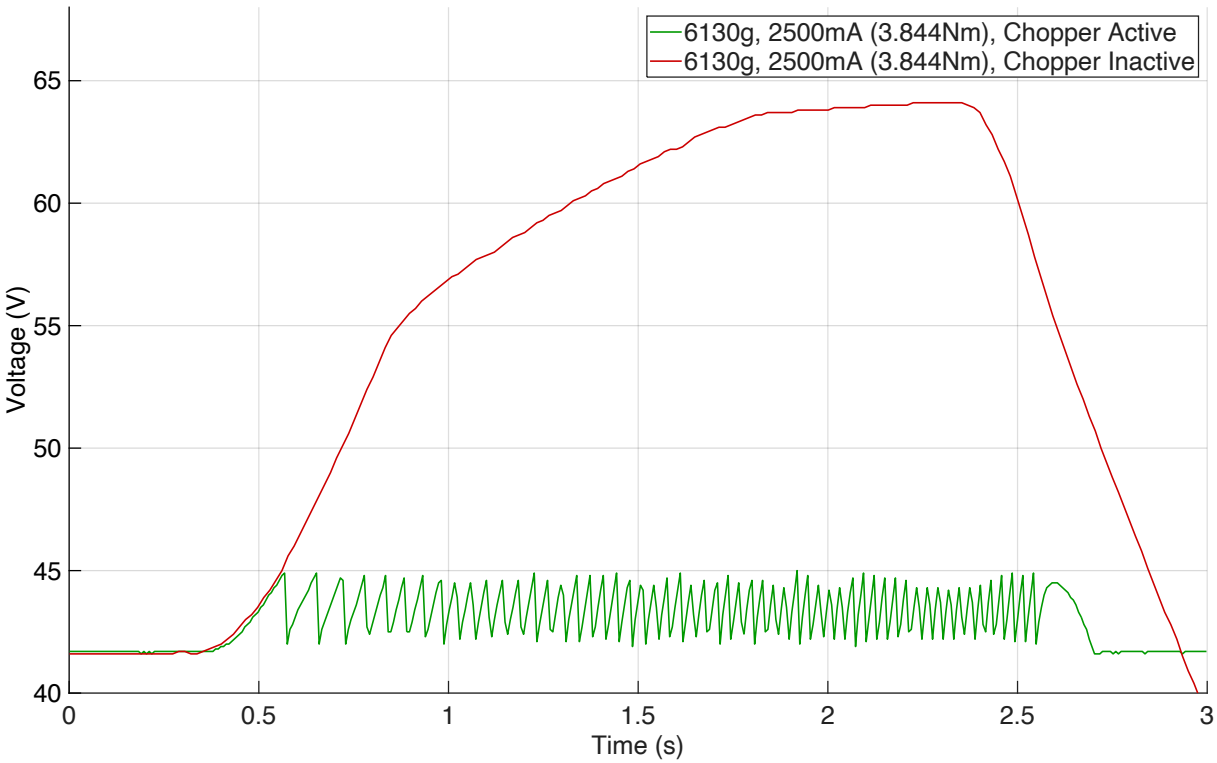

Figure 21. Effect of brake chopper on high-load drop test DC bus voltage.

As seen in Figure 21, the voltage measured by the motor controller greatly exceeds the rated voltage of the motor (48V) when a brake-chopper is not used. Once the brake-chopper is implemented and activated, it successfully keeps the voltage between 42.5 and 45V. All subsequent tests were completed with an active brake-chopper.

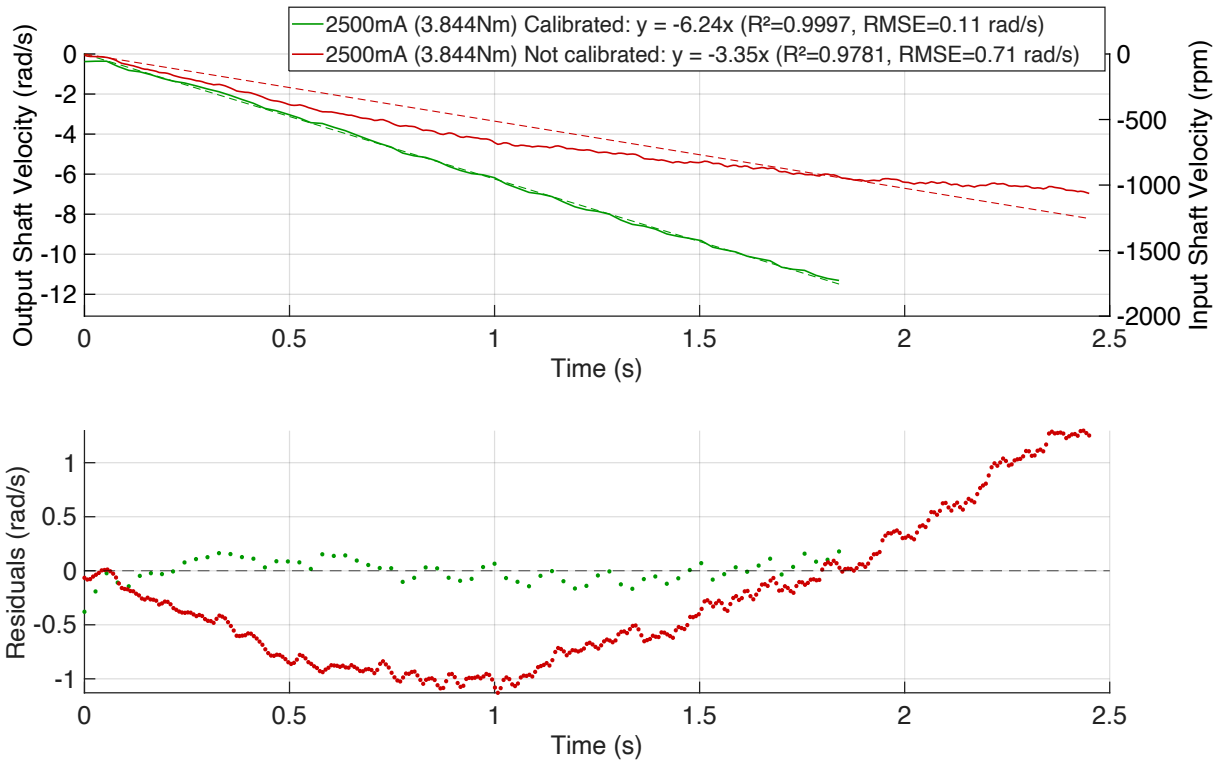

Figure 22. Drop test velocity trace with and without friction compensation.

The drop test that did not use the calibration curve for real-time compensation (Figure 22) deviates from the expected constant torque. It displays the same decreasing rate of increase in velocity as seen in the gearbox-only and preliminary system tests. The same test conditions with the active compensation being used can successfully maintain a constant torque, as demonstrated by the nearly perfect linear fit. The residuals for the uncalibrated curve have a clear pattern, while those for the calibrated curve are all closer to 0 and show a sinusoidal pattern that can be explained by the motor control loop.

To validate the real-time compensation's ability to achieve a constant torque, drop tests across a range of resisting torques were completed using the same pulley system as the initial benchmarking. The results of these tests are shown in Figure 23. A best fit line, using a linear least square regression, is used to illustrate the ability of the system to achieve a linear increase in velocity, which is indicative of constant acceleration and thus constant torque.

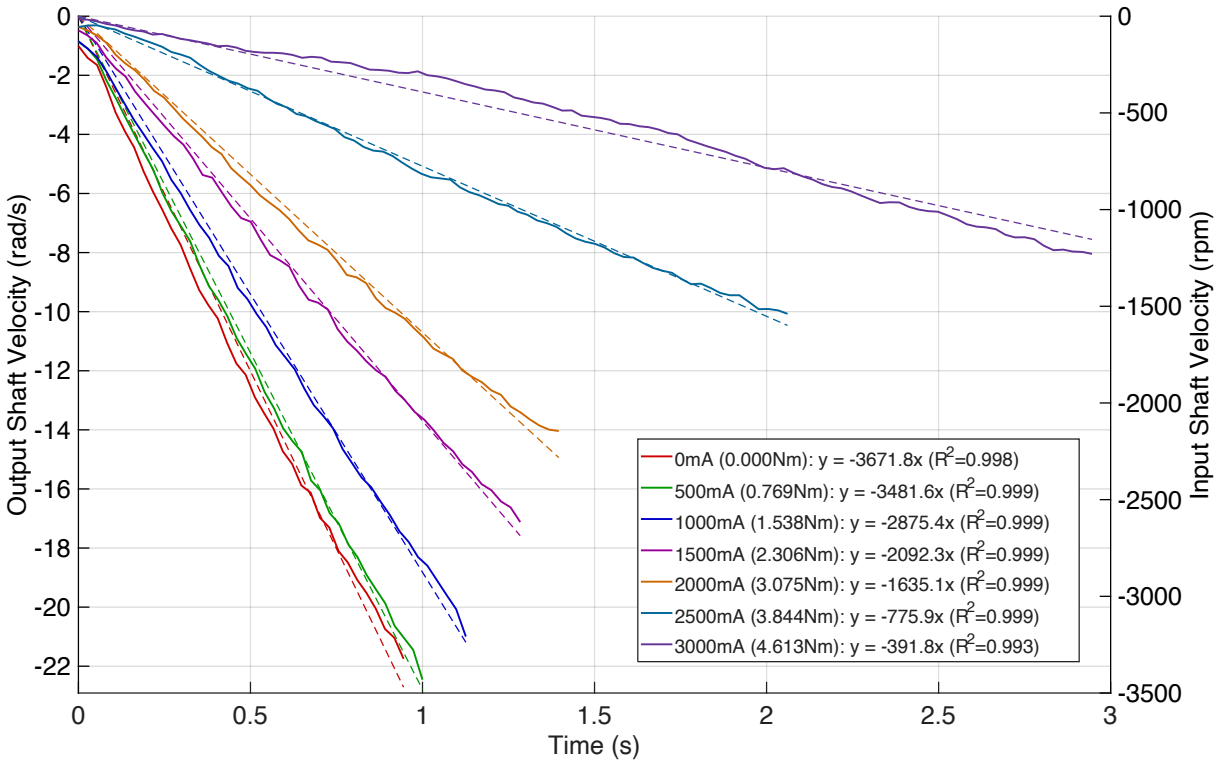

Figure 23. Drop test velocity traces with friction compensation across full resisting torque range.

The results in *Figure 23* show that as resistance increases, the magnitude of acceleration (the slope of the velocity curve) decreases. This is consistent with the lower net torque. Each line has an $R^2 \geq 0.99$ indicating that more than 99% of the variability is captured by a linear fit, validating the assumption of constant acceleration.

6.6. Isometric Testing Validation

To calibrate the torque arm, strain gauges, and ADS1256, multiple weights ranging from 0-33N were tied to the horizontal 15cm torque arm while the brake was engaged. The voltage outputs of the ADS1256 were recorded without additional processing. The results of these tests are shown in Figure 24.

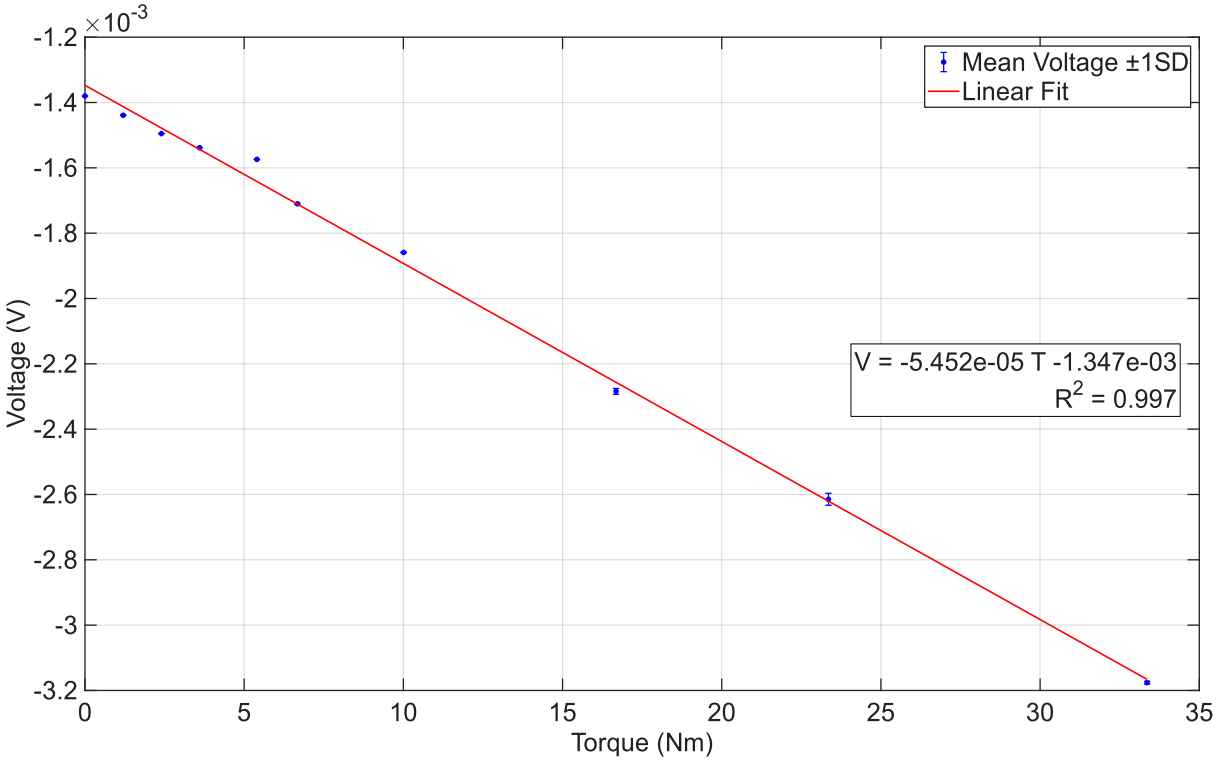

Figure 24. Strain-gauge torque calibration using known static loads.

The linear regression indicates that the torque arm's sensitivity is -5.45 x 10^{-5} V/N·m, with a -1.34 x 10^{-3} offset. It showed excellent linearity (R^2 = 0.997) and a low RMSE (2.95 x 10^{-5} V). The maximum error is 3.77% of the tested range, which corresponds to 2.7% of the full span (78 N·m)

7. Discussion

This chapter examines the experimental results as they relate to the characterization, calibration, real-time compensation and validation of the upper-limb dynamometer. The focus is on the need for a portable and affordable way to measure isotonic power, since gold-standard systems are large and expensive. There is a clear need for compact devices that can reliably provide a controlled resisting torque, which is essential for clinically meaningful results.

7.1. Overview

Precise resistive torque control in a backdriven scenario is an atypical motor application and presents significant challenges. While field-oriented control can in theory provide constant torque with precision, the gearbox losses meant that the system did not behave as an ideal torque source when integrated into the prototype. The gearbox introduced velocity dependent friction and inertial effects that caused a deviation from the expected linear velocity-time profiles. As a result, simply commanding constant torque and relying entirely on the FOC controller was insufficient. The experimental approach to obtaining a constant resistive torque under load required a combination of drop tests and passive deceleration experiments to isolate and characterize the sources of nonlinear behaviour. By separating and analyzing the system's primary components, the motor and the gearbox, the correct source of the observed behaviour is determined before significant characterization efforts are taken. The apparent predictability in preliminary benchmarks and baseline tests suggests that a calibration curve designed to compensate for the gearbox losses could provide the foundation for real-time compensation.

The discussion begins by evaluating the full system's behaviour in its off-the-shelf configuration and highlights the need for an adjustment to the control strategy. It then identifies the sources of unwanted behaviour by testing the motor's ability to maintain constant resisting torque in isolation, and the gearbox's behaviour during drop tests. A detailed analysis of the inertia and friction modeling procedure, and its results follows. Finally, the validation of the calibration curve, a discussion of the practical applications of each result, and the limitation of the current prototype completes the discussion.

7.2. Interpretation of Full System Drop Test Behaviour

Drop tests on the fully assembled system provide a baseline for the dynamometer's response when commanded to resist a constant, known external torque with a constant resisting torque. Figure 10 and Figure 11 show velocity-time profiles for two drop tests under different conditions. In both cases, the motor was commanded to resist motion

with a fixed torque by limiting the motor current and attempting to maintain a velocity of 0. This resulted in the motor attempting to stop the motion but only with the amount of torque it could provide with the limited current. For an ideal system, angular velocity would increase linearly (due to a constant net torque, and a constant acceleration), as a mass falls under the influence of gravity. The velocity profile, shown in Figure 10, deviates significantly from this ideal. The velocity profile, as measured by the NDI Polaris Vega camera, shows a rapid initial increase in velocity at the beginning of the drop test, consistent with the expected acceleration due to the falling mass under gravity. The velocity then quickly reaches a plateau. This nonlinearity and plateau suggest that the internal resistance is not constant, and that it requires further investigation.

The system's general torque equation is:

$$\tau_{net} = I\alpha = \tau_{gravity} - \tau_{motor} - \tau_{resistance/losses}$$

where τ_{motor} is set by the controller, $\tau_{gravity}$ is determined by the dropping mass, and $\tau_{resistance/losses}$ is internal resistance. A constant resistance would simply appear as an additional constant resisting torque, reducing the net torque on the shaft, but would maintain a linear velocity profile. Figure 10 and Figure 11 suggest that as velocity increases, the internal resistance to motion increases, further reducing the net torque and slowing down the acceleration of the falling mass. The system cannot maintain the consistent and constant resisting torque required for accurate isotonic dynamometry.

The nonlinearity in the velocity profiles shows that the internal resistance is not purely linear with velocity, so coulomb friction is unlikely to be a major contributor. Comparing the two tests, the first (Figure 10) used a 4.13 kg mass and 1500mA current limit, while the second (Figure 11) used a 5.5 kg mass and a 500mA current limit. The higher torque and lower motor resistance ensures that the second test reaches higher peak velocities. The increase in velocity once again decreases in rate as the test progresses. This suggests that the increase in internal resistance is non-linear with velocity, and that it causes a decrease in the net effect of an external load on the dynamometer. The behaviour is also observed in a range of torque/velocity conditions.

The most likely sources of this internal resistance are mechanical friction, back electromotive force (back-emf) from the motor, and electrical losses such as winding resistance or controller limitations. The exact source of the observed behaviour is likely complex and composed of a combination of these factors. The experimental setup and the design of the dynamometer minimized the effects of electrical losses and controller limitations by ensuring the system operated within the specified range as recommended by the manufacturers. Mechanical friction, especially in the gearbox and bearings, is a likely source of this resistance. If friction is a dominant factor, resistive torque would increase either linearly or non-linearly, depending on the mix of coulomb and viscous

friction within the gearbox. If back-emf is a dominant factor, the velocity-time curve would approach a terminal velocity when the applied external torque (the falling mass), is balanced by the back-emf resistance. Although the choice of field-oriented control as a core control strategy is intentional and could theoretically handle the back-emf on its own, these tests were insufficient to isolate the exact sources of the resistance and the relative contributions.

A fixed current limit as the only method to apply a constant resistance is insufficient for applications that require precise torque control while a motor is backdriven, especially across a wide range of velocities and with unknown losses. The system's performance is limited by nonlinear resistance which cannot be compensated by simply commanding the motor to maintain a constant torque. This was a critical challenge in dynamometry with the proposed approach (using an active motor). Accurate and consistent resistive torque is essential for a valid measurement, and the inability to achieve this goal limits the use of such devices in clinical and research settings.

The observed behaviour, and the inability to isolate the motor's electrical effects from the gearbox's passive resistive effects, justify separating the motor from the gearbox for further testing. This allows the characterization of each component's contributions and allows the development of component-specific compensations as required.

7.3. Component-Level Analysis (Individual Motor and Gearbox Characterizations)

To understand the system's internal resistance, the assembly was separated into its primary components: the motor and the gearbox. Drop tests were completed on each individual component. These drop tests clarify the origin of the observed non-linearity and justify the subsequent characterization and modeling efforts.

7.3.1. Motor-Only Drop Tests

The motor-only configuration was achieved by removing the gearbox from the assembly and directly coupling the motor shaft to the test wheel that held the passive markers. The test wheel was part of the pulley system holding the mass used for drop tests. The 0.25 kg mass used in these tests resulted in a nearly perfect linear velocity-time profile (Figure 12), as confirmed by a linear least squares regression's R^2 of 0.997. Under a fixed current limit of 3A, corresponding to 0.29 N·m (Kt = 0.096 N·m/A), the motor produces a nearly constant resistive torque as indicated by the system's angular acceleration remaining constant.

$$\tau_{net} = I\alpha = \tau_{gravity} - \tau_{motor} - \tau_{resistance}$$

Where τ is torque (N·m), I is inertia (kg·m^2), and α is acceleration (rad/s^2) the summarized results of all motor-only drop tests, shown in Table 2, confirm that these results are consistent across the full range of tested motor torques. The low standard deviation for tests at 0.5-2.500 A suggests a high level of precision and consistency in torque output since the coefficient of variation is consistently below 0.66%. The high linearity of the velocity curve confirms that the motor and controller's contributions to the velocity-dependent resistance are negligible. The tests completed with higher motor torque (3 A) had a slow acceleration of $2.112 \pm 0.138\, rad/s^2$, suggesting the torque control may be less effective at lower velocities, or the resistance at lower velocities causes more variability. This is sufficient to confirm that the FOC controller, and the motor are not the cause of the non-linear velocity profile observed in Figure 10 and Figure 11. In addition, a plot of the acceleration vs resisting torque indicates a nearly perfect linear relationship between the two (Figure 12), indicating that the motor's torque command scales proportionally to the resistance it provides against a constant external torque. This is the expected behaviour.

7.3.2. Gearbox-Only Drop Tests

The gearbox was tested alone by mounting the shaft directly to the same test wheel and pulley system used for motor tests. Drop tests were done with the following weights: 1.032 kg, 2.058 kg, 3.073 kg, and 4.099 kg. These tests were passive since the motor was removed. No external resisting torque was provided. Results from these drop tests, shown in Figure 13, reveal a rapid increase in angular velocity, followed by a clear decrease in the rate of change of velocity. The tests with the smaller masses reached a plateau similar to the lower velocity baseline test in Figure 10. The 3.073kg and 4.099 kg drops reached a higher velocity than the others and had a similar decrease in acceleration as the full system test shown in Figure 11.

Figure 13 also shows that the non-linearities appear in the full range of tested weights. The observations provide direct evidence that the gearbox is the dominant source of non-linearity and that frictional losses are major contributors. The velocity profile observed in the gearbox mirrors the one seen in the fully assembled system, while the motor tests remain linear. This justifies the subsequent focus on gearbox friction for characterization and calibration. The passive nature of the gearbox, and fact that the non-linearity is observed in all weights tested, strongly supports the idea that a calibration curve can be developed for use in active compensation of the varying gearbox resistance.

The 1032g tests, in particular, can provide some information regarding the gearbox's dynamic characteristics because it reaches a state of constant velocity. This can only be achieved when the torque is balanced. The velocity time-trace indicates that the falling mass accelerates initially, then the rate of increase in velocity decreases to a plateau

where the mass continues to fall for $\approx 2s$ without acceleration. The fundamental equation describing this is:

$$T_{net} = T_{gravity} - T_{friction} = I \times \alpha$$

where I is the inertia of the gearbox and wheel (kg·m^2).

Since the test reaches a steady state and drops at constant velocity,

$$T_{net} = 0$$

$$T_{gravity} = F \times r = (1.032kg \times 9.81\,{}^{\mathrm{m}}/_{s^2}) \times 0.15m$$

$$T_{friction} = T_{gravity}$$

$$T_{friction} = 1.519Nm$$

This is the friction in the gearbox when operating at a low constant velocity of 3.91 rad/s (Figure 13). At such low velocities, the main contributor is typically coulomb friction. While this gives an idea of friction losses in the gearbox, it does not account for velocity-dependent non-linear frictional effects such as viscous friction, shaft seal drag and other bearing losses. For the high-fidelity measurements needed in isotonic dynamometry, further characterization is required to correct for those losses.

7.4. Passive Deceleration Tests: Experimentally Determining the Inertia and Friction of The Gearbox

A robust calibration curve is necessary for the active friction compensation required for this system to achieve a constant resisting torque when backdriven. This section discusses the experimental strategy, data processing, and results that lead to a friction calibration curve capable of accurately predicting the gearbox's behaviour in the full range of velocities required for this application.

The approach uses passive deceleration testing with various weights and velocities, regression analysis, and the development of a power-law friction equation. The friction compensation equation is then validated with drop tests.

7.4.1. Passive Deceleration and Data Processing

The friction and inertia of the system are two variables required to understand the behaviour of the gearbox. Since friction is observed in the form of an opposing torque, the two variables are not independent. The equation describing the full system's behaviour as it rotates a known mass is:

$$\tau_{net} = I\alpha = \tau_{motor} - \tau_{friction}$$

To isolate and quantify the frictional and inertial properties separately, passive deceleration tests were performed. These tests required a custom fixture, detailed in the methodology (section 5.2), which allowed the motor to drive the load to a fixed velocity. Once that velocity was reached, the motor was disconnected from the gearbox. This eliminated any external forces from the system, leaving friction as the only force decelerating the rotating masses and reducing the fundamental equation to:

$$\tau_{net} = I\alpha = -\tau_{friction}$$

Multiple trials were completed, with varying weight. This changing inertia is what allowed the empirical estimate of the gearbox's real inertia.

As illustrated in Figure 15, the filtered data eliminates most of the noise without affecting the general trend. Most importantly, the filtered data closely follows the deceleration phase. This ensures that the decelerations derived from this methodology reflect the actual behaviour of the system and are not a result of data processing artifacts. The slope of the velocity curve during the deceleration phase was identified by linear regression and used as the instantaneous deceleration for that trial. The high R^2 values across all trials documented in Table 5.2 confirm the validity of the linear regression approach. The relatively low standard deviations suggest a good repeatability in the experimental method and through repeated tests. The median deceleration was used, rather than the mean, for its robustness against outliers.

A key strength in this approach is the ability to isolate the frictional contribution of the gearbox from all other effects. The physical decoupling of the motor allows the masses to decelerate passively, and the results exclusively reflect the mechanical losses in the gearbox. More complex, closed-loop systems, such as tests done with the gearbox and motor still connected, cannot achieve this level of isolation. Potential sources of error and additional mechanical losses can stem from minor misalignments in the test setup and friction in the bearings used specifically in this fixture. This is mitigated by careful assembly, the use of multiple trials, statistical methods, and a final validation of the compensation strategy. These sources still represent an inherent limitation of the test setup, and the experimental nature of the characterization effort.

7.4.2. Power Law Friction Equation

The relationship between angular acceleration and initial velocity, based on gearbox passive deceleration tests, was non-linear. For each combination of test weight and initial velocity, the median deceleration of 6 tests was plotted against velocity. The passive deceleration tests all resulted in a similar curve (as shown in Figure 17 and Figure 18). Several regression models were evaluated. A two-term power law consistently produced the lowest error, and the model was fit using the following linear regression described in equation (5.6). Although not a mechanistic model, it was able to

capture the linear and nonlinear effects with sufficient accuracy. The 95% confidence intervals closely follow the best-fit line in Figure 19, and goodness-of-fit metrics for each tested weight support the use of a two-term power law (Figure 18). A high coefficient of determination ($R^2 > 0.97$) in all tested weights indicates that this regression model closely represents the data regardless of the added inertia. The use of medians mitigates the influence of outliers and ensures that the model reflects the central tendency. The composite plots of all deceleration curves (Figure 18) reveal consistent shapes and spacing, demonstrating that the power law is robust across test conditions. Their curves appear to directly translate as weight increases, which supports the generalizability of the friction model and its use in real-time compensation.

The fitted parameters have a physical basis, for example, the parameter c accounts for a baseline resisting torque, likely from bearing drag or misalignment during the tests. The leading coefficient a and the exponent b were estimated with high precision, giving confidence that the behaviour is captured correctly. The precision of the parameters is evaluated during the leave-one-out analysis, where the 95% confidence intervals are tabulated in Table 4.

The power law friction equation is an empirical fit and has its limitations. While it generalizes well across the tested conditions, its extrapolation to untested conditions should be avoided unless further characterization or validation is completed in those conditions. In addition, the model does not account for temperature-dependent effects or long-term wear, which can alter the frictional characteristics. The device is intended to be used indoors, at temperatures near standard room temperature, and with low enough cycle times that the gearbox will remain in relatively similar temperatures to those that occur during calibration. Long term wear, however, may require periodic re-calibration. While these limitations are important, they occur in any data-driven, experimentally established calibration. Recalibration is also part of regular maintenance requirements.

7.4.3. Inertia Estimation and Friction Curve

The deceleration test protocol was developed to allow the inertia parameter estimation by linear regression. Using the method described in 5.2.1, and the analysis described in section 6.4.1, an inertia of $0.011\ kg \cdot m^2 \pm 0.005\ kg \cdot m^2$ was obtained. This value corresponds to $4.3 \times 10^{-5}\ kg \cdot m^2$ at the output shaft, which is consistent with reported inertias in the order of $3\ to\ 4 \times 10^{-5}\ kg \cdot m^2$ for direct gearboxes of similar size and gear ratio. The Kollmorgen G34VI-x-0160, for example, has a motor reflected inertia of $3.86 \times 10^{-5}\ kg \cdot m^2$. The gearbox inertia was then used to calculate the friction consistent with the observed decelerations[187].

Using the equation $\tau = I \times \alpha$, with the known inertia I and the experimentally measured declerations α, the torque due to friction could be calculated for each deceleration curve. Since friction should only depend on velocity, the friciton curves should theoretically be the same. The results of this analysis, as seen in Figure 19, gives a mean friction curve $T_{\text{friction}} = -1.809 \cdot \omega^{0.1307} + 1.71$ that represents the gearbox friction as a function of angular velocity. The constant term (1.71 N·m) corresponds to the baselline losses due to static friction, seal drag and slight misalignments. The velocity dependent term represents the viscous friction, gear mesh friction and bearing losses that are typically non-linear. In this case, they obey a power law within the tested velocity range. Friction, in this application, introduces errors in torque calculations that become problematic when attempting to maintain a constant resisting torque. The ability to characterize the gearbox correctly and obtain a friction curve that can be used for real-time compensation is essential to isotonic dynamometry. Friction typically also introduces heat, though this only becomes a challenge during continuous operation. Patients that require dynamometer will only be doing a few sets at a time so the use will be intermittent. The tight confidence intervals, as visualized in Figure 19 and tabulated in Table 4 indicate that repeated measurements, and in this case, multiple friction curves, yield similar results. This suggests good repeatability in the data, and that a control system design based on these parameters is likely to be effective.

7.4.4. Real-Time Friction Compensation Implementation

The characterization of the gearbox's friction profile was the foundation for developing the real-time compensation required for constant resisting torque during isotonic dynamometry. The passive deceleration tests successfully quantified the velocity-dependent friction relationship using the power-law relationship: $T_{\text{friction}} = -1.809 \cdot \omega^{0.1307} + 1.71$, but the practical implementation required careful integration with the existing FOC controller. This was achieved by transforming the equation into a feedforward algorithm that could operate in real-time while maintaining the precision and responsiveness needed for torque control. This was the transition from theoretical characterization to practical application, where the success of the implementation directly determines the dynamometer's ability to provide constant resistance.

The feedforward compensation algorithm implemented with the microcontroller used the relationship: $T_{command} = T_{target} - T_{friction}(\omega)$. T_{target} is the user specified maximum torque (usually a percentage of the maximum voluntary contraction) and its value is set before a test begins and represents the total resistance that should be provided throughout the test. The microcontroller reads the encoder's velocity outputs, calculates $T_{friction}$ using the power-law friction curve, and subtracts the friction torque from the target before sending the torque command to the FOC controller. The FOC controller can then act as a black box to provide the desired torque while using its own control

algorithms. This approach anticipates and compensates for velocity related errors before they could manifest as errors in the torque output. The angular velocity measurements were obtained and processed through the power law relationship at each control cycle.

A full compensation cycle in the current implementation of the dynamometer occurs in 27ms (30 Hz). The control loop within the microcontroller has explicit 1ms delays that occur at each communication with the FOC controller (4 in total). The microcontroller to FOC controller request-response cycles took 8-12 ms. Console print operations take 1-3 ms, and a 10 ms delay exists at the end of each loop. These delays were initially longer for communication diagnostics and were reduced but kept in place for reliable console outputs while developing the dynamometer. The request-response cycles were to monitor the voltage, monitor the velocity, set the torque and monitor the torque of the motor and were necessary to observe the behaviour and stability of the dynamometer while it is in operation. They confirmed that the brake-chopper addressed the voltage spikes effectively (as demonstrated in Figure 21), that the control loop was working as intended, and that the motor controller was responding to microcontroller commands appropriately. It is important to note that the friction compensation loop and the FOC control loop are different, and that the FOC controller operates at faster speeds. The manufacturer of the TMCM-1636 FOC controller states a PWM and current control loop of up to 100 kHz. Though this is a theoretical ceiling, it is reasonable to expect a velocity control loop of 10-20 kHz given the claimed performance and the extensive tuning the controller allows. Accordingly, the slower 30 Hz friction compensation loop issues setpoints that the TMCM-1636 enforces at its kHz rates until the next update.

Accurate real-time monitoring of parameters other than velocity is unnecessary during normal operation since the motor controller has internal safety measures to stop operation in abnormal conditions. Removal of the diagnostic messages, the delays and all request-response cycles except reading velocity and returning the friction torque compensation should reduce the cycle down to 4 ms, making it a 250 Hz system. The velocity-dependent friction calculation was implemented using fixed-point arithmetic to reduce computational overhead and minimize execution time. Memory allocation included dedicated storage for the friction model parameters and intermediate calculation variables. This approach was used due to the simplicity of power-law function, the simplicity of the mathematical operations, and the ease with which coefficients can be adjusted during development without rebuilding lookup tables.

7.5. Validation of the Friction Compensation System

Having established the friction compensation algorithm and its implementation, it was essential to validate the system's performance under controlled conditions. This validation was done by first ensuring safe operation of the system by implementing a brake-chopper to prevent voltage spikes, and completing drop tests with 6.13 kg (9 N·m on the output shaft) to compare velocity with an without an active brake-chopper, then, by completing drop tests at 6.13 kg at varying resisting torques to ensure constant torque is achieved in a full range of resistances.

Figure 21 shows the voltage results of a drop test with and without brake-chopper as reported by the motor controller. The brake-chopper dissipates excess energy into heat using a braking resistor. This test was done with a mass of 6.1 kg (9 N·m on the output shaft), and the lowest safe resisting torque of 2500 mA (3.84 N·m on the output shaft) to ensure that the voltage spike experienced in initial benchmarking could be replicated. Lower resisting torques resulted in an immediate system shutdown due to overvoltage. As seen in Figure 21, the drop tests with an inactive chopper had a voltage that quickly rose to 55 V and stabilized near 65 V before a system shutdown at 2.5 s. The voltage of the test with an inactive brake-chopper quickly dropped to 0 V, preventing further use of the dynamometer until the system was power cycled. This voltage increase is due to the motor acting as a generator when being backdriven. The test with an active chopper successfully maintains a lower voltage, protecting the motor and allowing it to function as intended regardless of the external torque applied. Its trigger point was 45 V, which allowed it to remain below the rated motor voltage and return to the baseline 42 V. As seen in the voltage plot for the test with an active chopper, the voltage increase is identical until it reaches the 45 V trigger, then rapidly drops back to 42 V before increasing again. This cycles quickly as the brake-chopper is activated as needed. Once the test is completed, the voltage remains stable at 42 V allowing further testing without a full system reset. Qualitative assessment of the braking resistor indicated negligible increases in temperature, suggesting that the intermittent use of the device, even at extreme weight to motor resistance ratios, would not affect the temperature enough to require cooling.

The velocity curves for a drop test with the same parameters is shown in Figure 22. The drop test without real-time compensation and an active brake-chopper, has a decreasing rate of increase in velocity, until impact with the ground at 7 rad/s. This is similar to the behaviour observed in gearbox-only and initial full-system tests. The drop test with real-time compensation and an active brake-chopper has a linear velocity profile indicating that it successfully maintains a constant torque throughout the test. This demonstrates that the friction compensation works as intended to keep a constant

resistance, and that further validation can continue with the existing compensation parameters and algorithm.

The brake-chopper's ability to mitigate bus-voltage spikes was confirmed first. The ability to maintain a constant resisting torque using the compensation method under high external loads, even when the resisting torque was lower, was then verified. Next, the functionality of the system was tested at 500 mA increments (0.77 N·m on the wheel) to verify the compensation over a wide range of resisting torques. These results, shown in Figure 23, demonstrate a linear velocity profile at all tested resistances, indicating that the resisting torque is constant. As the resisting torque was increased, the falling mass's measured acceleration decreased, which is consistent with applying a greater constant resistance. This is the behaviour that was expected for isotonic dynamometry. It further confirms that the system works as intended to keep a constant resisting torque against an external load.

7.6. Clinical Performance and Measurement Validity

The portable upper-limb dynamometer achieved excellent linearity in torque control as evidenced by the $R^2 \geq 0.90$ across the 0.61 N·m to 4.61 N·m range.

The experimental validation demonstrates that the system can maintain a constant resistance during drop tests where gravity and a falling mass provide a constant external torque. The successful friction compensation was implemented through an empirically derived power-law equation $T_{friction} = -1.809^{0.1307} + 2.71$. It achieved a linear velocity profile ($R^2 \geq 0.98$) across the entire tested range. Drop tests with 6.13 kg weight (9 N·m on the output shaft) and a range of resisting torques (0.77 N·m - 4.61 N·m) confirmed that the system maintains a constant resistive torque regardless of the movement velocity.

Response time analysis revealed that the current implementation has a 27ms control cycle, which includes communication between the main microcontroller and the FOC controller, in addition to diagnostic console messages to enable development and troubleshooting. These additional messages and diagnostic delays enabled troubleshooting during integration and preliminary testing, but had a control loop frequency of 30 Hz, which was still sufficient to maintain torque stability. As evidenced by the low RMSE of 0.11 rad/s of the calibrated test in Figure 22, the compensation algorithm worked despite the delays and console outputs. Even with the R^2 of 0.98 and RMSE of 0.71 rad/s, the residual plot for the uncalibrated test shows a clear systematic bias. The residuals for the calibrated test also have a small-amplitude sinusoidal pattern centered around 0 rad/s. This sinusoidal ripple is consistent with a torque control loop that is correcting to maintain a constant torque.

While the ability to maintain a constant torque in this use case is an advancement, performance limitations in the current iteration of the device require acknowledgement. The 30 Hz control loop, while sufficient to maintain a constant torque against a constant external load, falls short of the 500 Hz recommended minimum in literature for Rate of Force Development measurements. Simply removing all diagnostic functions will achieve a 4ms correction cycle (250 Hz), making the control much smoother. Further optimizations, such as the implementation of a real-time operating system and direct memory access could allow the separation of velocity update frequency from the motor control loop. This would give the dynamometer the ability to give more frequent velocity updates. Implementing the friction compensation directly in the motor controller as a lookup table could allow it to reduce the control loop even further but would sacrifice the ability to make quick adjustments to the parameters. The 27 ms control cycle, while suitable for isotonic assessment, represents a constraint for rate of force development applications.

The velocity measurement is currently tied to the motor control loop. Separating the velocity readings could theoretically allow an update frequency of 1000 counts per revolution of the motor shaft, as per the manufacturer's datasheet[176]. For a 0.5 rad/s angular velocity at the 16:1 gearbox output shaft, this would be a 1.27 kHz update frequency.

$$MotorShaftVelocity = 0.5\,rad/s \times 16 \div 2\pi\,rad/rev = 1.273\,rev/s$$

$$UpdateFrequency = 1.273\,rev/s \times 1000CPR = 1273Hz$$

With direct memory access, and the current implementation of CAN communication, this would be the minimum velocity sampling frequency during low-speed movements. The current implementation of CAN communication has a theoretical maximum of 9.2 kHz with the standard data frame and 1Mbit/s rate.

$$MaxUpdateFrequency = 1 \times 10^6\,\frac{bits}{s} \div 108bits = 9250\,\frac{frames}{s}$$

This makes the encoder the primary bottleneck in velocity measurement. The encoder is removable and can be replaced with higher resolution options, though the current implementation if fully optimized should be sufficient to obtain the 500Hz minimum, and could theoretically achieve the recommended 1kHz.

The system's sensitivity can be quantified for two measurement/control chains: torque sensing (isometric), and torque generation (isotonic). For the torque sensing chain, the strain-gage half-bridge uses 350Ω gauges with 0.76mm grid length [156], digitized by an ADS1256 (24-bit, up to 30kSPS, PGA1-64). The ADS input referred RMS noise at 1000 SPS is up to 2.93 μV [156]. The measured torque calibration, shown in Figure 24, has a sensitivity of 54.5 μV/N·m, and a max error of 0.19 N·m over the tested span. For the

torque generation chain, resisting torque is produced via FOC torque-axis current. The static torque actuation sensitivity, defined as the change in output torque per unit current at constant speed, is set by the motor torque constant and gearbox ratio. It is a fixed electromechanical property of the motor-gearbox combination. Using the motor datasheet values, Kt ≈ 0.096 N·m/A, so with a 16:1 gearbox the output torque sensitivity is ≈1.5 N·m/A [176], [177]. Angular velocity is derived from the encoder for friction compensation. At 4500rpm (471.24 rad/s) and 1000 CPR, this corresponds to ~75,000 counts/s at the highest expected velocity. Given the controller sampling interval, this sets the number of counts per update for velocity estimation and the smallest change in velocity used for friction compensation. In dynamic testing, the encoder resolution and velocity estimation do not alter this static sensitivity, but they do affect net torque accuracy during motion by introducing a speed-dependent torque bias and tracking error in the friction compensation.

The power-law friction equation is empirically derived and may not extrapolate beyond tested conditions, though 22 rad/s represents a reasonable range for most healthy patients as evidenced by the maximum velocity of 19 rad/s in elbow flexion and 27.9 rad/s in elbow extension achieved by athletes[169]. Long-term wear could alter frictional characteristics, requiring periodic re-calibration though the current implementation demonstrates excellent generalization across tested load and velocity conditions. Temperature variations are limited in controlled clinical environments, and low cycle times relative to the gearbox and motor's design for continuous operation ensure that the temperatures stay low.

The constant torque capability provides an advantage for valid isotonic assessments that cannot be achieved by less rudimentary methods such as lifting a weight. It provides a direct measure of velocity and power against a constant load throughout the entire movement and can track changes throughout a movement with high resolution. Standardized position can also control and mitigate any body momentum that can be used to assist the motion, ensuring that only the muscles normally involved in a movement are tracked and assistance from swinging motions or different positioning does not affect the results. In addition, the smooth and precise delivery of resisting torque can reassure patients[92], [136] who may be nervous around medical devices or have limited strength. Jerkiness with slower control systems can give the perception of instability which could affect the patient's trust and confidence in the device[131], [188].

7.7. Comparison with Existing Literature and Gold Standard Devices

The critical assessment of the system's capability to maintain a constant resistive torque, completed in section 6.6, establishes the foundation for direct comparison with existing

technologies. This section synthesizes the results of the technical characterization and validation and compares them with benchmarks from the literature on existing devices.

7.7.1. Technical Performance Benchmarking

The portable upper-limb dynamometer developed in this study was validated across a range of 0-4.61N·m of resisting torque (0-3000mA) due to safety considerations during benchtop testing on an open enclosure, and motor control troubleshooting. This represents 40% of the rated motor torque (7490mA), and 20% of the peak torque (14000mA), demonstrating proof-of-concept within conservative and safe limits for the developer and the device. The theoretical maximum resistance that the current motor, gearbox and controller combination can provide is 21N·m. Observations of the motor current measurement noise when the motor is static, and the thresholds for torque control activation by the controller, indicate that the controller begins to correct torque when a threshold of 400mA is reached (0.61N·m). As such, the theoretical range that can be achieved with full optimization of the system, and torque limits set to the maximum safe limits for the motor, is 0.61N·m to 21N·m. The mean MVC torque for healthy adults is frequently reported to be between 45N·m and 65N·m, with male dominant values higher, and female values closer to 50N·m[170], [189]. If full capabilities are unlocked, the motor-gearbox combination is capable of completing tests at up to 50% MVC for most healthy patients and up to 30% MVC for the strongest healthy adults. Operation at those peak values should be tested for temperature effects since the motor would be operating at its peak, though the low duty cycle and the time between tests should result in a negligible temperature increase.

Isokinetic testing protocols typically force a velocity limit in the 60°/s to 180°/s range (1 rad/s to 3.14 rad/s)[167], [190] though healthy humans can achieve angular velocities up to 25.6 ± 5.8 rad/s under controlled laboratory conditions when movement was completed with an isolated joint in the tested direction only. Tests that allowed countermovement, or tests that were completely unrestricted had slightly higher values[169].The portable dynamometer developed in this work was tested to velocities up to 22 rad/s while maintaining a constant torque. The velocity was only limited by the total available drop height and weight combination, since the tests ended when the weight reached the ground. Additional tests should be completed to ensure validity beyond the tested range.

The friction compensation curves that form the basis for this dynamometer's ability to complete isotonic power tests have been developed for velocities up to 22 rad/s, independent of the external torque. It has been validated for torque ranges of 0-4.61N·m and showed that the friction compensation algorithm is effective at maintaining the constant resistive torque required by the application. This demonstrated performance establishes a solid foundation for clinical application, with the primary

limitation being the need for validation across the full operational range and thermal characterization at peak operating conditions.

7.7.2. Portable Dynamometry Landscape

Handheld dynamometers are limited to peak force measurements and depend on the examiner for stabilization[22]. Isokinetic dynamometers can provide torque curves, and a measure of power, but their substantial footprint and complexity limit their accessibility to clinics[36], [75], [92], [97], [101]. The portable dynamometer with its reasonable weight of ≈19kg, and its compact dimensions addresses those practical barriers while providing both isometric and isotonic measurement capabilities.

Bench testing results demonstrate the successful achievement of constant resistive torque, distinguishing this device from existing portable solutions that lack friction compensation [191]. The 30Hz control loop, however, represents a limitation compared to the 500Hz minimum recommended for rate of force development measurements, though optimization to 250Hz is readily achievable. This control loop represents the rate of friction correction. FOC torque adjustments are independent, and velocity readings can be obtained at rates greater than 1kHz when decoupled from the friction corrections.

7.7.3. Patient Population Considerations

The device's technical capabilities address common challenges faced by patient populations with reduced limb function. Lawrence et al. found that upper limb weakness affects 77.4% of stroke patients, making it one of the populations for whom this device would be the most beneficial[192]. Similarly, spinal cord injuries often affect the upper-limb, with tetraplegia accounting for 51% of cases at discharge in the US[193], and 62% of traumatic cases in Canada [194], [195]. The validated torque range of 0.61N·m-4.61N·m, and capability to test up to 23N·m accommodates the various strength capabilities of those patients. In many existing systems, testing at lower torque would require a separate dedicated dynamometer. In contrast, the modularity of the prototype allows this to be achieved simply by changing the gearbox and recalibrating, rather than designing an entirely new device. Alternative gearbox options could potentially provide a wider torque range, and for the patients with the most pronounced functional limitations, running the dynamometer without a gearbox is an option.

7.8. Research Contributions and Innovation

The achievement of constant resisting torque during testing with an external load is the primary technical contribution of this portable dynamometer. Its ability to do this

successfully distinguishes it from handheld devices that only give peak force, and its small size distinguishes it from the large isokinetic dynamometers that are considered the gold standard. The technical challenge in maintaining the constant torque required systematic characterization of the main sources of error, integration of all components, and a real-time compensation algorithm.

The compensation developed in this work is an extension beyond conventional FOC applications documented in literature. The implementation of friction compensation in backdriven applications such as dynamometry required an atypical empirical characterization approach. The power-law friction equation $T_{friction} = -1.809\omega^{0.1307} + 1.71$ developed through the passive deceleration tests addressed velocity dependent losses that are not typically assessed in conventional FOC implementations, where the motor is driving the load. The compensation method taken in this work represents a hybrid approach that maintains the independent and rapid millisecond torque adjustments of the FOC controller while providing friction correction every 27ms as per the external microcontroller's control cycle.

The system's ability to maintain a constant torque, and its direction independent friction characterization and algorithm design represent an advancement in portable dynamometry. One of the fundamental challenges in upper-limb dynamometry is maintaining measurement accuracy and precision with varying movement speeds and external loads. This is directly addressed by the power-law friction equation developed through passive deceleration tests. The correction of velocity dependent losses achieves a linear velocity profile ($R^2 \geq 0.98$) when tested with constant external torque, indicating that the correction is successful. The low velocity error (RMSE = 0.11 rad/s) is important because velocity is a direct component of power ($P = T \times \omega$). High precision in velocity measurement ensures that calculated power values are reliable and can detect meaningful changes even in noisy environments.

The prototype's 0.61-4.61N·m calibrated range, provided through field-oriented control of a BLDC motor, can provide a constant resisting torque and perform isotonic power tests in addition to the strength measurements. This places it in a distinct category and addresses the gap identified for isotonic power assessments. While preliminary testing was limited to this calibrated range, the motor-gearbox combination is capable of producing torques of up to 23N·m. Unlocking the full capacity would make the device suitable to measure a wide range of patients. The ability of the isotonic power upper-limb dynamometer to provide a constant resistance throughout the full range of motion regardless of movement velocity enables the power calculation $P = T \times \omega$, giving clinicians important information that would otherwise be missed.

This technical capability, combined with the demonstrated precision of the friction compensation, positions the device to fill the identified need for portable isotonic power measurement tools while maintaining accessibility.

7.9. Future Direction

The focus of this project was to develop a small device capable of maintaining a constant resisting torque using a BLDC motor with FOC control. Building on the technical validation, a systematic roadmap is presented to address the limitations of the current iteration of the device. This will ensure robust clinical reliability and ensure that the device is ready for testing with a larger group of healthy subjects.

In the immediate term, some high impact and low effort changes can provide large improvements in performance. The removal of all diagnostic messaging and reduction of fixed delays can accelerate the control loop to 250Hz, giving better control over the torque and more frequent velocity measurements. Changing the torque limit from the rated 7.49A to the peak 14.98A as indicated in the datasheet [176] would immediately enable the motor to resist with a torque up to 23N·m. These small changes will enable testing over the full capabilities of the hardware. Further software optimizations, such as the implementation of a real-time operating system and the use of direct memory access for encoder readings would enable velocity sampling rates greater than 1kHz. This would not only satisfy the requirement for accurate rate of force development measurements, but also further reduce the control loop and allow friction correction at 500Hz. The microcontroller would no longer have to request and receive velocity values as part of the main control loop. If more performance is needed, implementing the friction compensation directly in the FOC controller's routines as a lookup table can further increase the speed by eliminating the need to communicate with the external microcontroller, and by eliminating the need to calculate the friction torque. The FOC controller would have to interpolate from values in the lookup tables, sacrificing some precision in favour of correction speed.

Testing of the motor's torque constant and rotor inertia should also be done to ensure that the system is fully characterized before re-assembly. Once the full capabilities are available, temperature characterization at peak operational loads must be done to define duty cycle limitations. The effects of running consecutive tests at the peak 23N·m are uncharacterized. They could affect motor performance, and friction equation accuracy.

Over the medium term, once these optimizations are completed, direct rotational inertia measurement of the dynamometer should be completed. While empirical

characterization of each separate component was needed during development, the final product should be characterized as a whole. The initial drop tests had voltage spikes that risked damaging the motor and controller, so gearbox characterization was done independent of the motor. Now that the brake-chopper functionality has been implemented and has been demonstrated to work effectively, full system characterization over the entire possible range can be done. Friction characterization should push the motor to the peak datasheet velocity of 4500rpm (29.5 rad/s at the test wheel)[176]. A new friction torque curve, following a similar protocol (with the full assembly, without disconnecting the motor), can be done. The brake-chopper is essential here since rotating heavy masses at peak velocities and immediately letting the motor coast will cause it to generate enough energy to damage the electronics if that energy has nowhere to go. Now that the torque limit can be set to its peak without risking damage, drop tests should be completed while achieving the full range of velocities, and full range of resisting torque (up to 23 N·m at the wheel). Cross-calibration with existing commercial dynamometers would be feasible at this step by repeating the same standardized protocol on both systems and comparing results, consistent with their manufacturer's verification procedures. Additional features could include a self-calibration procedure. Since parameter drift can happen over time and with operating conditions, the friction-compensation coefficients can be treated as self-calibrating parameters and re-identified periodically using automated sweeps. These can be repeated spin down tests at fixed velocities and inertias. The microcontroller can use these re-calculate each friction-curve coefficient and store them for use in subsequent testing.

Regarding the physical design of the device, a few additional circuits were required for safety beyond bench tests. Internal organization of the additional circuit boards and wires is required to completely close and seal the dynamometer. This will be necessary before larger scale laboratory and clinical tests are done with volunteers. In addition, while the arm could withstand torque in the intended direction with a wide enough margin of safety, off-axis torque can cause bending, which will cause significant measurement uncertainty. A new arm will be necessary to mitigate this. The development of a new torque arm will require new strain gauges and re-calibration of the isometric torque measurement.

Finally, implementing the digital user interface and external memory storage would complete the stand-alone operation. The device in its current state is tethered to a computer and requires serial communication, which slows its control loop significantly. A handheld controller will complete the goal of portability and stand-alone use, getting the device ready for transportation and validation with human testers.

Once these steps are completed, the focus can shift to the development of a normative dataset and a standardized protocol. Volunteers should span a wide range of target populations that includes healthy individuals of all ages, genders, and upper-limb functional status. This will provide reference values for clinical interpretation. Protocol standardization and validation should be part of this process and should include measurements that can be compared with other dynamometers. In practice, the benchmark for cross-validation would be the well characterized commercial dynamometers (such as the Biodex), using their published calibration and verification procedures[92]. Clinical validation can be accomplished by comparing this prototype against the commercial dynamometers in isotonic mode [37], and testing the same participants using the same joint setup and protocols, then quantifying test-retest reliability and agreement between devices [121]. A standardized protocol would specify patient positioning, joint alignment, range of motion and test conditions. Normative datasets (reference sets of strength/power by demographics) exist in literature for isometric strength [170], and isokinetic power [98], [167]. The isometric datasets can be used for direct comparison. This will ensure measurement consistency and comparability. Isotonic power, however, does not have the same extent of available data, so comparison with multiple existing isotonic studies, can provide contextual benchmarks. To demonstrate the device's consistency outside of a controlled laboratory setting, the testing in clinics and alternative settings should be completed to ensure that all potential sources of error are addressed, that the standardized protocol works in all scenarios where the dynamometer will be used, and that it produces the same results regardless of the operator. The recording of normative data with the device after technical validation, clinical validation, and usability studies, will address the current lack of standardized isotonic testing protocols. It can establish the device as a standard assessment tool once human factors and reliability studies are completed.

In the long term, hardware improvements can include the use of a higher resolution encoder for finer control and increased velocity sampling rate. Motors designed for high performance industrial robot arms, such as frameless BLDC motors, are becoming more popular and less expensive. The high torque density of such motors would enable them to function in a direct-drive configuration (without a gearbox), completely eliminating the need for friction compensation, further expanding the device's precision and accuracy. In addition, software updates can add significant functionality to the dynamometer. For example, the FOC controller in the current iteration is already operating in velocity mode, with a set-point of 0rpm. As such, it resists external torque by attempting stop rotation and maintain a velocity of 0. The control of the maximum allowable resisting torque is used to complete the isotonic power tests. A software update, with an associated user interface update, can set the motor to have a maximum velocity instead of maximum torque, giving it isokinetic testing functionality. These

updates and generational upgrades add value to the device without significantly increasing the production cost per unit.

Regulatory approval will be required for commercial deployment, and mass production will require automated calibration procedures to ensure efficient characterization. This would enable each individual unit to be calibrated to the same standard and ensure that the data from each clinical or laboratory study is reliable.

8. Conclusion

This thesis demonstrates the successful achievement of developing a portable device capable of measuring isotonic power in elbow flexion and extension. The research was motivated by a need for objective, standardized measurement capabilities that bridge the gap between the inexpensive but feature limited handheld dynamometers, and the cost-prohibitive gold-standard isokinetic systems. Through systematic characterization, friction compensation, and technical validation, this work is the foundation for a clinically viable solution to portable isotonic power assessment.

8.1. Achievement of Research Objectives

While the device is not ready for clinical use, the primary objectives outlined in section 1.2 form the groundwork upon which an optimized and clinically validated tool can be deployed.

Objective 1: Evaluation of Field-Oriented Control (FOC) Viability

This research demonstrates that FOC is a viable strategy to achieve precise and constant resisting torque in dynamometry applications. The motor-only drop tests revealed a linear relationship between velocity and time, indicating a constant acceleration and thus a constant torque. The theoretical advantages of FOC, including the independent control of torque and flux, the rapid response times, and the low torque ripple were validated experimentally. This confirmed FOC's ability to maintain a constant resistance while the motor is backdriven. However, the research also showed that FOC alone cannot account for mechanical losses in the drivetrain in this application, as evidenced by velocity-dependent errors.

Objective 2: Development of a Table-top Prototype

A functional prototype capable of isometric strength and isotonic power testing was developed successfully. The mechanical design is compact and weighs less than the targeted 20kg. This makes it possible for a clinician to transport and set up on their own. The prototype had the ability to perform both measurement modes through software controls. It required the examiner to actuate a manual brake for isometric tests, but it

could complete isotonic power tests without any further physical interaction with the patient or volunteer. The modular design approach, with off-the-shelf components including a NEMA 34 BLDC motor, two stage 16:1 planetary gearbox, and FOC controller successfully balanced performance requirements with cost-effectiveness.

Objective 3: Validation of Constant Resisting Torque Capability

In addition to the physical design, the systematic component-level characterization formed the basis for a functional device. While initial benchmarks revealed a velocity-dependent friction characteristic to the gearbox, subsequent passive deceleration tests and drop tests led to the development of a power-law compensation equation: $T_{friction} = -1.81\omega^{0.13} + 1.71$. This equation was derived from the experimental results of these tests. Real-time compensation was achieved using a feedforward controller on top of the standard FOC control system. By reading the instantaneous velocity during movement, the friction is calculated, and motor torque is reduced, resulting in a constant resistance applied to the user. The compensation strategy allows the system to function rapidly and react to the velocity changes rather than the user's torque. The system successfully maintained a constant resisting torque across the tested range of 0.61N·m to 4.61N·m during drop tests, demonstrating its ability to function as intended despite the typical losses inherent to real mechanical systems. The friction compensated drop tests had linear velocity profiles, with excellent correlation ($R^2 \geq 0.98$) and low error (0.11 rad/s RMSE) over the range of 0 rad/s to 22 rad/s, which covers what is needed for most clinical applications.

8.2. Overall Impact and Future Outlook

This work contributes to the fields of dynamometry in biomechanics, functional performance assessments, and clinical device development by demonstrating that field-oriented control, when combined with an empirically derived friction compensation strategy, enables precise constant resisting torque. This capability allows isotonic power testing to be performed reliably in a lightweight, cost-effective system. This bridges the gap between the low-cost handheld devices that measure strength, and the expensive laboratory-grade isokinetic systems currently used for power testing. The prototype demonstrates that isometric and isotonic assessments can be completed by a single device without sacrificing portability. This offers clinicians an accessible tool to capture functionally relevant power measurements. While further optimization, normative data-collection, and clinical validation are needed, this research serves as a foundation for the future development of isotonic dynamometer, and the protocols associated to their use. This thesis highlights a pathway for making isotonic power assessment more widely available. The device developed in this work has the potential to expand research

capabilities, increase the amount of available research on this form of assessment, and ultimately improve patient outcomes in populations with upper-limb impairments.

9. References

[1] D. K. Moon *et al.*, "Common Upper Extremity Disorders and Function Affect Upper Extremity-Related Quality of Life: A Community-Based Sample from Rural Areas," *Yonsei Med. J.*, vol. 59, no. 5, p. 669, 2018, doi: 10.3349/ymj.2018.59.5.669.

[2] S. S. H. Wu and C. Ahn, "3.2 Physical and Rehabilitation Medicine – Clinical Scope: Specific Health Problems and Impairments," *J. Int. Soc. Phys. Rehabil. Med.*, vol. 2, no. Suppl 1, pp. S29–S34, June 2019, doi: 10.4103/jisprm.jisprm_10_19.

[3] A. Pollock *et al.*, "Interventions for improving upper limb function after stroke," *Cochrane Database Syst. Rev.*, vol. 2014, no. 11, Nov. 2014, doi: 10.1002/14651858.CD010820.pub2.

[4] C.-M. Chen, C.-C. Tsai, C.-Y. Chung, C.-L. Chen, K. P. Wu, and H.-C. Chen, "Potential predictors for health-related quality of life in stroke patients undergoing inpatient rehabilitation," *Health Qual. Life Outcomes*, vol. 13, no. 1, p. 118, Dec. 2015, doi: 10.1186/s12955-015-0314-5.

[5] L. Ada, "Stroke patients have selective muscle weakness in shortened range," *Brain*, vol. 126, no. 3, pp. 724–731, Mar. 2003, doi: 10.1093/brain/awg066.

[6] S. M. Dyer *et al.*, "A critical review of the long-term disability outcomes following hip fracture," *BMC Geriatr.*, vol. 16, no. 1, p. 158, Sept. 2016, doi: 10.1186/s12877-016-0332-0.

[7] B. R. McDonald, S. Vogrin, and C. M. Said, "Factors affecting hospital admission, hospital length of stay and new discharge destination post proximal humeral fracture: a retrospective audit," *BMC Geriatr.*, vol. 24, no. 1, p. 334, Apr. 2024, doi: 10.1186/s12877-024-04928-z.

[8] H. Johansen, K. Østlie, L. Ø. Andersen, and S. Rand-Hendriksen, "Health-related quality of life in adults with congenital unilateral upper limb deficiency in Norway. A cross-sectional study," *Disabil. Rehabil.*, vol. 38, no. 23, pp. 2305–2314, Nov. 2016, doi: 10.3109/09638288.2015.1129450.

[9] M. Alm, H. Saraste, and C. Norrbrink, "Shoulder pain in persons with thoracic spinal cord injury: Prevalence and characteristics," *J. Rehabil. Med.*, vol. 40, no. 4, pp. 277–283, 2008, doi: 10.2340/16501977-0173.

[10] R. Núñez-Cortés *et al.*, "Association Between Pain Coping and Symptoms of Anxiety and Depression, and Work Absenteeism in People With Upper Limb Musculoskeletal Disorders: A Systematic Review and Meta-analysis," *Arch. Phys. Med. Rehabil.*, vol. 105, no. 4, pp. 781–791, Apr. 2024, doi: 10.1016/j.apmr.2023.07.003.

[11] L. Ada, C. Canning, and T. Dwyer, "Effect of muscle length on strength and dexterity after stroke," *Clin. Rehabil.*, vol. 14, no. 1, pp. 55–61, Feb. 2000, doi: 10.1191/026921500671430626.

[12] J. Burridge *et al.*, "A Systematic Review of International Clinical Guidelines for Rehabilitation of People With Neurological Conditions: What Recommendations Are Made for Upper Limb Assessment?," *Front. Neurol.*, vol. 10, p. 567, June 2019, doi: 10.3389/fneur.2019.00567.

[13] K. Nas, "Rehabilitation of spinal cord injuries," *World J. Orthop.*, vol. 6, no. 1, p. 8, 2015, doi: 10.5312/wjo.v6.i1.8.

[14] L. Miller *et al.*, "Functional Electrical Stimulation for Foot Drop in Multiple Sclerosis: A Systematic Review and Meta-Analysis of the Effect on Gait Speed," *Arch. Phys. Med. Rehabil.*, vol. 98, no. 7, pp. 1435–1452, July 2017, doi: 10.1016/j.apmr.2016.12.007.

[15] U. Keller *et al.*, "Robot-Assisted Arm Assessments in Spinal Cord Injured Patients: A Consideration of Concept Study," *PLOS ONE*, vol. 10, no. 5, p. e0126948, May 2015, doi: 10.1371/journal.pone.0126948.

[16] Y. Tao *et al.*, "The role of robot-assisted training on rehabilitation outcomes in Parkinson's disease: a systematic review and meta-analysis," *Disabil. Rehabil.*, vol. 46, no. 18, pp. 4049–4067, Aug. 2024, doi: 10.1080/09638288.2023.2266178.

[17] R. Wang, Y. Wang, F. Yan, J. Sun, and T. Zhang, "Assessment of mesenchymal stem cells for the treatment of spinal cord injury: a systematic review and network meta-analysis," *Front. Cell. Neurosci.*, vol. 19, p. 1532219, Apr. 2025, doi: 10.3389/fncel.2025.1532219.

[18] V. Tabar *et al.*, "Phase I trial of hES cell-derived dopaminergic neurons for Parkinson's disease," *Nature*, vol. 641, no. 8064, pp. 978–983, May 2025, doi: 10.1038/s41586-025-08845-y.

[19] S. Y. Yoon, "Update on Parkinson's Disease Rehabilitation," *Brain NeuroRehabilitation*, vol. 15, no. 2, p. e15, July 2022, doi: 10.12786/bn.2022.15.e15.

[20] J. E. Lexell and D. Y. Downham, "How to Assess the Reliability of Measurements in Rehabilitation:," *Am. J. Phys. Med. Rehabil.*, vol. 84, no. 9, pp. 719–723, Sept. 2005, doi: 10.1097/01.phm.0000176452.17771.20.

[21] S. Rodríguez-Rodríguez *et al.*, "Correlation between Power Elbow Flexion and Physical Performance Test: A Potential Predictor for Assessing Physical Performance in Older Adults," *J. Clin. Med.*, vol. 12, no. 17, p. 5560, Aug. 2023, doi: 10.3390/jcm12175560.

[22] R. W. Bohannon, "Considerations and Practical Options for Measuring Muscle Strength: A Narrative Review," *BioMed Res. Int.*, vol. 2019, pp. 1–10, Jan. 2019, doi: 10.1155/2019/8194537.

[23] K. F. Reid and R. A. Fielding, "Skeletal Muscle Power: A Critical Determinant of Physical Functioning in Older Adults," *Exerc. Sport Sci. Rev.*, vol. 40, no. 1, pp. 4–12, Jan. 2012, doi: 10.1097/JES.0b013e31823b5f13.

[24] C. Liu, D. Marie, A. Fredrick, J. Bertram, K. Utley, and E. E. Fess, "Predicting hand function in older adults: evaluations of grip strength, arm curl strength, and manual dexterity," *Aging Clin. Exp. Res.*, vol. 29, no. 4, pp. 753–760, Aug. 2017, doi: 10.1007/s40520-016-0628-0.

[25] M. O. Conrad and D. G. Kamper, "Isokinetic strength and power deficits in the hand following stroke," *Clin. Neurophysiol.*, vol. 123, no. 6, pp. 1200–1206, June 2012, doi: 10.1016/j.clinph.2011.10.004.

[26] P. S. Lum, C. Patten, D. Kothari, and R. Yap, "Effects of velocity on maximal torque production in poststroke hemiparesis," *Muscle Nerve*, vol. 30, no. 6, pp. 732–742, Dec. 2004, doi: 10.1002/mus.20157.

[27] L. R. Nascimento, L. F. Teixeira-Salmela, J. C. Polese, L. Ada, C. D. C. M. Faria, and G. E. C. Laurentino, "Strength deficits of the shoulder complex during isokinetic testing in people with chronic stroke," *Braz. J. Phys. Ther.*, vol. 18, no. 3, pp. 268–275, June 2014, doi: 10.1590/bjpt-rbf.2014.0030.

[28] C. M. Kim, D. H. Kothari, P. S. Lum, and C. Patten, "Reliability of Dynamic Muscle Performance in the Hemiparetic Upper Limb," *J. Neurol. Phys. Ther.*, vol. 29, no. 1, pp. 9–17, Mar. 2005, doi: 10.1097/01.NPT.0000282257.74325.2b.

[29] L. A. Ingram, A. A. Butler, S. R. Lord, and S. C. Gandevia, "Use of a physiological profile to document upper limb motor impairment in ageing and in neurological conditions," *J. Physiol.*, vol. 601, no. 12, pp. 2251–2262, June 2023, doi: 10.1113/JP283703.

[30] S. K. Subramanian, J. Yamanaka, G. Chilingaryan, and M. F. Levin, "Validity of Movement Pattern Kinematics as Measures of Arm Motor Impairment Poststroke," *Stroke*, vol. 41, no. 10, pp. 2303–2308, Oct. 2010, doi: 10.1161/STROKEAHA.110.593368.

[31] B. J. Thompson, "It's time to re-evaluate the reporting of common measures from isokinetic dynamometers: isokinetic for torque, isotonic for power," *Front. Sports Act. Living*, vol. 7, p. 1472712, Feb. 2025, doi: 10.3389/fspor.2025.1472712.

[32] M. Foldvari *et al.*, "Association of Muscle Power With Functional Status in Community-Dwelling Elderly Women," *J. Gerontol. Ser. A*, vol. 55, no. 4, pp. M192–M199, Apr. 2000, doi: 10.1093/gerona/55.4.M192.

[33] F. Aerts *et al.*, "Reliability and Agreement of Hand-Held Dynamometry Using Three Standard Rater Test Positions," *Int. J. Sports Phys. Ther.*, vol. 20, no. 2, Feb. 2025, doi: 10.26603/001c.128286.

[34] J. B. Wikholm and R. W. Bohannon, "Hand-held Dynamometer Measurements: Tester Strength Makes a Difference," *J. Orthop. Sports Phys. Ther.*, vol. 13, no. 4, pp. 191–198, Apr. 1991, doi: 10.2519/jospt.1991.13.4.191.

[35] P. A. Massey, C. Montgomery, J. Paulos, B. Branch, C. Lobrano, and K. Perry, "Are luggage scales a viable alternative to hand-held dynamometers for the measurement of shoulder scaption strength?," *JSES Int.*, vol. 8, no. 1, pp. 212–216, Jan. 2024, doi: 10.1016/j.jseint.2023.09.007.

[36] Y. Myong *et al.*, "Development and validation of a portable articulated dynamometry system to assess knee extensor muscle strength," *Sci. Rep.*, vol. 13, no. 1, p. 11887, July 2023, doi: 10.1038/s41598-023-39062-0.

[37] M. Jokiel *et al.*, "Biomechanical Examination of Wrist Flexors and Extensors with Biodex System Dynamometer—Isometric, Isokinetic and Isotonic Protocol Options," *Medicina (Mex.)*, vol. 60, no. 7, p. 1184, July 2024, doi: 10.3390/medicina60071184.

[38] M. V. Narici and N. Maffulli, "Sarcopenia: characteristics, mechanisms and functional significance," *Br. Med. Bull.*, vol. 95, no. 1, pp. 139–159, Sept. 2010, doi: 10.1093/bmb/ldq008.

[39] S. Van Driessche, E. Van Roie, B. Vanwanseele, and C. Delecluse, "Test-retest reliability of knee extensor rate of velocity and power development in older adults using the isotonic mode on a Biodex System 3 dynamometer," *PLOS ONE*, vol. 13, no. 5, p. e0196838, May 2018, doi: 10.1371/journal.pone.0196838.

[40] S. Van Driessche, C. Delecluse, I. Bautmans, B. Vanwanseele, and E. Van Roie, "Age-related differences in rate of power development exceed differences in peak power," *Exp. Gerontol.*, vol. 101, pp. 95–100, Jan. 2018, doi: 10.1016/j.exger.2017.11.009.

[41] L. Santisteban, M. Térémetz, J.-P. Bleton, J.-C. Baron, M. A. Maier, and P. G. Lindberg, "Upper Limb Outcome Measures Used in Stroke Rehabilitation Studies: A Systematic Literature Review," *PLOS ONE*, vol. 11, no. 5, p. e0154792, May 2016, doi: 10.1371/journal.pone.0154792.

[42] G. B. Prange-Lasonder *et al.*, "European evidence-based recommendations for clinical assessment of upper limb in neurorehabilitation (CAULIN): data synthesis from systematic reviews, clinical practice guidelines and expert consensus," *J. NeuroEngineering Rehabil.*, vol. 18, no. 1, p. 162, Dec. 2021, doi: 10.1186/s12984-021-00951-y.

[43] N. Wilson, D. Howel, H. Bosomworth, L. Shaw, and H. Rodgers, "Analysing the Action Research Arm Test (ARAT): a cautionary tale from the RATULS trial," *Int. J. Rehabil. Res. Int. Z. Rehabil. Rev. Int. Rech. Readaptation*, vol. 44, no. 2, pp. 166–169, June 2021, doi: 10.1097/MRR.0000000000000466.

[44] J. H. Bae, S. H. Kang, K. M. Seo, D.-K. Kim, H. I. Shin, and H. E. Shin, "Relationship Between Grip and Pinch Strength and Activities of Daily Living in Stroke Patients," *Ann. Rehabil. Med.*, vol. 39, no. 5, p. 752, 2015, doi: 10.5535/arm.2015.39.5.752.

[45] J. G. Betts *et al.*, "11.5 Muscles of the Pectoral Girdle and Upper Limbs - Anatomy and Physiology 2e | OpenStax." Accessed: Sept. 07, 2025. [Online]. Available: https://openstax.org/books/anatomy-and-physiology-2e/pages/11-5-muscles-of-the-pectoral-girdle-and-upper-limbs

[46] J. G. Betts *et al.*, "Ch. 9 Chapter Review - Anatomy and Physiology 2e | OpenStax." Accessed: Sept. 07, 2025. [Online]. Available: https://openstax.org/books/anatomy-and-physiology-2e/pages/9-chapter-review

[47] M. A. Clark, M. Douglas, J. Choi, M. A. Clark, M. Douglas, and J. Choi, "38.1 Types of Skeletal Systems - Biology 2e | OpenStax." Accessed: Sept. 07, 2025. [Online]. Available: https://openstax.org/books/biology-2e/pages/38-1-types-of-skeletal-systems

[48] S. U. Islam, A. Glover, R. J. MacFarlane, N. Mehta, and M. Waseem, "The Anatomy and Biomechanics of the Elbow," *Open Orthop. J.*, vol. 14, no. 1, pp. 95–99, Aug. 2020, doi: 10.2174/1874325002014010095.

[49] G. Coratella *et al.*, "Biceps Brachii and Brachioradialis Excitation in Biceps Curl Exercise: Different Handgrips, Different Synergy," *Sports*, vol. 11, no. 3, p. 64, Mar. 2023, doi: 10.3390/sports11030064.

[50] J. G. Betts *et al.*, "8.2 Bones of the Upper Limb - Anatomy and Physiology | OpenStax." Accessed: Sept. 07, 2025. [Online]. Available: https://openstax.org/books/anatomy-and-physiology-2e/pages/8-2-bones-of-the-upper-limb

[51] J. Acosta Batlle, L. Cerezal, M. D. López Parra, B. Alba, S. Resano, and J. Blázquez Sánchez, "The elbow: review of anatomy and common collateral ligament complex pathology using MRI," *Insights Imaging*, vol. 10, no. 1, p. 43, Dec. 2019, doi: 10.1186/s13244-019-0725-7.

[52] M. Patel and M. A. Varacallo, "Anatomy, Shoulder and Upper Limb, Arm Nerves," *StatPearls Publ.*, 2025.

[53] J. G. Betts *et al.*, "13.4 The Peripheral Nervous System - Anatomy and Physiology 2e | OpenStax." Accessed: Sept. 07, 2025. [Online]. Available: https://openstax.org/books/anatomy-and-physiology-2e/pages/13-4-the-peripheral-nervous-system

[54] J. G. Betts *et al.*, "20.5 Circulatory Pathways - Anatomy and Physiology 2e | OpenStax." Accessed: Sept. 07, 2025. [Online]. Available: https://openstax.org/books/anatomy-and-physiology-2e/pages/20-5-circulatory-pathways

[55] Y. Kawakami, K. Nakazawa, T. Fujimoto, D. Nozaki, M. Miyashita, and T. Fukunaga, "Specific tension of elbow flexor and extensor muscles based on magnetic resonance imaging," *Eur. J. Appl. Physiol.*, vol. 68, no. 2, pp. 139–147, Feb. 1994, doi: 10.1007/BF00244027.

[56] M. A. Plantz and B. Bordoni, "Anatomy, Shoulder and Upper Limb, Brachialis Muscle," in *StatPearls*, Treasure Island (FL): StatPearls Publishing, 2025. Accessed: Sept. 07, 2025. [Online]. Available: http://www.ncbi.nlm.nih.gov/books/NBK551630/

[57] T. Kleiber, L. Kunz, and C. Disselhorst-Klug, "Muscular coordination of biceps brachii and brachioradialis in elbow flexion with respect to hand position," *Front. Physiol.*, vol. 6, Aug. 2015, doi: 10.3389/fphys.2015.00215.

[58] "Anatomy and Physiology (Boundless)".

[59] B. Harwood, A. W. Davidson, and C. L. Rice, "Motor unit discharge rates of the anconeus muscle during high-velocity elbow extensions," *Exp. Brain Res.*, vol. 208, no. 1, pp. 103–113, Jan. 2011, doi: 10.1007/s00221-010-2463-4.

[60] J. Singh, M. H. Elvey, Z. Hamoodi, and A. C. Watts, "Current perspectives on elbow dislocation and instability," *Ann. Jt.*, vol. 6, pp. 10–10, Jan. 2021, doi: 10.21037/aoj-19-186.

[61] J. G. Betts *et al.*, "10.4 Nervous System Control of Muscle Tension - Anatomy and Physiology 2e | OpenStax." Accessed: Sept. 07, 2025. [Online]. Available: https://openstax.org/books/anatomy-and-physiology-2e/pages/10-4-nervous-system-control-of-muscle-tension

[62] M. C. Gash, P. F. Kandle, I. V. Murray, and M. A. Varacallo, "Physiology, Muscle Contraction," in *StatPearls*, Treasure Island (FL): StatPearls Publishing, 2025. Accessed: Sept. 07, 2025. [Online]. Available: http://www.ncbi.nlm.nih.gov/books/NBK537140/

[63] J. Alcazar, R. Csapo, I. Ara, and L. M. Alegre, "On the Shape of the Force-Velocity Relationship in Skeletal Muscles: The Linear, the Hyperbolic, and the Double-Hyperbolic," *Front. Physiol.*, vol. 10, p. 769, June 2019, doi: 10.3389/fphys.2019.00769.

[64] R. L. Lieber and S. R. Ward, "Skeletal muscle design to meet functional demands," *Philos. Trans. R. Soc. B Biol. Sci.*, vol. 366, no. 1570, pp. 1466–1476, May 2011, doi: 10.1098/rstb.2010.0316.

[65] D. Jandačka and P. Beremlijski, "Determination of Strength Exercise Intensities Based on the Load-Power-Velocity Relationship," *J. Hum. Kinet.*, vol. 28, no. 2011, pp. 33–44, June 2011, doi: 10.2478/v10078-011-0020-2.

[66] K. E. Wilk, C. A. Arrigo, and G. J. Davies, "Isokinetic Testing: Why it is More Important Today than Ever," *Int. J. Sports Phys. Ther.*, vol. 19, no. 4, Apr. 2024, doi: 10.26603/001c.95038.

[67] D. Lum, G. G. Haff, and T. M. Barbosa, "The Relationship between Isometric Force-Time Characteristics and Dynamic Performance: A Systematic Review," *Sports*, vol. 8, no. 5, p. 63, May 2020, doi: 10.3390/sports8050063.

[68] N. A. Maffiuletti, P. Aagaard, A. J. Blazevich, J. Folland, N. Tillin, and J. Duchateau, "Rate of force development: physiological and methodological considerations," *Eur. J. Appl. Physiol.*, vol. 116, no. 6, pp. 1091–1116, June 2016, doi: 10.1007/s00421-016-3346-6.

[69] S. D. Lomborg, U. Dalgas, and L. G. Hvid, "The importance of neuromuscular rate of force development for physical function in aging and common neurodegenerative disorders - a systematic review," *J. Musculoskelet. Neuronal Interact.*, vol. 22, no. 4, pp. 562–586, Dec. 2022.

[70] W. M. Murray, T. S. Buchanan, and S. L. Delp, "Scaling of peak moment arms of elbow muscles with upper extremity bone dimensions," *J. Biomech.*, vol. 35, no. 1, pp. 19–26, Jan. 2002, doi: 10.1016/S0021-9290(01)00173-7.

[71] W. M. Murray, S. L. Delp, and T. S. Buchanan, "Variation of muscle moment arms with elbow and forearm position," *J. Biomech.*, vol. 28, no. 5, pp. 513–525, May 1995, doi: 10.1016/0021-9290(94)00114-J.

[72] C. Y. Seow, "Hill's equation of muscle performance and its hidden insight on molecular mechanisms," *J. Gen. Physiol.*, vol. 142, no. 6, pp. 561–573, Dec. 2013, doi: 10.1085/jgp.201311107.

[73] T. Tajika *et al.*, "Flexor pronator muscles' contribution to elbow joint valgus stability: ultrasonographic analysis in high school pitchers with and without symptoms," *JSES Int.*, vol. 4, no. 1, pp. 9–14, Mar. 2020, doi: 10.1016/j.jses.2019.10.003.

[74] R. A. Kaufmann, T. Wilps, V. Musahl, and R. E. Debski, "Elbow Biomechanics: Soft Tissue Stabilizers," *J. Hand Surg.*, vol. 45, no. 2, pp. 140–147, Feb. 2020, doi: 10.1016/j.jhsa.2019.10.034.

[75] D. Borms, A. Maenhout, and A. M. Cools, "Upper Quadrant Field Tests and Isokinetic Upper Limb Strength in Overhead Athletes," *J. Athl. Train.*, vol. 51, no. 10, pp. 789–796, Oct. 2016, doi: 10.4085/1062-6050-51.12.06.

[76] S. C. Cuthbert and G. J. Goodheart, "On the reliability and validity of manual muscle testing: a literature review," *Chiropr. Osteopat.*, vol. 15, no. 1, p. 4, Dec. 2007, doi: 10.1186/1746-1340-15-4.

[77] W. H. Schmitt and S. C. Cuthbert, "Common errors and clinical guidelines for manual muscle testing: 'the arm test' and other inaccurate procedures," *Chiropr. Osteopat.*, vol. 16, no. 1, p. 16, Dec. 2008, doi: 10.1186/1746-1340-16-16.

[78] S. O'Neill, S. L. T. Jaszczak, A. K. S. Steffensen, and B. Debrabant, "Using 4+ to grade near-normal muscle strength does not improve agreement," *Chiropr. Man. Ther.*, vol. 25, no. 1, p. 28, Dec. 2017, doi: 10.1186/s12998-017-0159-6.

[79] F. Bittmann, S. Dech, M. Aehle, and L. Schaefer, "Manual Muscle Testing—Force Profiles and Their Reproducibility," *Diagnostics*, vol. 10, no. 12, p. 996, Nov. 2020, doi: 10.3390/diagnostics10120996.

[80] T. Paternostro-Sluga *et al.*, "Reliability and validity of the Medical Research Council (MRC) scale and a modified scale for testing muscle strength in patients with radial palsy," *J. Rehabil. Med.*, vol. 40, no. 8, pp. 665–671, 2008, doi: 10.2340/16501977-0235.

[81] K. Vijian, Y. T. Cheng, Z. Idris, A. R. Izaini Ghani, S. Abdul Halim, and J. M. Abdullah, "Manual Muscle Testing of the Scapula and the Upper Limb through Bedside Examination," *Malays. J. Med. Sci.*, vol. 30, no. 1, pp. 198–212, Feb. 2023, doi: 10.21315/mjms2023.30.1.17.

[82] F. N. Bittmann, S. Dech, and L. V. Schaefer, "Another Way to Confuse Motor Control: Manual Technique Supposed to Shorten Muscle Spindles Reduces the Muscular Holding Stability in the Sense of Adaptive Force in Male Soccer Players," *Brain Sci.*, vol. 13, no. 7, p. 1105, July 2023, doi: 10.3390/brainsci13071105.

[83] J. Lesnak, D. Anderson, B. Farmer, D. Katsavelis, and T. L. Grindstaff, "VALIDITY OF HAND-HELD DYNAMOMETRY IN MEASURING QUADRICEPS STRENGTH AND RATE OF TORQUE DEVELOPMENT," *Int. J. Sports Phys. Ther.*, vol. 14, no. 2, pp. 180–187, Apr. 2019, doi: 10.26603/ijspt20190180.

[84] R. W. Bohannon, J. Kindig, G. Sabo, A. E. Duni, and P. Cram, "Isometric knee extension force measured using a handheld dynamometer with and without belt-stabilization," *Physiother. Theory Pract.*, vol. 28, no. 7, pp. 562–568, Oct. 2012, doi: 10.3109/09593985.2011.640385.

[85] V. Baltzopoulos and D. A. Brodie, "Isokinetic Dynamometry: Applications and Limitations," *Sports Med.*, vol. 8, no. 2, pp. 101–116, Aug. 1989, doi: 10.2165/00007256-198908020-00003.

[86] K. Warneke *et al.*, "Maximal strength measurement: A critical evaluation of common methods—a narrative review," *Front. Sports Act. Living*, vol. 5, p. 1105201, Feb. 2023, doi: 10.3389/fspor.2023.1105201.

[87] M. Brookshaw, A. Sexton, and C. A. McGibbon, "Reliability and Validity of a Novel Wearable Device for Measuring Elbow Strength," *Sensors*, vol. 20, no. 12, p. 3412, June 2020, doi: 10.3390/s20123412.

[88] E. Ekstrand, J. Lexell, and C. BrogÃ¥rdh, "Isometric and isokinetic muscle strength in the upper extremity can be reliably measured in persons with chronic stroke," *J. Rehabil. Med.*, vol. 47, no. 8, pp. 706–713, 2015, doi: 10.2340/16501977-1990.

[89] L. A. Frey-Law, A. Laake, K. G. Avin, J. Heitsman, T. Marler, and K. Abdel-Malek, "Knee and Elbow 3D Strength Surfaces: Peak Torque-Angle-Velocity Relationships," *J. Appl. Biomech.*, vol. 28, no. 6, pp. 726–737, Dec. 2012, doi: 10.1123/jab.28.6.726.

[90] P. Gentil *et al.*, "Comparison of elbow flexor isokinetic peak torque and fatigue index between men and women of different training level," *Eur. J. Transl. Myol.*, vol. 27, no. 4, Dec. 2017, doi: 10.4081/ejtm.2017.7070.

[91] M. Cozette, P.-M. Leprêtre, C. Doyle, and T. Weissland, "Isokinetic Strength Ratios: Conventional Methods, Current Limits and Perspectives," *Front. Physiol.*, vol. 10, p. 567, May 2019, doi: 10.3389/fphys.2019.00567.

[92] "SYSTEM 4: Isokinetic dynamometer instructions For use," Biodesx Medical Systems Inc., 20-001-CLR, Mar. 2024. Accessed: Sept. 05, 2025. [Online]. Available: https://biodexrehab.com/wp-content/uploads/2024/08/20-001-CLR-System-4-IFU-Rev-E.pdf

[93] K. Takeno, V. L. Katch, G. E. Norte, and C. D. Ingersoll, "Validity and reliability of a novel portable tension-gauge dynamometer for isometric and isotonic seated knee extension strength measurement," *The Knee*, vol. 56, pp. 646–656, Oct. 2025, doi: 10.1016/j.knee.2025.07.013.

[94] K.-S. Sung, Y. G. Yi, and H.-I. Shin, "Reliability and validity of knee extensor strength measurements using a portable dynamometer anchoring system in a supine position," *BMC Musculoskelet. Disord.*, vol. 20, no. 1, p. 320, Dec. 2019, doi: 10.1186/s12891-019-2703-0.

[95] "International Vocabulary of Metrology – Basic and general concepts and associated terms (VIM), 3rd edition." Accessed: Dec. 17, 2025. [Online]. Available: https://www.bipm.org/doi/10.59161/JCGM200-2012

[96] T. K. Koo and M. Y. Li, "A Guideline of Selecting and Reporting Intraclass Correlation Coefficients for Reliability Research," *J. Chiropr. Med.*, vol. 15, no. 2, pp. 155–163, June 2016, doi: 10.1016/j.jcm.2016.02.012.

[97] B. F. Mentiplay *et al.*, "Assessment of Lower Limb Muscle Strength and Power Using Hand-Held and Fixed Dynamometry: A Reliability and Validity Study," *PLOS ONE*, vol. 10, no. 10, p. e0140822, Oct. 2015, doi: 10.1371/journal.pone.0140822.

[98] T. Stark, B. Walker, J. K. Phillips, R. Fejer, and R. Beck, "Hand-held Dynamometry Correlation With the Gold Standard Isokinetic Dynamometry: A Systematic Review," *PM&R*, vol. 3, no. 5, pp. 472–479, May 2011, doi: 10.1016/j.pmrj.2010.10.025.

[99] A. Nordez, P. Casari, and C. Cornu, "Accuracy of Biodex system 3 pro computerized dynamometer in passive mode," *Med. Eng. Phys.*, vol. 30, no. 7, pp. 880–887, Sept. 2008, doi: 10.1016/j.medengphy.2007.11.001.

[100] "Biodex System 4 Pro," Arrowhead Medical Online Store. Accessed: Sept. 05, 2025. [Online]. Available: https://arrowheadmedstore.com/product/biodex-system-4-pro/

[101] D. Santos, A. Bravo-Sánchez, L. A. Peyré-Tartaruga, F. Simini, and R. Zacca, "Isometric Force–Time Curve Assessment: Accuracy, Precision, and Repeatability of a Mobile Application and Portable and Lightweight Device," *Sports*, vol. 12, no. 10, p. 268, Oct. 2024, doi: 10.3390/sports12100268.

[102] E. P. Washabaugh, T. E. Augenstein, M. Koje, and C. Krishnan, "Functional Resistance Training With Viscous and Elastic Devices: Does Resistance Type Acutely Affect Knee Function?," *IEEE Trans. Biomed. Eng.*, vol. 70, no. 4, pp. 1274–1285, Apr. 2023, doi: 10.1109/TBME.2022.3214773.

[103] C. McMillin, B. Melton, N. Murray, and C. D'Adamo, "Machine Resistance Curve Analysis of Seven Resistance Training Machines: Original Research," *Res. Directs Strength Perform.*, vol. 4, no. 1, Apr. 2024, doi: 10.53520/rdsp2024.105118.

[104] A. Spaggiari and E. Dragoni, "Analytical and numerical modeling of shape memory alloy Negator springs for constant-force, long-stroke actuators," *J. Intell. Mater. Syst. Struct.*, vol. 25, no. 9, pp. 1139–1148, June 2014, doi: 10.1177/1045389X13493354.

[105] R. B. Williams, C. D. Fisher, and J. C. Gallon, "Practical Considerations for using Constant Force Springs in Space-Based Mechanisms," in *54th AIAA/ASME/ASCE/AHS/ASC Structures, Structural Dynamics, and Materials Conference*, Boston, Massachusetts: American Institute of Aeronautics and Astronautics, Apr. 2013. doi: 10.2514/6.2013-1574.

[106] X. Li, K. Sun, and H. Liu, "A modified constant-torque spring hinge toward synchronous deployment," *Adv. Space Res.*, vol. 70, no. 11, pp. 3301–3310, Dec. 2022, doi: 10.1016/j.asr.2022.08.005.

[107] F. Gao, Y. Liu, and W.-H. Liao, "Cam Profile Generation for Cam-Spring Mechanism With Desired Torque," *J. Mech. Robot.*, vol. 10, no. 4, p. 041009, Aug. 2018, doi: 10.1115/1.4040270.

[108] Y. Liu, D. Yu, and J. Yao, "Design of an adjustable cam based constant force mechanism," *Mech. Mach. Theory*, vol. 103, pp. 85–97, Sept. 2016, doi: 10.1016/j.mechmachtheory.2016.04.014.

[109] E. Simeu and D. Georges, "Modeling and control of an eddy current brake," *Control Eng. Pract.*, vol. 4, no. 1, pp. 19–26, Jan. 1996, doi: 10.1016/0967-0661(95)00202-4.

[110] Hong-Je Ryoo, Jong-Soo Kim, Do-Hyun Kang, Geun-Hie Rim, Yong-Ju Kim, and Chung-Yuen Won, "Design and analysis of an eddy current brake for a high-speed railway train with constant torque control," in *Conference Record of the 2000 IEEE Industry Applications Conference. Thirty-Fifth IAS Annual Meeting and World Conference on Industrial Applications of Electrical Energy (Cat. No.00CH37129)*, Rome, Italy: IEEE, 2000, pp. 277–281. doi: 10.1109/IAS.2000.881123.

[111] K. Lee and K. Park, "Optimal robust control of a contactless brake system using an eddy current," *Mechatronics*, vol. 9, no. 6, pp. 615–631, Sept. 1999, doi: 10.1016/S0957-4158(99)00008-2.

[112] T. Kikuchi, K. Kobayashi, and A. Inoue, "Gap-Size Effect of Compact MR Fluid Brake," *J. Intell. Mater. Syst. Struct.*, vol. 22, no. 15, pp. 1677–1683, Oct. 2011, doi: 10.1177/1045389X11428674.

[113] P.-B. Nguyen, X.-P. Do, J. Jeon, S.-B. Choi, Y. D. Liu, and H. J. Choi, "Brake performance of core–shell structured carbonyl iron/silica based magnetorheological suspension," *J. Magn. Magn. Mater.*, vol. 367, pp. 69–74, Oct. 2014, doi: 10.1016/j.jmmm.2014.04.061.

[114] G. C. Henderson and J. Ueda, "Pneumatically powered robotic exercise device to induce a specific force profile in target lower extremity muscles," *Robotica*, vol. 32, no. 8, pp. 1281–1299, Dec. 2014, doi: 10.1017/S0263574714001556.

[115] D. U. Campos-Delgado, D. R. Espinoza-Trejo, and E. Palacios, "Closed-loop Torque Control of an Absorbing Dynamometer for a Motor Test-Bed," in *2007 IEEE International Symposium on Industrial Electronics*, Vigo, Spain: IEEE, June 2007, pp. 2113–2118. doi: 10.1109/ISIE.2007.4374934.

[116] J. Zongxia, L. Chenggong, and R. Zhiting, "The extraneous torque and compensation control.on the electric load simulator", doi: 10.1117/12.521962.

[117] X. Wang, S. Wang, and X. Wang, "Electrical load simulator based on velocity-loop compensation and improved fuzzy-PID," in *2009 IEEE International Symposium on Industrial Electronics*, Seoul, South Korea: IEEE, July 2009, pp. 238–243. doi: 10.1109/ISIE.2009.5213288.

[118] K. Chen, H. Guo, L. Sun, and J. Yan, "Dynamic Torque Control Incorporating Tracking Differentiator for Motor-Driven Load Simulator," in *AsiaSim 2013*, vol. 402, G. Tan, G. K. Yeo, S. J. Turner, and Y. M. Teo, Eds., in Communications in Computer and Information Science, vol. 402. , Berlin, Heidelberg: Springer Berlin Heidelberg, 2013, pp. 276–287. doi: 10.1007/978-3-642-45037-2_26.

[119] I. A. Stringer and K. J. Bullock, "A Regenerative Road Load Simulator," presented at the 20th FISITA Congress (1984), Vienna, Austria, Vienna, Austria, Jan. 1984, p. 845115. doi: 10.4271/845115.

[120] J. M. Gregson, M. J. Leathley, A. P. Moore, T. L. Smith, A. K. Sharma, and C. L. Watkins, "Reliability of measurements of muscle tone and muscle power in stroke patients", doi: 10.1093/ageing/29.3.223.

[121] J. M. Drouin, T. C. Valovich-mcLeod, S. J. Shultz, B. M. Gansneder, and D. H. Perrin, "Reliability and validity of the Biodex system 3 pro isokinetic dynamometer velocity, torque and position measurements," *Eur. J. Appl. Physiol.*, vol. 91, no. 1, pp. 22–29, Jan. 2004, doi: 10.1007/s00421-003-0933-0.

[122] "TMCM-1636 Hardware Manual," TRINAMIC Motion Control GmbH & Co. KG, Hamburg, Germany, Hardware Manual TMCM-1636, Mar. 2021. Accessed: June 05, 2022. [Online]. Available: https://www.analog.com/en/products/TMCM-1636.html

[123] "TMCM-1636 TMCL™ Firmware Manual," TRINAMIC Motion Control GmbH & Co. KG, Hamburg, Germany, Firmware Manual TMCM-1636, Mar. 2021. Accessed: June 05, 2022. [Online]. Available: https://www.analog.com/en/products/TMCM-1636.html

[124] Microchip Technology Inc., "Sensorless Field Oriented Control for a Permanent Magnet Synchronous Motor Using a PLL Estimator and Equation-based Flux Weakening," Microchip Technology Inc., AN2520, Application Note DS00002520D, Dec. 2024. Accessed: Sept. 08, 2025. [Online]. Available: https://ww1.microchip.com/downloads/aemDocuments/documents/MCU32/ApplicationNotes/ApplicationNotes/AN2520-Sensorless-Field-Oriented-Control-for-a-Permanent-Magnet-Synchronous-Motor-Using-a-PLL-Estimator-and-Equation-based-Flux-Weakening-DS00002520.pdf

[125] R. Ramamoorthy, B. Larimore, and M. Bhardwaj, "Sensored Field Oriented Control of 3-Phase Permanent Magnet Synchronous Motors Using TMS320F2837x," Texas Instruments Incorporated, Application Report SPRABZ0A, May 2021. Accessed: Sept. 08, 2025. [Online]. Available: https://www.ti.com/lit/an/sprabz0a/sprabz0a.pdf?ts=1757384427361

[126] TRINAMIC Motion Control GmbH & Co. KG, "TMC4671 Datasheet," Analog Devices, Inc., Hamburg, Germany., Datasheet, Feb. 2019.

[127] Fred Flett, "Space Phasor Model of PMSM.," in *A Tutorial in AC Induction and Permanent Magnet Synchronous Motors: Vector Control with Digital Signal Processors.*, Wilmington, MA, USA: Analog Devices, Inc., 1994, pp. 63–70. Accessed: Sept. 08, 2025. [Online]. Available: https://www.analog.com/media/en/training-

seminars/design-handbooks/tutorial-ac-induction-permanent-magnet/Part2-Chapter3.pdf

[128] ABB, "Technical_guide_No_8_3AFE64362534_RevC," ABB, 3AFE64362534, May 2018. [Online]. Available: https://library.e.abb.com/public/20be376000f34dd6b9c513580cf56423/Technical_guide_No_8_3AFE64362534_RevC.pdf

[129] J. Bullick, "VFD Regenerative Applications," KEB. Accessed: Sept. 08, 2025. [Online]. Available: https://www.kebamerica.com/blog/vfd-regenerative-applications/

[130] B. Akin and M. Bhardwaj, "Sensorless Trapezoidal Control of BLDC Motors (Rev. A)," Texas Instruments Incorporated, Application Report SPRABQ7A, 2013. Accessed: Sept. 08, 2025. [Online]. Available: https://www.ti.com/lit/an/sprabq7a/sprabq7a.pdf

[131] D.-K. Kim, D.-M. Kim, J.-C. Park, S.-G. Lee, J. Yoo, and M.-S. Lim, "Torque Ripple Reduction of BLDC Traction Motor of Electric Wheelchair for Ride Comfort Improvement," *J. Electr. Eng. Technol.*, vol. 17, no. 1, pp. 351–360, Jan. 2022, doi: 10.1007/s42835-021-00875-6.

[132] "PMSM FeedForward Control - Decouple d-axis and q-axis current to eliminate disturbance - Simulink." Accessed: Sept. 08, 2025. [Online]. Available: https://www.mathworks.com/help/mcb/ref/pmsmfeedforwardcontrol.html

[133] B. Podmiljšak *et al.*, "The Future of Permanent-Magnet-Based Electric Motors: How Will Rare Earths Affect Electrification?," *Materials*, vol. 17, no. 4, p. 848, Feb. 2024, doi: 10.3390/ma17040848.

[134] B. Boggess, J. Moffit, J. Morales, and T. Anderson, "The Effects of Kinetic Energy on Concentric and Eccentric Isokinetic Work," *J. Sports Sci. Med.*, vol. 7, no. 1, pp. 84–90, Mar. 2008.

[135] Kollmorgen, "Evolving the Rules of Inertia Matching," Kollmorgen, White paper KM_WP_000379_RevB_EN, Jan. 2022. Accessed: Sept. 09, 2025. [Online]. Available: https://www.kollmorgen.com/sites/default/files/kol_3361_Inertia_Mismatch_WP_update.pdf

[136] D. Laparidou, F. Curtis, J. Akanuwe, K. Goher, A. Niroshan Siriwardena, and A. Kucukyilmaz, "Patient, carer, and staff perceptions of robotics in motor rehabilitation: a systematic review and qualitative meta-synthesis," *J. NeuroEngineering Rehabil.*, vol. 18, no. 1, p. 181, Dec. 2021, doi: 10.1186/s12984-021-00976-3.

[137] J. Pinto-Ramos *et al.*, "Handheld dynamometer reliability to measure knee extension strength in rehabilitation patients—A cross-sectional study," *PLOS ONE*, vol. 17, no. 5, p. e0268254, May 2022, doi: 10.1371/journal.pone.0268254.

[138] J. W. J. Van Unnik *et al.*, "Portable fixed dynamometry enables home-based, reliable assessment of muscle strength in patients with amyotrophic lateral sclerosis: a pilot study," *Amyotroph. Lateral Scler. Front. Degener.*, vol. 24, no. 7–8, pp. 651–660, Oct. 2023, doi: 10.1080/21678421.2023.2231494.

[139] L. P. James, J. Weakley, P. Comfort, and M. Huynh, "The Relationship Between Isometric and Dynamic Strength Following Resistance Training: A Systematic Review, Meta-Analysis, and Level of Agreement," *Int. J. Sports Physiol. Perform.*, vol. 19, no. 1, pp. 2–12, Sept. 2023, doi: 10.1123/ijspp.2023-0066.

[140] G. A. Power, B. H. Dalton, C. L. Rice, and A. A. Vandervoort, "Power loss is greater following lengthening contractions in old versus young women," *Age*, vol. 34, no. 3, pp. 737–750, June 2012, doi: 10.1007/s11357-011-9263-z.

[141] T. Dos'Santos, P. A. Jones, J. Kelly, J. J. McMahon, P. Comfort, and C. Thomas, "Effect of Sampling Frequency on Isometric Midthigh-Pull Kinetics," *Int. J. Sports Physiol. Perform.*, vol. 14, no. 4, pp. 525–530, Apr. 2019, doi: 10.1123/ijspp.2019-2015-0222.

[142] B. J. Thompson, "Influence of signal filtering and sample rate on isometric torque – time parameters using a traditional isokinetic dynamometer," *J. Biomech.*, vol. 83, pp. 235–242, Jan. 2019, doi: 10.1016/j.jbiomech.2018.12.006.

[143] Z. B. Moussa, S. Zouita, F. Ben Salah, D. Behm, and A. Chaouachi, "ISOKINETIC TRUNK STRENGTH, VALIDITY, RELIABILITY, NORMATIVE DATA AND RELATION TO PHYSICAL PERFORMANCE AND LOW BACK PAIN: A REVIEW OF THE LITERATURE," *Int. J. Sports Phys. Ther.*, vol. 15, no. 1, pp. 160–174, Feb. 2020.

[144] K. C. Wong *et al.*, "User Perceptions and Experiences of a Handheld 12-Lead Electrocardiographic Device in a Clinical Setting: Usability Evaluation," *JMIR Cardio*, vol. 5, no. 2, p. e21186, Aug. 2021, doi: 10.2196/21186.

[145] M.-P. T. Le *et al.*, "Comparison of four handheld point-of-care ultrasound devices by expert users," *Ultrasound J.*, vol. 14, p. 27, July 2022, doi: 10.1186/s13089-022-00274-6.

[146] T. R. Waters, V. Putz-Anderson, A. Garg, and L. J. Fine, "Revised NIOSH equation for the design and evaluation of manual lifting tasks," *Ergonomics*, vol. 36, no. 7, pp. 749–776, July 1993, doi: 10.1080/00140139308967940.

[147] C. C. for O. H. and S. Government of Canada, "CCOHS: NIOSH Lifting Equation - Calculating Recommended Weight Limit (RWL)." Accessed: Sept. 09, 2025. [Online]. Available: https://www.ccohs.ca/oshanswers/ergonomics/niosh/calculating_rwl.html

[148] *Packaging — Complete, filled transport packages and unit loads — Dimensions of rigid rectangular packages*, International Standard ISO 3394:2012, Nov. 2012. Accessed: Sept. 09, 2025. [Online]. Available: https://www.iso.org/standard/50990.html

[149] "Ergonomic Guidelines for Manual Material Handling," California Department of Industrial Relations (Cal/OSHA); National Institute for Occupational Safety and Health (NIOSH), CDC., Sacramento, CA., DHHS (NIOSH) Publication 2007–131, 2007.

[150] R. Brack and E. H. Amalu, "A review of technology, materials and R&D challenges of upper limb prosthesis for improved user suitability," *J. Orthop.*, vol. 23, pp. 88–96, Jan. 2021, doi: 10.1016/j.jor.2020.12.009.

[151] U.S. Food and Drug Administration, "Applying Human Factors and Usability Engineering to Medical Devices.," U.S. Food and Drug Administration, Guidance for Industry and Food and Drug Administration Staff. 1757., Feb. 2016. Accessed: Sept. 09, 2025. [Online]. Available: https://www.fda.gov/media/80481/download

[152] U.S. Food and Drug Administration., "Reprocessing Medical Devices in Health Care Settings: Validation Methods and Labeling," U.S. Department of Health and Human Services; Food and Drug Administration; Center for Devices and Radiological Health; Center for Biologics, Guidance for Industry and Food and Drug Administration Staff 1748, Mar. 2015. [Online]. Available: https://www.fda.gov/media/80265/download

[153] M. Bernard, E. Jubeli, M. D. Pungente, and N. Yagoubi, "Biocompatibility of polymer-based biomaterials and medical devices – regulations, *in vitro* screening and risk-management," *Biomater. Sci.*, vol. 6, no. 8, pp. 2025–2053, 2018, doi: 10.1039/C8BM00518D.

[154] J. Gaudet and G. Handrigan, "Assessing the Validity and Reliability of A Low-Cost Microcontroller-Based Load Cell Amplifier for Measuring Lower Limb and Upper Limb Muscular Force," *Sensors*, vol. 20, no. 17, p. 4999, Sept. 2020, doi: 10.3390/s20174999.

[155] G. J. Wilson and A. J. Murphy, "The Use of Isometric Tests of Muscular Function in Athletic Assessment," *Sports Med.*, vol. 22, no. 1, pp. 19–37, July 1996, doi: 10.2165/00007256-199622010-00003.

[156] Texas Instruments Incorporated, "ADS1255/ADS1256: Very Low Noise, 24-Bit Analog-to-Digital Converter," Datasheet, Datasheet Datasheet, Sept. 2013.

[157] V. Baltzopoulos, J. G. Williams, and D. A. Brodie, "Sources of Error in Isokinetic Dynamometry: Effects of Visual Feedback on Maximum Torque Measurements," *J. Orthop. Sports Phys. Ther.*, vol. 13, no. 3, pp. 138–142, Mar. 1991, doi: 10.2519/jospt.1991.13.3.138.

[158] N. Kanemura *et al.*, "Effect of Visual Feedback on Muscle Endurance in Normal Subjects," *J. Phys. Ther. Sci.*, vol. 11, no. 1, pp. 25–29, 1999, doi: 10.1589/jpts.11.25.

[159] I. J. B. Nascimento *et al.*, "Barriers and facilitators to utilizing digital health technologies by healthcare professionals," *Npj Digit. Med.*, vol. 6, no. 1, p. 161, Sept. 2023, doi: 10.1038/s41746-023-00899-4.

[160] J. Zhang, T. R. Johnson, V. L. Patel, D. L. Paige, and T. Kubose, "Using usability heuristics to evaluate patient safety of medical devices," *J. Biomed. Inform.*, vol. 36, no. 1–2, pp. 23–30, Feb. 2003, doi: 10.1016/S1532-0464(03)00060-1.

[161] J. Mitchell, C. Shirota, and K. Clanchy, "Factors that influence the adoption of rehabilitation technologies: a multi-disciplinary qualitative exploration," *J. NeuroEngineering Rehabil.*, vol. 20, no. 1, p. 80, June 2023, doi: 10.1186/s12984-023-01194-9.

[162] CME Corp, "Baseline Economy Push/Pull Dynamometer With Attachments," CME Corp. [Online]. Available: https://www.cmecorp.com/fei-baseline-economy-push-pull-dynamometer-with-attachments.html

[163] FEI Retail, "MicroFET / ErgoFET Instruments for Strength and Range-of-Motion Evaluation Archives," Fabrication Enterprises Retail Sales Corp. Accessed: Sept. 09, 2025. [Online]. Available: https://www.feiretail.com/evaluation/strength/microfet-ergofet-instruments-for-strength-and-range-of-motion-evaluation/

[164] S. Gallagher, J. S. Moore, and T. J. Stobbe, *Physical strength assessment in ergonomics*. Fairfax, Va: American Industrial Hygiene Association, 1998.

[165] "HUMAC NORM Isokinetic Testing & Exercise system," MEDELCO. Accessed: Sept. 09, 2025. [Online]. Available: https://medelco.ca/products/humac-norm-isokinetic-testing-exercise-system

[166] T. S. Ellenbecker and E. P. Roetert, "Isokinetic Profile of Elbow Flexion and Extension Strength in Elite Junior Tennis Players," *J. Orthop. Sports Phys. Ther.*, vol. 33, no. 2, pp. 79–84, Feb. 2003, doi: 10.2519/jospt.2003.33.2.79.

[167] I. F. S. R. Schindler *et al.*, "A Systematic Review of Isokinetic Muscle Strength in a Healthy Population With Special Reference to Age and Gender," *Sports Health Multidiscip. Approach*, vol. 15, no. 3, pp. 328–332, May 2023, doi: 10.1177/19417381221146258.

[168] J. A. Parraca, J. C. Adsuar, F. J. Domínguez-Muñoz, S. Barrios-Fernandez, and P. Tomas-Carus, "Test-Retest Reliability of Isokinetic Strength Measurements in Lower Limbs in Elderly," *Biology*, vol. 11, no. 6, p. 802, May 2022, doi: 10.3390/biology11060802.

[169] D. M. Jessop and M. T. G. Pain, "Maximum Velocities in Flexion and Extension Actions for Sport," *J. Hum. Kinet.*, vol. 50, no. 1, pp. 37–44, Apr. 2016, doi: 10.1515/hukin-2015-0139.

[170] S. H. P. Kotte, J. Viveen, K. L. M. Koenraadt, B. The, and D. Eygendaal, "Normative values of isometric elbow strength in healthy adults: a systematic review," *Shoulder Elb.*, vol. 10, no. 3, pp. 207–215, July 2018, doi: 10.1177/1758573217748643.

[171] M. Fidan, A. Bayrak, and U. Karli, "A novel adaptable isometric strength analysis and exercise development system design," *Proc. Inst. Mech. Eng. [H]*, vol. 235, no. 8, pp. 913–926, Aug. 2021, doi: 10.1177/09544119211015562.

[172] R. Montoro-Bombú, B. B. Gomes, A. Santos, and L. Rama, "Validity and Reliability of a Load Cell Sensor-Based Device for Assessment of the Isometric Mid-Thigh Pull Test," *Sensors*, vol. 23, no. 13, p. 5832, June 2023, doi: 10.3390/s23135832.

[173] O. Andrades-Ramírez, D. Ulloa-Díaz, B. Alfaro Castillo, P. Arroyo-Jofré, A. Castillo-Paredes, and L. Chirosa-Ríos, "Test–Retest Reliability of an Isometric and Isometric/Vibratory Muscular Strength Protocol with Functional Electro-Mechanical Dynamometry," *Sports*, vol. 12, no. 7, p. 175, June 2024, doi: 10.3390/sports12070175.

[174] B. L. Riemann, K. E. Wilk, and G. J. Davies, "Reliability of Upper Extremity Functional Performance Tests for Overhead Sports Activities," *Int. J. Sports Phys. Ther.*, vol. 18, no. 3, June 2023, doi: 10.26603/001c.74368.

[175] B. J. Thompson and J. Xu, "Isokinetic Dynamometer Leg Extensor Peak Torque Measurement: A Time-Delayed Reliability and Score Selection Analysis Study," *J. Funct. Morphol. Kinesiol.*, vol. 8, no. 2, p. 62, May 2023, doi: 10.3390/jfmk8020062.

[176] "BL34E34-01D-05RO Brushless DC Motor Datasheet," Lin Engineering, Datasheet BL34E34-01D-05RO, Mar. 2022. [Online]. Available: https://lin-docs.s3.us-west-2.amazonaws.com/datasheets/external/bldc/BL34E34-01D-05RO.pdf

[177] Anaheim Automation, Inc., "GBPH-090x-NS Series Spec Sheet," Anaheim Automation, Inc, Anaheim, CA, USA, Datasheet L010455, 2023.

[178] "STM32F407G-DISC1-Datasheet," STMicroelectronics, Geneva, Switzerland, Datasheet DS8626 Rev 9, Aug. 2020. Accessed: Apr. 05, 2022. [Online]. Available: https://www.st.com/en/microcontrollers-microprocessors/stm32f407-417/documentation.html

[179] "STM32F407G-DISC1 Evaluation Board Schematic," STMicroelectronics, Geneva, Switzerland, Schematic MB997E, Sept. 2020. Accessed: Apr. 05, 2022. [Online]. Available: https://www.st.com/en/microcontrollers-microprocessors/stm32f407-417/documentation.html

[180] "STM32F407/417 Reference Manual," STMicroelectronics, Geneva, Switzerland, Reference Manual RM0090 Rev 19, Feb. 2021. Accessed: Apr. 05, 2022. [Online]. Available: https://www.st.com/en/microcontrollers-microprocessors/stm32f407-417/documentation.html

[181] MEAN WELL Enterprises Co., Ltd., "SE-600 Series 600W Single Output Power Supply Specification," MEAN WELL Enterprises Co., Ltd., New Taipei City, Taiwan, Specification Sheet (Datasheet) SE-600-SPEC, Sept. 2024. [Online]. Available: https://www.meanwell.com/Upload/PDF/SE-600/SE-600-SPEC.PDF

[182] "General Purpose Strain Gages — Single Linear (S5145)," Vishay Precision Group, Inc. – Micro-Measurements, Malvern, Pennsylvania, USA, Datasheet 12134-EN (Rev. 21-Jul-2020), July 2020. Accessed: Nov. 21, 2024. [Online]. Available: https://docs.micro-measurements.com/?id=12134

[183] "BL34E34-01-RO," DigiKey Electronics. Accessed: Dec. 18, 2025. [Online]. Available: https://www.digikey.ca/en/products/detail/lin-engineering/BL34E34-01-RO/11564448

[184] "GBPH-0902-NS-040." Accessed: Dec. 18, 2025. [Online]. Available: https://anaheimautomation.com/gbph-0902-ns-040.html

[185] "TMCM-1636-24V-CANOPEN," DigiKey Electronics. Accessed: Dec. 18, 2025. [Online]. Available: https://www.digikey.ca/en/products/detail/analog-devices-inc-maxim-integrated/TMCM-1636-24V-CANOPEN/12699250

[186] "SE-600-48," DigiKey Electronics. Accessed: Dec. 18, 2025. [Online]. Available: https://www.digikey.ca/en/products/detail/mean-well-usa-inc/SE-600-48/7706618

[187] "Planetary Gearmotors," Kollmorgen (Industrial Devices Corporation), Catalog I_Gearmotors, Jan. 2000. Accessed: May 02, 2024. [Online]. Available:

https://www.kollmorgen.com/sites/default/files/legacy%20-%20idc/documentation/%E2%80%93//I_Gearmotors.pdf

[188] C. Hannum, R. Li, and W. Wang, "A Trust-Assist Framework for Human–Robot Co-Carry Tasks," *Robotics*, vol. 12, no. 2, p. 30, Feb. 2023, doi: 10.3390/robotics12020030.

[189] R. Yoshida, K. Kasahara, Y. Murakami, and M. Nakamura, "Maximum Isokinetic Eccentric Elbow Flexor Muscle Force Can Be Estimated Using Maximum Isometric Contraction Force," *Cureus*, Oct. 2024, doi: 10.7759/cureus.70878.

[190] D. Janicijevic, O. M. Knezevic, A. Garcia-Ramos, D. Cvetic, and D. M. Mirkov, "Isokinetic Testing: Sensitivity of the Force-Velocity Relationship Assessed through the Two-Point Method to Discriminate between Muscle Groups and Participants' Physical Activity Levels," *Int. J. Environ. Res. Public. Health*, vol. 17, no. 22, p. 8570, Nov. 2020, doi: 10.3390/ijerph17228570.

[191] B. Jeoung, M. Choi, and A. Kim, "Development and Performance Evaluation of a Smart Upper-Limb Rehabilitation Exercise Device," *Sensors*, vol. 24, no. 2, p. 659, Jan. 2024, doi: 10.3390/s24020659.

[192] E. S. Lawrence *et al.*, "Estimates of the Prevalence of Acute Stroke Impairments and Disability in a Multiethnic Population," *Stroke*, vol. 32, no. 6, pp. 1279–1284, June 2001, doi: 10.1161/01.STR.32.6.1279.

[193] National Spinal Cord Injury Statistical Center (NSCISC), "2023 Annual Statistical Report for the Spinal Cord Injury Model Systems.," University of Alabama at Birmingham, Birmingham, Alabama, 2023. [Online]. Available: https://www.nscisc.uab.edu

[194] M. Bond *et al.*, "Epidemiology of Spinal Cord Injury in British Columbia, Canada: 20 Years of Population-Based Administrative Data," *Neurotrauma Rep.*, vol. 6, no. 1, pp. 311–321, Apr. 2025, doi: 10.1089/neur.2025.0012.

[195] Praxis Spinal Cord Institute, "Rick Hansen Spinal Cord Injury Registry: A look at Spinal Cord Injury in Canada in 2022," Praxis Spinal Cord Institute., Vancouver, BC, RHSCIR Report, Sept. 2024. [Online]. Available: https://praxisinstitute.org/a-look-at-spinal-cord-injury-in-canada-in-2022/